João Otávio Dourado Monteiro

LAMINAR FLAME SPEED OF FUEL MIXTURES APPLIED TO SPARK IGNITION INTERNAL COMBUSTION ENGINES

Dissertation submitted to the Mechanical Engineering Graduate Program of the Federal University of Santa Catarina in partial fulfillment of the requirements for the degree of Master of Mechanical Engineering.

Supervisor: Prof. Amir Antônio Martins de Oliveira Jr., PhD.

Florianópolis
2015

Ficha de identificação da obra elaborada pelo autor,
através do Programa de Geração Automática da Biblioteca Universitária da UFSC.

Monteiro, Joao Otavio Dourado
Laminar Flame Speed of Fuel Mixtures Applied to Spark Ignition Internal Combustion Engines / Joao Otavio Dourado Monteiro ; orientador, Amir Antônio Martins de Oliveira Jr. - Florianópolis, SC, 2015.
150 p.

Dissertação (mestrado) - Universidade Federal de Santa Catarina, Centro Tecnológico. Programa de Pós-Graduação em Engenharia Mecânica.

Inclui referências

1. Engenharia Mecânica. 2. Reator de volume constante. 3. Velocidade de chama laminar. 4. Gasolina. 5. Etanol. I. Oliveira Jr., Amir Antônio Martins de. II. Universidade Federal de Santa Catarina. Programa de Pós-Graduação em Engenharia Mecânica. III. Título.

João Otávio Dourado Monteiro

LAMINAR FLAME SPEED FOR FUEL MIXTURES FOR SPARK IGNITION COMBUSTION ENGINES

This Dissertation was considered adequate to obtain the degree of Master of Mechanical Engineering and was approved on its final version by the Mechanical Engineering Graduate Program.

Florianópolis, September 30th 2015.

_____
Prof. Armando Albertazzi Gonçalves Jr., Dr. Eng.
Mechanical Engineering Graduate Program Chair

Examining board:

_____
Prof. Amir Antônio Martins de Oliveira Jr., PhD
Supervisor
Federal University of Santa Catarina

_____
Prof. Armando Albertazzi Gonçalves Jr., Dr.Eng.
Federal University of Santa Catarina

_____
Prof. Cesar José Deschamps, Ph.D.
Federal University of Santa Catarina

_____
Prof. Fernando Marcelo Pereira, Dr.Eng.
Federal University of Rio Grande do Sul

ACKNOWLEDGEMENTS

I thank my parents, Ana Rita Ribas Dourado and Avelino José Monteiro, my brother José Vitor Dourado Monteiro, and my sister Maria Clara Dourado Monteiro, also my girlfriend Luana Cristina Wilvert.

I thank my supervisor Amir Antônio Martins Oliveira Jr., and the professors of the combustion and termal systems laboratory Leonel Rincón Cancino and Edson Bazzo.

I thank the LabCET staff and colleagues, Gilson Nunes Maia, Ricardo Morel Hartmann, Eduardo Morel Hartmann, Amir Roberto De Toni, Leandro Alves de Oliveira, Camila Rigoni Medeiros, Roberto Wolf Francisco Jr., Renzo Fabricio Figueroa Piña, Alexandre Schmidt Ferreira.

I thank the company PETROBRAS and the CNPq for the financial support and the employees Edimilson Jesus de Oliveira and Mauro Iurk Rocha.

I thank the Federal University of Santa Catarina and the Mechanical Engineering Graduate Program and everyone that contributed to the development of this work and my formation as an engineer.

ABSTRACT

The laminar flame speed is a physicochemical parameter of the combustion of premixed mixtures. It is relevant in the design and analysis of combustion systems, such as internal combustion engines and gas turbines, in risk analysis of accidents with gas fuels, as well as, a global target to the development of detailed chemical kinetics models for combustion. Here, the laminar flame speeds of ethanol, iso-octane, n-heptane, gasoline, gasoline with 27% ethanol in volume, two surrogates for the gasoline and the gasoline with ethanol, in mixture with dry air were measured at 100 kPa, temperature range from 298 K to 408 K, and equivalence ratio from 0.6 to 1.4. The measurements were made in a constant volume reactor equipped with a high-speed camera (10000 FPS), for the visualization of the spherically expanding flame front propagation using the Schlieren method. Unstretched laminar flame speed was obtained through extrapolation using a linear relation between flame stretch rate and flame propagation velocity. The effect of temperature on flame speed was evidenced and two empirical equations were curve fitted to the measurements relating the flame speed to the equivalence ratio. A global equation to calculate laminar flame speed as a function of equivalence ratio and temperature was also curve-fitted for each fuel. The results agree with values found in the literature for the pure substances within 10 %. The temperature dependence parameter is also in good agreement with the literature within an error band of 10 % of the measurement. The deviation from the curve-fitted equations and the measurements is smaller than 4%. The surrogate proposed also represented with great accuracy the laminar flame speed of the gasoline and the gasoline with ethanol addition, with a maximum difference of 2 %.

Keywords: Constant volume reactor, Laminar flame speed, Gasoline, Ethanol, Gasoline surrogate.

Título: MEDIÇÃO DE VELOCIDADE DE CHAMA LAMINAR DE MISTURAS AR-COMBUSTÍVEL PARA MOTORES DE IGNIÇÃO POR CENTELHA

RESUMO

A velocidade de chama laminar é uma característica físico-química da combustão de misturas contendo oxidante e combustível pré-misturados. É um parâmetro utilizado no projeto e análise de sistemas de combustão, como motores e turbinas a gás, nas análises de risco, como em acidentes envolvendo gases, e como parâmetro global para o desenvolvimento de modelos de cinética química de combustão. Nesse trabalho, a velocidade de chama laminar foi medida para os seguintes combustíveis: etanol, iso-octano, n-heptano, gasolina, gasolina com adição de 27% de etanol, e duas misturas que emulam o comportamento (*surrogates*) da gasolina e da gasolina com adição de etanol. As condições iniciais para os experimentos foram 100 kPa, temperaturas variando de 298 K até 408 K, e razão de equivalência de 0,6 até 1,4. Os experimentos foram realizados em um reator de volume constante, equipado com uma câmera de alta velocidade (10000 FPS) usada para a visualização da propagação da frente de chama no interior do reator com o método Schlieren. A velocidade de chama laminar plana foi obtida através da extrapolação linear da relação entre a velocidade de propagação da chama e a taxa de estiramento. O parâmetro de dependência com a temperatura foi calculado para cada combustível em cada razão de equivalência. Duas curvas de ajuste dos dados experimentais (função polinomial de terceiro grau e exponencial) foram obtidas para relacionar velocidade de chama laminar e razão de equivalência para cada temperatura. Uma equação global para calcular velocidade de chama laminar em função de temperatura e razão de equivalência para cada combustível também foi determinada. O resultados obtidos mostram uma boa concordância com a literatura, com diferenças menores que 10 % para as substâncias puras. O parâmetro de dependência com a temperatura também está em boa concordância com os valores encontrados na literatura dentro da faixa de erro experimental de 10 % do valor medido. O uso da equação global resulta em desvio menor que 4 % para os valores medidos. Os *surrogates* investigados representam a velocidade de chama laminar da gasolina e da gasolina com adição de etanol dentro de um desvio de máximo de 2 %.

Palavras-chave: Reator de volume constante, Velocidade de chama laminar, Gasolina, Etanol, Surrogate.

RESUMO ESTENDIDO

Introdução: A velocidade de chama laminar é um dos parametros essenciais para a análise e predição da performance das mais variadas máquinas a combustão. A maioria dos modelos de combustão turbulenta requerem o conhecimento da velocidade de chama laminar da mistura ar/combustível em função da razão de equivalência, temperatura e pressão. Além disso, dados experimentais confiáveis são necessários para testar e calibrar modelos cinéticos de combustão. A velocidade de chama laminar também é importante no projeto de queimadores, turbinas a gás, e para predições de explosões.

A velocidade de chama laminar de misturas de ar com iso-octano, n-heptano e etanol, foi investigada extensivamente principalmente na última década. Porém, mesmo assim a diferença entre medições com diferentes métodos é muitas vezes maior que a incerteza experimental, o que leva a crer que medições ainda são necessárias a fim de se estabelecer uma valor mais correto. Além destes combustíveis puros, também se faz necessário testar combustíveis convencionais, como a gasolina, principalmente por não ser viável representar quimicamente através de um modelo cinético de combustão toda a complexidade de elementos que compõem a gasolina. Desta forma também é importante que sejam estabelecidos *surrogates* confiáveis e que representem com devida precisão as propriedades da gasolina.

Objetivos: O objetivo principal é medir a velocidade de chama laminar de misturas de hidrocarbonetos e ar para motores a combustão interna com ignição por centelha. Objetivos específicos são: medir e comparar com a literatura disponível a velocidade de chama laminar de combustíveis puros como iso-octano, n-heptano e etanol, para validar as medições. Mediar a velocidade de chama laminar da Gasolina A (sem adição de etanol) e Gasolina C (Mistura de gasolina A e 27 % de etanol em volume). Propor um *surrogate* para a gasolina A, composto por uma mistura binária de iso-octano e n-heptano, e um *surrogate* para a gasolina C, formulado adicionando 27 % de etanol ao *surrogate* para a gasolina A, e finalmente averiguar a concordância entre a velocidade de chama laminar entre os *surrogates* e os combustíveis reais a fim de acertar se estes resultam em uma boa simulação da velocidade de chama laminar das gasolinas A e C. Além disso, através das medições feitas são determinadas relações empíricas para que a velocidade de chama laminar possa ser obtida também fora dos pontos experimentais, e também é feita a determinação do parâmetro de dependência com a temperatura

Método: Para se realizarem as medições de velocidade de chama laminar um reator de volume constante é utilizado.

O reator consiste em dois hemisférios juntos formando uma esfera de raio de 150 mm, os hemisférios possuem cada um uma janela de quartzo de 75 mm de raio e 5 mm em espessura através das quais luz pode passar pelo reator possibilitando a visualização da chama, O reator tem um volume total de 14,8 L.

O reator é equipado com sistema de controle de temperatura, composto por uma manta térmica com uma potência máxima de aquecimento de 900 W e duas lâmpadas de 250 W totalizando um sistema de aquecimento de 1400 W, o reator pode ser aquecido até 135 ºC e a temperatura é controlada por 3 termopares localizados nas superfícies externas do reator, e um termopar em seu interior cuja ponta se encontra a 40 mm do centro afim de se controlar a temperatura dos gases antes da combustão.

A pressão no interior da câmara é monitorada por um transdutor de pressão localizado na parede do reator que mede a evolução da pressão na câmara conforme a reação de combustão ocorre. Além disso a pressão de ar com a qual o reator e preenchido também é controlada por outro transdutor na linha de alimentação de ar.

Para o sistema de ignição é utilizado um sistema de controle elétrico para controlar a energia descarregada pela centelha. Em todos os experimentos o sistema de controle descarrega sempre a mesma energia na centelha. A centelha por sua vez ocorre no centro do reator, para tal são utilizadas duas velas automotivas prolongadas por fios de cobre de 1 mm em diâmetro que se encontram a uma distância de 2 mm entre um e outro no centro geométrico do reator, é nesta distância em que a centelha de ignição de estabelece.

Para a obtenção de imagens da propagação da chama esférica no interior do reator é utilizado o método *Schllieren* com uma montagem tipo Z. Este sistema ótico de obtenção de imagens é composto por dois espelhos esféricos com 152,4 mm em diâmetro e uma distância focal de 1524 mm um ponto de luz composto por um LED de 5 mm e uma faca para melhorar a precisão da imagem. Através da montagem deste sistema é utilizada uma câmera digital de alta velocidade capaz de obter 10000 FPS e capturar pela diferença da densidade entre os gases queimados e não-queimados a posição da frente de chama a cada instante de tempo.

O combustível é injetado no reator utilizando uma seringa, previamente à injeção do combustível a bomba de vácuo é acionada, criando uma pressão absoluta de 0,2 mPa o que possibilita a completa evaporação do combustível. O reator, após a evaporação do combustível, é preenchido com ar seco até a pressão inicial previamente selecionada.

A velocidade de propagação da chama obtida através das imagens adquiridas pela câmera de alta velocidade é igual a velocidade de chama estirada em relação aos gases queimados. Para que seja possível relacionar esta velocidade com a velocidade de chama laminar é necessário empregar

uma modelo que relaciona a velocidade de chama estirada a taxa de estiramento e a velocidade de chama não-estirada. O modelo utilizado é o modelo linear, largamente utilizado na literatura e que forneceu bons resultados.

Desta forma foram feitos experimentos e foi medida a velocidade de chama laminar para todos os combustíveis (iso-octano, n-heptano, etanol, gasolina A, gasolina C, *surrogate* A, e *surrogate* C).

O *surrogate* A foi desenvolvido através de uma mistura de 66 % de iso-octano e 33 % de n-heptano em volume e o *surrogate* C é resultado da mistura dentre *surrogate* A e 27 % de etanol em volume.

Resultados: Os resultados obtidos foram satisfatórios, para as substâncias puras (iso-octano, n-heptano e etanol) em todos os 5 níveis de temperaturas testados e todas as razões de equivalência os resultados de velocidade de chama estiveram de acordo com a literatura revisada. O parâmetro de dependência com a temperatura para estes combustíveis apesar da grande incerteza experimental associada, em torno de 10 %, também mostrou uma boa concordância com a literatura revisada.

Os resultados obtidos com as substâncias puras em comparação com a literatura revisada, pela boa concordância, possibilitaram a segurança necessária para se realizar medições com as gasolinas, que são combustíveis cuja comparação com outros resultados experimentais não é possível devido a grande diferença de composição.

Como resultados dos experimentos com gasolina A, C e *surrogates* A e C, pode-se afirmar que ambos os *surrogates* modelam com precisão a velocidade de chama laminar respectiva gasolina, para todas as faixas de temperatura e também de razão de equivalência testadas, uma vez que a diferença entre os pontos experimentais nunca foi maior de 2 %. O parâmetro de dependência da temperatura dos *surrogates* também teve um resultado satisfatório uma vez que a diferença entre os valores dos *surrogates* e das gasolinas sempre esteve dentro das incertezas experimentais.

Desta forma como uma conclusão geral pode-se afirmar que os *surrogates* A e C testados representam com a qualidade esperada a velocidade de chama laminar da gasolina A e C respectivamente.

Além disso, as equações empíricas para todos os combustíveis testados também modelaram com grande qualidade os resultados experimentais obtidos, uma vez que o uso de qualquer equação empírica resultou em uma diferença de no máximo 4 % do real valor medido para o combustível em questão.

LIST OF FIGURES

Figure 2-1 – Explosion limits 36
Figure 2-2 – Schematic of the classification of flame type 39
Figure 2-3 – Flame front propagation. 40
Figure 2-4 – Representation of the flame in the CVR. 41
Figure 2-5 - Mallard–Le Chatelier description of the temperature in a laminar flame wave. 45
Figure 2-6 – Control volume and boundary conditions for the Spalding's model for flame speed 47
Figure 2-7 – Influence of equivalence ratio on laminar flame speed. 50
Figure 2-8 - Influence of unburnt mixture temperature on laminar flame speed. 51
Figure 2-9 - Influence of unburnt mixture temperature on laminar flame speed. 52
Figure 2-10 – Categorization of flame speed measurement experiments. 54
Figure 2-11 - Schematic diagram of the reactor developed by Metghalchi and Keck. 57
Figure 2-12 - Experimental apparatus used by Eisazadeh-Far (2010). 58
Figure 2-13 – Diagram of a simple Schlieren system. 59
Figure 2-14 – Differences of knife-edge positions and forms in Schlieren imaging: (a) Circular knife-edge; (b) Vertical knife-edge; (c) Horizontal knife-edge. 61
Figure 2-15 – Representation of a typical Z-type Schlieren arrangement. 62
Figure 2-16 – Coma aberration representation. 62
Figure 2-17 - Astigmatism aberration representation. 64
Figure 3-1 – Exploded view of the CVR's main components. 71
Figure 3-2 – Air filling system schematic. 73
Figure 3-3 - Evacuation system schematic. 73
Figure 3-4 - Dimensions of the optical system. 75
Figure 3-5 – Optical system photo. 1- punctual light source; 2 and 4- spherical mirrors; 3- CVR; 5- cutting edge; 6- camera. 76
Figure 3-6 – Experimental apparatus. 76
Figure 3-7 – Pressure and flame radius data. 79
Figure 3-8 – Stretched flame speed versus strech rate. 80
Figure 3-9 – Selected data for linear regression. 81
Figure 4-1– Spherical flame evolution. N-heptane at T_u= 398 K. 86
Figure 4-2 – Comparison for extrapolation of the third degree and exponential fitting curves for laminar flame speed as a function of equivalence ratio. 87
Figure 4-3 – Comparison of wrinkle in flames. T_u = 398 K; ϕ = 1.4 r_f = 50 mm. (a) n-hepthane; (b) gasoline A; (c) iso-octane; (d) ethanol. 89

Figure 4-4 – Results of laminar flame speed of n-heptane versus equivalence ratio at 298 K. 90
Figure 4-5 – Results of laminar flame speed of n-heptane versus equivalence ratio at 323 K. 90
Figure 4-6– Results of laminar flame speed of n-heptane versus equivalence ratio at 348 K. Other references measured at different temperatures. 91
Figure 4-7– Results of laminar flame speed of n-heptane versus equivalence ratio at 373K. 91
Figure 4-8– Results of laminar flame speed of n-heptane versus equivalence ratio at 398 K. 92
Figure 4-9 – Laminar flame speed versus unburned mixture temperature. 94
Figure 4-10 – Temperature dependence parameter versus equivalence ratio for n-heptane. 95
Figure 4-11 - Deviation in percentage of the flame speed measured values from the flame speed calculated values using the global fitting curve versus normalized equivalence ratio for n-heptane. 96
Figure 4-12 – Results of laminar flame speed of iso-octane versus equivalence ratio at 298 K. 98
Figure 4-13 – Results of laminar flame speed of iso-octane versus equivalence ratio at 323 K. 98
Figure 4-14– Results of laminar flame speed of iso-octane versus equivalence ratio at 348 K. 99
Figure 4-15– Results of laminar flame speed of iso-octane versus equivalence ratio at 373K. 99
Figure 4-16– Results of laminar flame speed of iso-octane versus equivalence ratio at 398 K. 100
Figure 4-17 – Laminar flame speed versus unburned mixture temperature for iso-octane. 102
Figure 4-18 – Temperature dependence parameter versus equivalence ratio for iso-octane. 103
Figure 4-19 - Deviation in percentage of the flame speed measured values from the flame speed calculated values using the global fitting curve versus normalized equivalence ratio for iso-octane. 104
Figure 4-20– Results of laminar flame speed of ethanol versus equivalence ratio at 348 K. 105
Figure 4-21– Results of laminar flame speed of ethanol versus equivalence ratio at 373K. 105
Figure 4-22– Results of laminar flame speed of ethanol versus equivalence ratio at 398 K. 106
Figure 4-23 – Laminar flame speed versus unburned mixture temperature for ethanol. 107
Figure 4-24 – Temperature dependence parameter versus equivalence ratio for ethanol. 108

Figure 4-25 - Deviation in percentage of the flame speed measured values from the flame speed calculated values using the global fitting curve versus normalized equivalence ratio for ethanol. 109
Figure 4-26– Results of laminar flame speed of gasoline A and surrogate A versus equivalence ratio at 373 K. 110
Figure 4-27– Results of laminar flame speed of gasoline A and surrogate A versus equivalence ratio at 398 K. 111
Figure 4-28– Results of laminar flame speed of gasoline A and surrogate A versus equivalence ratio at 408 K. 111
Figure 4-29 – Laminar flame speed versus unburned mixture temperature for gasoline A. 114
Figure 4-30– Laminar flame speed versus unburned mixture temperature for surrogate A. 114
Figure 4-31 – Temperature dependence parameter versus equivalence ratio for gasoline A and surrogate A. 116
Figure 4-32 - Deviation in percentage of the flame speed measured values from the flame speed calculated values using the global fitting curve versus normalized equivalence ratio for gasoline A. 117
Figure 4-33 - Deviation in percentage of the flame speed measured values from the flame speed calculated values using the global fitting curve versus normalized equivalence ratio for surrogate A. 118
Figure 4-34– Results of laminar flame speed of gasoline C and surrogate C versus equivalence ratio at 373 K. 119
Figure 4-35– Results of laminar flame speed of gasoline C and surrogate C versus equivalence ratio at 398 K. 119
Figure 4-36– Results of laminar flame speed of gasoline C and surrogate C versus equivalence ratio at 408 K. 120
Figure 4-37 – Laminar flame speed versus unburned mixture temperature for gasoline C. 122
Figure 4-38– Laminar flame speed versus unburned mixture temperature for surrogate C. 122
Figure 4-39 – Temperature dependence parameter versus equivalence ratio for gasoline C and surrogate C. 124
Figure 4-40 - Deviation in percentage of the flame speed measured values from the flame speed calculated values using the global fitting curve versus normalized equivalence ratio for gasoline C. 125
Figure 4-41 - Deviation in percentage of the flame speed measured values from the flame speed calculated values using the global fitting curve versus normalized equivalence ratio for surrogate C. 126
Figure 4-42 – Comparison of laminar flame speed versus equivalence ratio of all tested fuels at 398 K. 127

LIST OF TABLES

Table 2-1 – Literature review on n-heptane and iso-octane flame speeds measurements. 67
Table 2-2 – Content of ethanol in gasoline worldwide. Volume fraction. .. 68
Table 2-3 – Literature review on ethanol flame speeds measurements. 69
Table 3-1 – Initial parameters of example experiment. 79
Table 3-2 – Results of the linear regression parameters. 81
Table 3-3 – Results and inputs of the equilibrium calculation. 82
Table 3-4 – Variables relevant to flame speed determination and corresponding uncertainties. 83
Table 4-1 – Parameters of Equation (4.1) for n-heptane. 93
Table 4-2– Parameters of Equation (4.2) for n-heptane. 93
Table 4-3 – Parameters of Equation (4.3) for n-heptane. 94
Table 4-4 - Differences for utilizing the average or the quadratic function for the temperature dependence parameter. 97
Table 4-5– Parameters of Equation (4.1) for iso-octane. 101
Table 4-6– Parameters of Equation (4.2) for iso-octane. 101
Table 4-7 – Parameters of Equation (4.3) for iso-octane. 102
Table 4-8– Parameters of Equation (4.1) for ethanol. 106
Table 4-9– Parameters of Equation (4.2) for ethanol. 107
Table 4-10 – Parameters of Equation (4.3) for ethanol. 108
Table 4-11– Parameters of Equation (4.1) for gasoline A. 112
Table 4-12– Parameters of Equation (4.2) for gasoline A. 112
Table 4-13– Parameters of Equation (4.1) for surrogate A. 113
Table 4-14– Parameters of Equation (4.2) for surrogate A. 113
Table 4-15 – Parameters of Equation (4.3) for gasoline A. 115
Table 4-16 – Parameters of Equation (4.3) for surrogate A. 115
Table 4-17– Parameters of Equation (4.1) for gasoline C. 120
Table 4-18– Parameters of Equation (4.2) for gasoline C. 120
Table 4-19– Parameters of Equation (4.1) for surrogate C. 121
Table 4-20– Parameters of Equation (4.2) for surrogate C. 121
Table 4-21 – Parameters of Equation (4.3) for gasoline C. 123
Table 4-22 – Parameters of Equation (4.3) for surrogate C. 123

SYMBOL LIST

SYMBOL	*Description*	*Unity*
(A/F)	Air/fuel rate	-
$(A/F)_{stoic}$	Stoichiometric air/fuel rate	-
(F/A)	Fuel/air rate	-
$(F/A)_{stoic}$	Stoichiometric fuel/air rate	-
[f]	Volumetric molar concentration of fuel	mol/m^3
[O]	Volumetric molar concentration of oxidizer	mol/m^3
A	Area	m^2
a	Constant of the cubic fitting curve	m/s
b	Constant of the cubic fitting curve	m/s
c	Constant of the cubic fitting curve	m/s
c_0	Light speed in vacuum	m/s
c_p	Specific heat at constant pressure	J/(kgK)
CVR	Constant volume reactor	-
D	Mass diffusivity	m^2/s
d	Constant of the cubic fitting curve	m/s
E	Expansion factor	-
e	Constant of the quadratic fitting curve	-
E_A	Activation energy	J/mol
f	Constant of the quadratic fitting curve	-
g	Constant of the quadratic fitting curve	-
k	Thermal conductivity	W/(mK)
L_b	Markstein length of the unburned mixture	m
Le	Lewis number	-
m_a	Mass of air	kg
m_f	Mass of fuel	kg
$\dot{m}$	Mass flow rate	kg/s
$\dot{m}''$	Mass flow rate per area	$kg/(m^2s)$
MM_a	Molecular mass of air	kg/mol

$\mathbf{n}$	Refractive index	-
$\mathbf{n_a}$	Air mol number	mol
$\mathbf{N_c}$	Number of carbon atoms in the elementary molecular formula	-
$\mathbf{n_f}$	Fuel mol number	mol
$\mathbf{N_H}$	Number of hydrogen atoms in the elementary molecular formula	-
$\mathbf{N_O}$	Number of oxigen atoms in the elementary molecular formula	-
$\mathbf{P}$	Pressure	Pa
$\mathbf{P_0}$	Pressure of the reference state	Pa
$\mathbf{P_u}$	Pressure of the unburned mixture	Pa
$\mathbf{R^2}$	Adjusted R squared	-
$\mathbf{r_f}$	Flame radius	m
$\mathbf{r_M}$	Reactant limiting layer	m
$\mathbf{r_T}$	Thermal limiting layer	m
$\mathbf{R_u}$	Universal gas constant	J/(molK)
$\mathbf{S_L}$	Unstretched laminar flame speed in relation to the unburned mixture	m/s
$\mathbf{S_{L,b}}$	Unstretched laminar flame speed in relation to the burned mixture	m/s
$\mathbf{S_{L,u}}$	Unstretched laminar flame speed in relation to the unburned mixture	m/s
$\mathbf{S_{L0}}$	Laminar flame speed at reference state	m/s
$\mathbf{S_{n,b}}$	Stretched laminar flame speed in relation to the burned mixture	m/s
$\mathbf{S_{n,u}}$	Stretched laminar flame speed in relation to the unburned mixture	m/s
$\mathbf{t}$	Time	s
$\mathbf{T}$	Temperature	K
$\mathbf{T_0}$	Temperature of the reference state	K
$\mathbf{T_b}$	Temperature of the burned mixture	K
$\mathbf{T_i}$	Temperature of ignition	K
$\mathbf{T_u}$	Temperature of the unburned mixture	K
$\mathbf{u}$	Standard uncertainty	-

u_b	Velocity of the burned mixture	m/s
u_u	Velocity of the unburned mixture	m/s
V_{CVR}	Volume of the CVR	m^3
x_{7H16}	n-heptane molar fraction	-
x_{C8H18}	iso-octane molar fraction	-
x_{O2}	Oxygen molar fraction	-
Y_{dil}	Mass fraction of diluent	-
Y_f	Mass fraction of fuel	-
Y_O	Mass fraction of oxidizer	-
Y_P	Mass fraction of products	-
α	Temperature dependence parameter	-
α_T	Thermal diffusivity	m^2/s
$\bar{\alpha}$	Average temperature dependence parameter	-
β	Pressure dependence parameter	-
δ	Reaction zone thickness	m
Δ	Average of the deviation in percentage of the flame speed measured values from the flame speed calculated values using the global fitting curve and quadratic equation for the temperature dependence parameter	%
Δh_c	Heat of combustion	J
ε	Average of the deviation in percentage of the flame speed measured values from the flame speed calculated values using the global fitting curve and average for the temperature dependence parameter	%
η	Constant of the exponential fitting curve	-
θ	angle	^{o}
κ	Stretch rate	s^{-1}
ν	Mass ratio of oxidizer and fuel	-
ξ	Constant of the exponential fitting curve	-
ρ_b	Density of the burned mixture	kg/m^3
ρ_u	Density of the unburned mixture	kg/m^3
σ	Constant of the exponential fitting curve	-
τ_c	Chemical time	s

τ_t	Thermic time	s
ϕ	Equivalence ratio	-
ω	Constant of the exponential fitting curve	m/s
$\dot{\omega}$	Reaction rate	mol/(m^{3}s)
$\bar{\omega}$	Mean reaction rate	mol/(m^{3}s)

TABLE OF CONTENTS

1 INTRODUCTION 27
1.1 MOTIVATION 27
1.1.1 Biofuels 28
1.1.2 Vehicular energetic efficiency 30
1.2 OBJECTIVES 32
1.2.1 General objectives 32
1.2.2 Specific objectives 32
2 LITERATURE REVIEW 34
2.1 DEFINITIONS 34
2.1.1 Combustion and equivalence ratio 34
2.1.2 Explosion and flammability limits 35
2.1.3 Flame and basic flame types 38
2.1.4 Laminar flame speed and stretch rate 40
2.2 LAMINAR FLAME SPEED 44
2.2.1 Mallard and Le Chatelier's model 44
2.2.2 Spalding's Model 46
2.2.3 Governing elements of flame speed 49
2.2.4 Empiric formulations for flame speed modeling 52
2.3 FLAME SPEED MEASUREMENTS 53
2.4 CONSTANT VOLUME REACTOR 55
2.4.1 Bradley and Hundy (1971) – Leeds University 56
2.4.2 Metghalchi and Keck (1980) – MIT 56
2.4.3 Eisazadeh-Far (2010) - Northeastern University 57
2.4.4 The Schlieren optic method 58
2.4.5 Optic Method 64
2.5 FUELS AND BIOFUELS 66
2.5.1 Gasoline and surrogates 66
2.5.2 Biofuels 68
3 MATERIALS AND METHODS 71
3.1 EXPERIMENTAL APPARATUS 71
3.1.1 Constant volume reactor 71
3.1.2 Filling system 72
3.1.3 Evacuation system 73
3.1.4 Data acquisition and sensors system 74
3.1.5 Ignition system 74
3.1.6 Optical system 75
3.2 EXPERIMENTAL PROCEDURE 76
3.2.1 Step-by-step experimental procedure 77
3.3 METHOD TO CALCULATE THE LAMINAR FLAME SPEED 77
3.3.1 Equivalence ratio 77
3.3.2 Flame speed calculation example 78

3.3.3 Determination of uncertainties....82
3.4 COMPOSITION OF THE SURROGATE....83
4 RESULTS....85
4.1 N-HEPTANE....89
4.2 ISO-OCTANE....97
4.3 ETHANOL....104
4.4 GASOLINE A AND SURROGATE A....110
4.5 GASOLINE C AND SURROGATE C....118
5 CONCLUSIONS....128
BIBLIOGRAPHIC REFERENCE....131
APPENDIX A - Effects of stretch and Lewis number on spherical flame....137
APPENDIX B – Uncertainty analysis....142
APPENDIX C - Detailed step-by-step experimental procedure....146

1 INTRODUCTION

1.1 MOTIVATION

The study of combustion is of great importance in our society. In just one quick look around, one can realize the huge quantity of machines operating through combustion that sustain our life style. According to the Brazilian Energy Balance 2014 (2014), 82% of total primary energy consumption (electricity and fuels) is generated by means of a combustion process. This percentage corresponds to approximately 80% of industrial consumption and almost 100% of the transport sector. If the total amount of energy produced by combustion processes in Brazil is compared to the annual amount of electricity produced in a record year by Itaipu Hydroelectric Plant (in 2013 Itaipu produced an amount of energy equivalent to 8.48 Mtep) it would be comparable to 28.6 Itaipus. In terms of the amount of fuel consumed, the production of oil products in domestic refineries amounted to 107.8 Mtep, a value that has increased 6.5% over the previous year. Diesel and gasoline alone accounted for 39.2% and 20.5%, respectively, of the total. Besides being the 7th economy, worldwide, Brazil represents only 1.2% of the world´s energy consumption, giving a dimension of the world energy consumption produced by combustion. Therefore, our lives depend vastly on the work and heat harnessed by combustion systems. It is only logical to think that even a small contribution on the knowledge of combustion can contribute significantly on enhancing the quality of our life and of our environment.

There is a wide variety of conditions in which the combustion processes commonly occur, for example, as dictated by the variations of the amount of fuel and air in the combustible mixture and the mixture initial state, determined by the fuel type (gas, liquid or solid), temperature, and pressure. For transportation fuels, the different types of engines, such as alternative engines and gas turbines, and ignition strategies, such as spark or compression ignition, are just a few of the possible strategies used to better explore the heat and work provided by the combustion processes.

In order to understand which strategy is better in each case and to improve its efficiency, it is necessary to characterize the parameters of the combustion that are relevant to the desired engine type. In the engine point of view, overall parameters, such as, the amount of gas and particulate pollutants emitted by unit power or distance travelled, the fuel conversion efficiency (a First-Law efficiency), the engine performance in terms of torque and power are commonly measured, reported and optimized. The fuels usually have their thermo-physical properties, such as heat content, vapor pressure, density, dynamic viscosity and surface tension regulated within somewhat narrow bands. Besides these one-sided parameters, it is well recognized that

parameters that measure the properties for normal combustion and control of the combustion in the engine are also needed to be quantified in order to qualify the fuel as a suitable commercial fuel. The most commonly measured combustion characteristic for alternative internal combustion engines are the octane number (RON/MON), for the spark ignited engines, and the cetane number (CN), for the compression ignited engines. These parameters depend intimately on the formulation of the fuel, i.e., on the relative amount of each hydrocarbon family present in the fuel formulation. The fuel formulation is not completely set from design, but is mostly a product of the oil processing operations that take place in the oil refinery and, as such, may present variations that depend on the origin of the oil and profitability considerations. Nevertheless, the final engine parameters must remain within the bounds established by the regulations.

With the continued tightening environmental regulations imposed, the great variety of oils being produced word-wide nowadays, the fine tuning needed to optimize the profitability in the refinery operations, and the increase in the penetration of biofuels from different origins and submitted to different processing routes, it has become clear that the classical fuel quality as expressed by RON/MON, for example, are not enough to distinguish, predict and optimize engine design, control, and reliability. The fuel industry and engine manufacturers must rely in combustion characteristics that closely reproduce the conditions found in the combustion chambers of internal combustion engines. The combustion characteristics comprise those related to molecular mixing, ignition, flame or reaction propagation, transition from a deflagration to a detonation phenomena, flame quenching and ignition. These phenomena are closely related to properties of the fuel air-mixture, from which, the detailed path taken by the reactions, or detailed chemical reaction mechanism, form the most fundamental chemical characteristic. Since flames are propagating waves, the flow-chemistry interaction form the most important fundamental physical characteristic.

This work focuses on the flame propagation after initiated by an electrical spark, a condition found in spark ignited internal combustion engines. Therefore, flame initiation and propagation are the important combustion characteristic to be measured and analyzed. A secondary aspect is on the effect that biofuels exert in the combustion characteristic of oil derived fuels.

1.1.1 Biofuels

The main driving force to increase the use of biofuels is that they are renewable, something like liquid solar energy. Depending on how they are produced, they contribute very little to carbon emissions and climate change. According to IPCC (2014), in 2004 road transport accounted for 74%

of total CO_2 transport emissions, which in turn represents 23% of the world's energy-related CO_2 emissions. Biofuels could mitigate a significant fraction of these emissions. Another benefit of the use of biofuels is their effect in creating local value chains since their production is more evenly distributed over the planet than that of fossil fuels. For countries with limited availability of oil, they are a strategic option as well.

The idea of using biofuels, specially ethanol, as an automotive fuel is not new, but in fact it remounts to the very beginnings of the use of internal combustion engines (ICE). In 1826, Samuel Morey used ethanol in his early ICEs prototypes, as also did Nikolaus Otto, in 1860. Henry Ford introduced, in 1908, an ethanol adjusted carburetor for the "T" Model, and stated to the *New York Times,* in 1925, that ethanol was "the fuel of the future". Brazil is currently the country with the largest fleet fueled by ethanol, the first car reported as running on ethanol was a Ford that in 1925 ran for 230 km using hydrated ethanol with a percentage of water as high as 30%. PAGLIUSO (2010). According to the Brazilian Automotive Manufacturer Nacional Association ANFAVEA (2014), 75% of the 2.8 millions of light duty vehicles produced in 2012 run with both gasoline or ethanol and any mixture of both fuels and the country produces about 17 million cubic meters of ethanol per year.

Biogasoline can be understood as a liquid fuel for spark-ignited engines obtained from biomass, either vegetal or animal, as well as from waste. Alcohols, mainly ethanol, are by far the most used biofuel. Fermentation and distillation are the most frequently used processes for the production of biofuel. Several crops can be used, such as sugar cane, corn, beetroot, wheat, and sorghum. Many other processes aimed at producing fuels for spark-ignition engines from biomass are under research and development. ZHAO (2010). A few examples are enzymatic hydrolysis of cellulosic materials followed by fermentation; microorganisms able to deliver a diesel-like fuel instead of an alcohol; and conversion of butyric acid obtained from sugar fermentation to hexane. Other include microorganisms that could produce ethanol from syngas; blends of glycerol (a by-product of biodiesel) with propanol, propanediol and gasoline; and even conversion of dehydrated ethanol to biogasoline. Some of these processes seem promising; some seem more difficult to be successful. Production of dehydrated ethanol is energy demanding, in fact dehydration is one of the most important factors that drops energy efficiency in US corn-based production, taking about 14% of the gross energy input in the process. Likewise, conversion of dehydrated ethanol to biogasoline surely takes some extra energy, dropping energy efficiency even further. Finally, in small fractions, ethanol can be mixed easily with gasoline without any penalty for the engine and even benefiting the environment. PAGLIUSO (2010).

1.1.2 Vehicular energetic efficiency

Many other technologies, besides biofuels, are developed with the same goal of improving overall vehicular energy efficiency and reducing global emissions. The main driving force for this development are the regulations regarding emissions of greenhouse gases and other pollutants. One example is the introduction of high-speed direct injection compression ignition Diesel engines. This technology is the major responsible for the reduction of the emission of carbon monoxide in Europe in the last decade. Today it corresponds to approximately half of the cars sold in Western Europe.

Some of the promising research areas, with the goal of improving vehicular energetic efficiency are as listed by the US Energy Department (2015):

- Combustion engine research: focuses on improving new combustion strategies, by improving the efficiency in which the fuel is burnt. That can greatly improve engine efficiency and minimize the emissions formation in the engine itself. Some examples are: low temperature combustion and lean combustion.
- Emissions reduction research: focuses on reducing the cost and improving the efficiency of after treatment technologies that reduce exhaust emissions. It also has software to help calculate greenhouse gas and other emissions.
- Waste heat recovery research: focuses on improving technology that converts wasted engine heat into electricity that can power vehicle accessories and auxiliary loads.
- Fuel effects research: focuses on better understanding how fuels from new sources can affect advanced combustion systems. As an example: development of detailed kinetics mechanisms, or characterization of physical/chemical fuel properties. This is the context in which this work is inserted.
- Lubricants research: focuses on improving lubricants that can improve the fuel efficiency of future and current vehicles in the fleet.
- Idling reduction work: focuses on minimizing unnecessary idling from vehicles.
- Lightweighting research: focuses on lowering the cost and improving the performance of lightweight materials like high-strength steel, aluminum, magnesium, and carbon fiber.
- Aerodynamics and other parasitic loss research focuses on reducing the energy lost to non-engine sources such as drag,

braking, rolling resistance, and auxiliary loads like air conditioning.

Improvement in the efficiency in the conversion of fuels to work has also focused fossil fuels. Even with all the advantages provided by the biofuels, the combination of high calorific power and low refinery costs, still makes gasoline the main and most utilized fuel in light duty vehicles in the world. Pitz, Cernansky, *et al.* (2007) have highlighted the need of characterizing complex fuels using simpler surrogates. Computational combustion modeling is an essential, complementary tool to engine experiments. The combination of computational fluid dynamics (CFD) and detailed chemical kinetics provides the opportunity to efficiently optimizing ICE performance for a given fuel composition. Consequently, computational chemistry models are needed to represent the combustion of gasoline in practical devices such as homogeneous charge compression ignition (HCCI) engines and spark ignited (SI) engines. Unfortunately, it is not currently possible to represent the complex chemistry of full blend gasolines in a detailed chemical kinetic model. Not only are the kinetics of all of the components not well determined, but the chemical kinetic interactions among them are not fully understood. Moreover, the large number of components would lead to an unwieldy number of reactions, species, and thermochemical parameters. Even restricting the number of initial fuel species to be considered to less than ten results in a very large dimensional chemical model. In fact the inclusion of complex geometries and transport phenomena required in an engine combustion model and the available computational resources limit the number of species that can be considered within engine combustion codes. While the long-term goal to increase the number of species considered should remain, there are presently practical reasons to represent full blend gasoline chemical kinetics with a small number of pure components.

Within this scenario, this work focus the measurement of laminar flame speed for gasoline, ethanol, and surrogate mixtures formed by two components. The laminar flame speed is one of the most essential parameters for analysis and performance predictions of various combustion engines. The majority of turbulent combustion models require a knowledge of laminar flame speed of the fuel/air mixture as a function of equivalence ratio, temperature, and pressure. Also, reliable experimental data are needed in order to test and calibrate thermokinetic combustion models which have been quite successful for combustion predictions of hydrocarbon fuels. GÜLDER (1984). Laminar flame speed is also important in the design of burners, gas turbines, and for the prediction of explosions. DIRRENBERGER, GLAUDE, *et al.* (2014). Given the importance of this property, the following set of objectives is proposed for this work.

1.2 OBJECTIVES

1.2.1 General objectives

The main objective of this work is to measure the laminar flame speed of hydrocarbon fuels for spark ignited (SI) engines. The fuels include ethanol, refinery gasoline, commercial gasoline, a gasoline surrogate, and mixtures of the surrogate and ethanol.

The measurements are obtained from image analysis of Schlieren photography of the spherical flame propagation in a Constant Volume Reactor (CVR).

The measurement conditions are: Initial temperature from 298 K to 408 K, initial pressure of 100 kPa, and equivalence ratio from 0.8 to 1.3. These conditions provides a basis for the analysis of the combustion in spark ignited internal combustion engines.

1.2.2 Specific objectives

In order to accomplish the general objective, a set of specific objectives are listed:

- To compare the measurements obtained in the proposed experimental set up and method of analysis to results available in literature as a form of validation. This is made by comparing measurements of laminar flame speed for n-heptane and iso-octane, which are primary reference fuels, at initial temperature of 298 K, 323 K, 348 K, 373 K, and 398 K, and equivalence ratio of 0.8; 0.9; 1.0; 1.1; 1.2, and 1.3.
- To analyze the behavior of the experimental set-up in respect to the basics of premixed flame ignition and propagation and to established the uncertainty related to the measured laminar flame speeds.
- To measure the laminar flame speed of ethanol at the initial temperatures of 348 K, 373 K, and 398 K, and equivalence ratio of 0.8; 0.9; 1.0; 1.1; 1.2, and 1.3.
- To measure the laminar flame speed of the Brazilian pure gasoline, known as gasoline A, at the initial temperatures of 373 K, 398 K and 408 K, and equivalence ratio of 0.8; 0.9; 1.0; 1.1; 1.2 and 1.3.
- To measure the laminar flame speed of the Brazilian commercial gasoline, with 27% of ethanol addition, known as gasoline C, at the initial temperatures of 373 K, 398 K and 408 K, and equivalence ratio of 0.8; 0.9; 1.0; 1.1; 1.2 and 1.3.

- To propose a surrogate for gasoline A formed by a mixture of n-heptane and iso-octane that emulate the behavior of the laminar flame speed of the gasoline A, and to measure the laminar flame speed of the surrogate at the initial temperatures of 373 K, 398 K and 408 K, and equivalence ratio of 0.8; 0.9; 1.0; 1.1; 1.2 and 1.3.
- To propose a surrogate for gasoline C formed by a mixture of n-heptane, iso-octane, and ethanol that emulate the behavior of the laminar flame speed of the gasoline C, and to measure the laminar flame speed of the surrogate at the initial temperatures of 373 K, 398 K and 408 K, and equivalence ratio of 0.8; 0.9; 1.0; 1.1; 1.2 and 1.3.
- To discuss the differences among the results of laminar flame speed obtained for each fuel and surrogate.

The present work is part of a project developed in the Laboratory for Combustion and Thermal Systems Engineering of the Federal University of Santa Catarina, LabCET/UFSC, in partnership with PETROBRAS, entitled “Analysis of the combustion of alternative aviation fuels”. The main objective of the project is to study characteristics of chemical kinetics, combustion, and emissions, of hydrocarbons and oxygenated fuels, and its application to formulations of aviation fuels.

2 LITERATURE REVIEW

2.1 DEFINITIONS

In this section, the definitions of the most important variables and concepts explored in this work are explained.

2.1.1 Combustion and equivalence ratio

Combustion is defined as a "rapid chemical combination of a substance with oxygen, involving the production of heat and light." This definition as given by the Oxford Dictionary emphasizes at first the importance of chemical reactions in combustion. Also, it emphasizes the reason why combustion is so important: it converts the energy stored in the chemical bonds of the atoms in the fuel and the oxidizer into heat, that can be utilized in a great variety of ways, and harnessed in an engine to produce work. As a reference, 1 kg of gasoline at 298 K, 100 kPa, contains roughly 43 MJ of internal energy, that, when converted in an elapsed time of 1 s, would produce 43 MW of thermal energy. This is equivalent to the consumption of the CFM56-7B27 gas turbine used in the Boeing 737-800.

In a combustion reaction, the amount of oxidizer that will react completely with the fuel is defined as the stoichiometric quantity of the oxidizer, it can be expressed in molar or mass basis. In order to exemplify the application of this concept, take a generic fuel composed by a hydrocarbon of the type $C_\alpha H_\beta$, reacting with dry air. The global reaction is represented by Equation (2.1).

$$C_\alpha H_\beta + a\left(O_2 + 3{,}76N_2\right) \rightarrow xCO_2 + \left(y/2\right)H_2O + 3{,}76aN_2 \qquad (2.1)$$

Throughout this paper, dry air will be always taken to have the composition of 20.939±0.006 % of O_2 as determined by Picard, Davis, *et al.* (2008), and other gases are represented by nitrogen.

The parameter defined as air-fuel ratio is defined as the proportion between the masses of air and fuel in the Equation (2.1). Therefore, the air-fuel ratio is:

$$\left(\frac{A}{F}\right)_{stoic} = \left(\frac{m_a}{m_f}\right) = \frac{4{,}76a}{1}\frac{MM_a}{MM_f} \qquad (2.2)$$

in Equation (2.2), the subscripts a and f denote air and fuel, m is the mass in kilograms and MM the molar mass, the parameter a is the same one

found in the Equation (2.1). By balancing the Equation (2.1), and substituting the value of a in Equation (2.2), the air-fuel ratio is determined. As the Equation (2.1) represents the global equation to complete oxidation of fuel and consumption of oxygen this air-fuel ratio is denominated stoichiometric air-fuel ratio, and this is denoted by the subscript $stoic$.

When the system presents predetermined quantities of fuel and air, a new parameter is defined in order to quantify this ratio of air and fuel in relation to the stoichiometric ratio. This parameter is the *equivalence ratio* (ϕ):

$$\phi = \frac{\left(\frac{A}{F}\right)_{stoic}}{\left(\frac{A}{F}\right)} = \frac{\left(\frac{F}{A}\right)}{\left(\frac{F}{A}\right)_{stoic}} = \frac{\left(\frac{n_f}{n_a}\frac{MM_f}{MM_a}\right)}{\left(\frac{1}{4,76a}\frac{MM_f}{MM_a}\right)} \tag{2.3}$$

where n is the number of moles. Therefore, when $\phi > 1$, the mixture in question is composed by a greater fuel-air ratio then the stoichiometric mixture would be, thus it is denominated a fuel rich mixture, or simply "rich", while a value of $\phi < 1$ represents a mixture composed by a lesser fuel-air ratio then its stoichiometric counterpart, thus it is denominated a fuel lean mixture, or simply "lean". Finally a mixture where $\phi = 1$ is denominated a stoichiometric mixture.

Besides the composition, for a chemical reaction to happen, the reagent system must be submitted to specific thermodynamic conditions of temperature and pressure that will activate the initiation reactions by overcoming the activation energy. This is explored next.

2.1.2 Explosion and flammability limits

Mixtures of hydrocarbons and oxygen react very slowly at temperatures below 200°C. As the temperature increases, a variety of oxygen-containing compounds begin to form. GLASSMAN and YETTER (2008). As the temperature is increased further, CO and H_2O begin to predominate in the products and H_2O_2 (hydrogen peroxide), CH_2O (formaldehyde), CO_2 , and other compounds begin to appear. At 300–400°C, a faint light often appears, and this light may be followed by one or more blue flames that successively traverse the reaction vessel. These light emissions are called cool flames and can be followed by an explosion.

At temperatures around 300–400°C and slightly higher, explosive reactions in hydrocarbon–air mixtures can take place. Thus, explosion limits

exist in hydrocarbon oxidation. A general representation of the explosion limits of hydrocarbons is shown in Figure 2-1.

Figure 2-1 – Explosion limits

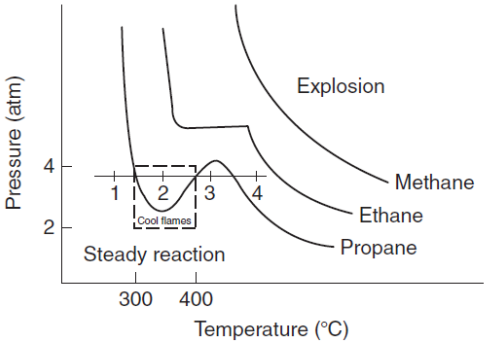

Source: GLASSMAN and YETTER (2008)

Understanding the existence and features of the explosion limits is important in this study, this problem is described as discussed by Glassman and Yetter (2008).

When the thermal conditions for point 1 exist, some oxidation reaction begins; thus, some heat must be released. If the experimental configuration is assumed to be non-adiabatic then the heat of reaction is dissipated infinitely fast and the temperature remains at its initial value. As a result steady reaction prevails and a slight pressure rise is observed. When conditions such as those at point 2 prevail, the rate of chain carrier generation exceeds the rate of chain termination; hence the reaction rate becomes progressively greater, and subsequently an explosion, or, in the context here, ignition occurs.

Generally, pressure is used as a measure of the extent of reaction, although, of course, other measures can be used as well. The sensitivity of the measuring device determines the point at which a change in initial conditions is first detected. Essentially, this change in initial conditions (pressure) is not noted until after some time interval and such interval can be related to the time required to reach degenerate branching stage or some other stage in which chain branching begins to affect overall reaction. This time interval is considered to be an induction period and to correspond to the ignition event. This induction period will vary considerably with temperature thus an increase in temperature increases the rates of the reactions leading to branching, thereby shortening the induction period. The isothermal events discussed in this paragraph essentially define chemical chain ignition.

Now if one begins at conditions similar to point 1—except that the experimental configuration is adiabatic—the reaction will self-heat until the temperature of the mixture moves the system into the explosive reaction regime. This type of event is called two-stage ignition and there are two induction periods, or ignition times, associated with it.

The first stage is associated with the time (τ_c , chemical time) to build up to the degenerate branching step or the critical concentration of radicals or other chain carriers, and the second (τ_t , thermal time) is associated with the subsequent steady reaction step and it is the time until the system reaches thermal explosion (ignition) condition. Generally, $\tau_c > \tau_t$.

If the initial thermal condition begins in the chain explosive regime, such as point 2, the induction period τ_c still exists; however, there is no requirement for self-heating, so the mixture immediately explodes. In essence, $\tau_t \rightarrow 0$.

In many practical systems, one cannot distinguish the two stages of ignition process since $\tau_c > \tau_t$; thus the time that one measures is predominantly the chemical induction period.

Sometimes point 2 will exist in the cool-flame regime. Again, the physical conditions of the non-adiabatic experiment can be such that the passage of the cool flame can raise the temperature so that the flame condition moves from a position characterized by point 1 to one characterized by point 4. This phenomenon is also called two-stage ignition. The region of point 4 is not a chain branching explosion, but a self-heating explosion. Again, an induction period τ_c is associated with the initial cool-flame stage and a subsequent time τ_t is associated with the self-heating aspect.

If the reacting system is initiated under conditions similar to point 4, pure thermal explosions develop and these explosions have thermal induction or ignition times associated with them.

It is the spark at the center of the reactor that is responsible for taking the system from a steady condition such as point 1, to a condition where thermal explosion is developed, such as point 4. This ignition form, spark ignition, is called forced ignition and there is a minimum ignition energy concept attached to its notion, which will be discussed later on.

The concept of flammability is related to the composition of the unburned gas mixture as explained by Turns (1996).

Experiments show that a flame will propagate only within a range of mixture strengths between the so-called lower and upper limits of flammability. The lower limit is the leanest mixture $\phi < 1$ that will allow steady flame propagation, while the upper limit represents the richest mixture $\phi > 1$.

Ignition can occur in mixtures above or under the flammability limits, but no flame propagation is observed. Such phenomena occurs

because the flame does not release enough heat thus the generation of chain carriers is lower than the rate of chain termination. As a result the flame cools and extinguishes.

Although flammability limits are physicochemical properties of the fuel-air mixture, experimental flammability limits are related to heat losses from the system, in addition to the mixture properties, and, hence, are generally 'apparatus dependent'. Even if conduction losses are minimal, radiation losses can account for the existence of flammability limits Turns (1996).

2.1.3 Flame and basic flame types

A flame is defined by Turns (1996), as "a self-sustaining propagation of a localized combustion zone at subsonic velocities". It is important to highlight some keywords of this definition. First, the flame must be "self-sustaining" that means, the reaction must generate sufficient heat to "pre-heat" the reactant's mixture to a point where the rate of chain carrier generation exceeds the rate of chain termination. Second, flame must be localized; that is, the flame occupies only a small portion of the combustible mixture at any instant. The third key word is subsonic. A discrete combustion wave that travels subsonically is termed a deflagration. It is also possible for combustion waves to propagate at supersonic velocities. Such a wave is called a detonation. The fundamental propagation mechanisms are different in deflagrations and detonations therefore these are distinct phenomena. Detonations are beyond the scope of this work.

At this point, this definition of flame is sufficient. Further complementation to the definition of the flame, like its modeling, regions, and velocity are discussed later on.

Flames are typically divided in two types regarding the sort of fuel and oxidizer mixing: premixed flames and nonpremixed flames. Each one of these two types are further characterized regarding the fluid motion: laminar and turbulent.

Figure 2-2 – Schematic of the classification of flame type

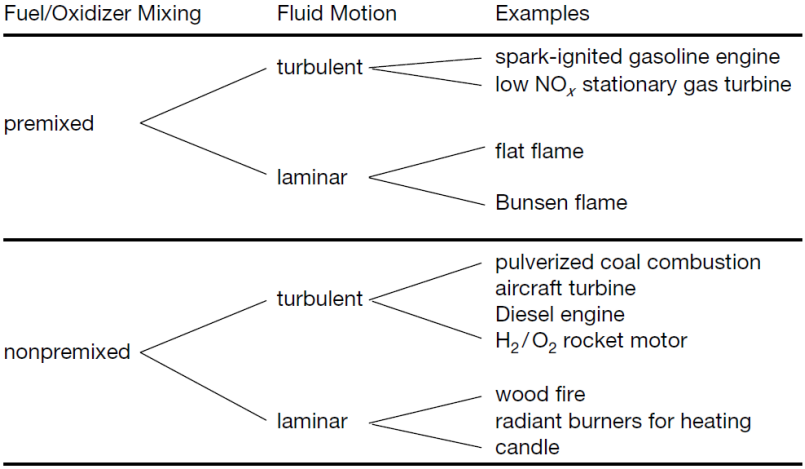

Source: WARNATZ, MAAS and DIBBLE (2006).

As described by Glassman and Yetter (2008), in nonpremixed flames the mixing rate of fuel and oxidizer is slow relative to the reaction rate thus the mixing controls the burning rate. The fuel and oxidizer come together in a reaction zone through molecular and/or turbulent diffusion. The fuel may be in the form of a gaseous jet or in condensed medium (either liquid or solid), and the oxidizer may be a flowing gas stream or the quiescent atmosphere. The distinctive characteristic of a diffusion flame is that the burning (or fuel consumption) rate is determined by the rate at which the fuel and oxidizer are brought together in proper proportions for reaction.

In a premixed flame, as the name suggests, fuel and oxidizer are mixed to a molecular level prior to the existence of the flame. If an ignition source applied locally raises the temperature substantially, or causes a high concentration of radicals to form, a flame will propagate through the gaseous mixture.

The Figure 2-2 presents a schematic of this classification, and practical examples of where each type of flame is found. Although it is difficult to observe a single type of flame in most practical machines, there is a governing regime, and in laboratory conditions these regimen are studied. For instance, in a spark-ignition engine, turbulent premixed flame is dominant but detonation can also occur. In addition, in compression-ignition engines, turbulent nonpremixed flames are dominant but premixed flames also play an important role.

This work presents a study of premixed laminar flames that are created inside a Constant Volume Reactor (CVR), and initiated by a spark.

These flames are produced and optically probed to evaluate laminar flame speed. As the flame grows, in specific cases, transition to turbulent regimen such as wrinkled or corrugated flames may occur. Such cases will be discussed in ensuing chapters.

2.1.4 Laminar flame speed and stretch rate

When a premixed gaseous fuel–oxidizer mixture within the flammability limits is contained in a long tube, with both ends opened, a combustion wave will propagate down the tube if an ignition source is applied at one end. The velocity of this wave is controlled by transport processes, mainly simultaneous heat conduction and diffusion of radicals. In this propagating combustion wave, subsequent reaction, after the ignition source is removed, is induced in the layer of gas ahead of the flame front by thermal and mass transport.

The flame velocity, or laminar flame speed, is more precisely defined by Glassman and Yetter (2008) as "the velocity at which unburned gases move through the combustion wave in the direction normal to the wave surface" in laminar flow. Therefore, if the wave propagating in the tube cited in the beginning of the section is completely planar, and do not loose heat to the walls of the tube, it will propagate at the laminar flame speed. The Figure 2-3 represents the flame front propagating at the laminar flame speed.

Figure 2-3 – Flame front propagation.

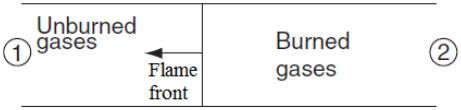

Source: GLASSMAN and YETTER (2008)

The laminar flame speed, denoted by S_L, (where S stands for "flame speed" and the subscript L for "unstretched and laminar") is a physical/chemical characteristic of reactants (fuel and equivalence ratio) and initial conditions of temperature and pressure.

In the context of the CVR, some considerations must be made. The speed in which the flame moves in the CVR experiment differs from the ideal experiment in two characteristics. First, the flame in the CVR is stretched, and second, the burned gas mixture expands in a region confined by the flame therefore 'masking' the real laminar flame speed. There are means to deal with both problems and the solution of the latter will aid in identifying some of the major characteristic of the flame and of the CVR experiment.

The CVR is a closed vessel where a spherical flame propagates radially from the center towards the walls. We exclude the initial flame development, where the flame growth is still governed by the spark, and also the moment where the flame front interacts with the wall increasing the pressure (and temperature) of the unburned gas due to adiabatic compression. These boundaries are used at all times in this work regarding laminar flame speed calculations and modeling. Furthermore, in this particular discussion, effects of flame curvature and stretching are ignored. The Figure 2-4 is a representation of the flame in the CVR's chamber.

Figure 2-4 – Representation of the flame in the CVR.

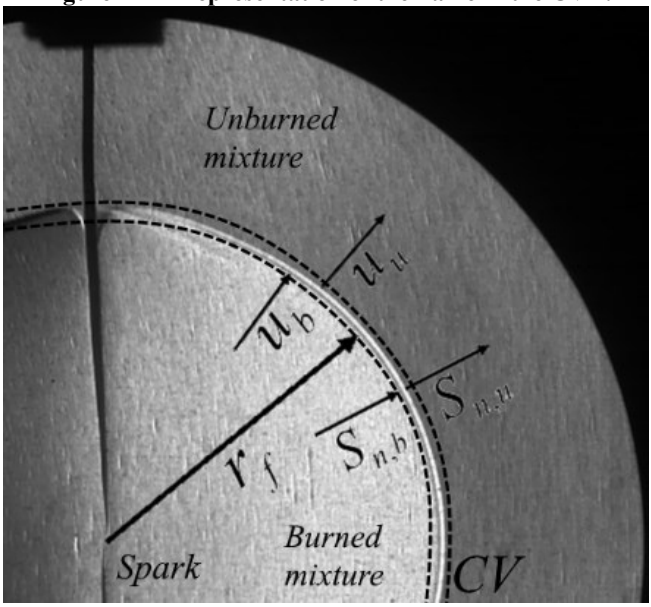

This model is presented by Peters (2000). The propagation velocity $\left(dr_f/dt\right)$, defined as the temporal variation of the radius of the spherical flame $\left(r_f\right)$, is captured by the high speed camera that records images of the flame development. The propagation velocity of the flame front results from an imbalance of the flow velocity of the mixture and the flame speed. Therefore, the propagation velocity in respect to a coordinate system fixed in the reactor is:

$$\frac{dr_f}{dt} = u_u - S_{n,u} \tag{2.4}$$

$$\frac{dr_f}{dt} = u_b - S_{n,b} \tag{2.5}$$

where u is the velocity of the mixture in respect to a coordinate system fixed in the reactor, and the subscripts u and b correspond to unburnt and burnt mixtures. The laminar flame speed is therefore the flow velocity relative to a control volume that moves with the flame front. The subscript n stands for *stretched* denoting that the flame is not planar, therefore: stretched.

In a moving reference, attached to the flame, the balance of mass flux through the flame front is:

$$\rho_u \left(u_u - \frac{dr_f}{dt} \right) = \rho_b \left(u_b - \frac{dr_f}{dt} \right) \tag{2.6}$$

where ρ is the density of the mixture. In this case of a laminar spherical flame, the flow velocity u_b of the burnt gas behind the flame front is zero, due to symmetry. Then, Equation (2.6) yields:

$$u_u = \frac{dr_f}{dt} \frac{\rho_u - \rho_b}{\rho_u} \tag{2.7}$$

Equation (2.7) states that the unburnt mixture velocity is induced by gas expansion within the flame front.

Recognizing that $u_b = 0$, in Equation (2.5):

$$\frac{dr_f}{dt} = S_{n,b} \tag{2.8}$$

which leads to the conclusion that the propagation velocity captured by the camera is equal to the stretched flame speed in relation to the burned mixture.

Working with Equations (2.4) and (2.7), it is found that:

$$S_{n,u} = S_{n,b} \left(\frac{\rho_b}{\rho_u} \right) \tag{2.9}$$

Which means that stretched flame speed in relation to the unburned mixture is equal to the stretched flame speed in relation to the burned mixture divided by the expansion factor. The expansion factor is defined by:

$$E = \frac{\rho_u}{\rho_b} \tag{2.10}$$

Note that the fact that the flame is stretched never interfered in the model, and it is possible to affirm that unstretched flame speed in relation to the unburned mixture is equal to unstretched flame speed in relation to the burned mixture divided by the expansion factor. That is:

$$S_{L,u} = \frac{S_{L,b}}{E} \tag{2.11}$$

A fundamental element of this example is that the flame is planar, if the flame is concave, convex, spherical, or in any other form, the propagation velocity is affected by stretch. The stretch rate acting on the flame is defined as:

$$\kappa = \frac{d(\ln A)}{dt} = \frac{1}{A}\frac{dA}{dt} \tag{2.12}$$

where κ is the stretch rate of the flame and A is the surface area of the flame. In the case studied in this work of a laminar spherical flame, then: $A = 4\pi r^2$ and the stretch rate is:

$$\kappa = \frac{1}{4\pi r_f^{\,2}}\frac{d(4\pi r_f^{\,2})}{dt} = \frac{2}{r_f}\frac{dr_f}{dt} \tag{2.13}$$

where r_f is the radius of the flame at a given instant of time

To obtain the unstretched flame speed in relation to the burned mixture, it is necessary to use models to correlate $S_{L,b}$, $S_{n,b}$ and the stretch rate κ. This is explored in the next sections of this work.

As the "unstretched laminar flame speed in relation to the unburned mixture" is the main subject of study of this work, the subscript u, in this specific case, may, for the sake of simplicity, be suppressed. The notation is then the one already pointed: S_L.

This concludes the section (2.1): definitions. Some further properties and physical variables that need definition are defined in the context where they are inserted.

The following section, entitled "Laminar flame speed" advances the topic, and treats about the physical and chemical structure of the flame, models for the flame speed and physical variables that govern its behavior.

2.2 LAMINAR FLAME SPEED

Initial theoretical analyses for the determination of the laminar flame speed fell into three categories: thermal theories, diffusion theories, and comprehensive theories. The historical development followed approximately the same order. Thermal theories for modeling laminar flame speeds initiate at the mass and energy conservation equations. These first models are very restrictive, and unfortunately cannot be used as a predictive tool, but they offer basic insights to understand most primary principles that govern laminar flame propagation.

Glassman and Yetter (2008) writes about the evolution of these models. Thermal theories date back to Mallard and Le Chatelier, who proposed that it is propagation of heat back through layers of gas that is the controlling, mechanism in flame propagation. Later, there were improvements in the thermal theories. Probably the most significant of these is the theory proposed by Zeldovich. The theory included the diffusion of molecules as well as heat, but did not include the diffusion of free radicals or atoms. As a result, their approach emphasized a thermal mechanism and was widely used in correlations of experimental flame velocities.

The theory was advanced further when it was postulated that the reaction mechanism can be controlled not only by heat, but also by the diffusion of certain active species such as radicals.

The theory of particle diffusion was first advanced in 1934 by Lewis and von Elbe. More recently, rate-ratio asymptotic analyses have been developed that provide formulas with greater accuracy and further clarification of the wave structure.

It is easily recognized that any exact solution of laminar flame propagation must make use of the basic equations of fluid dynamics modified to account for the liberation and conduction of heat and for changes of chemical species within the reaction zones.

To begin with, the Mallard and Le Chatelier thermal theory is explored, as it is approached by Glassman and Yetter (2008).

2.2.1 Mallard and Le Chatelier's model

To understand the analysis developed by Mallard and Le Chatelier, first it is necessary to have in mind the temperature distribution that is established in the combustion process. This distribution is presented in Figure 2-5.

Figure 2-5 - Mallard–Le Chatelier description of the temperature in a laminar flame wave.

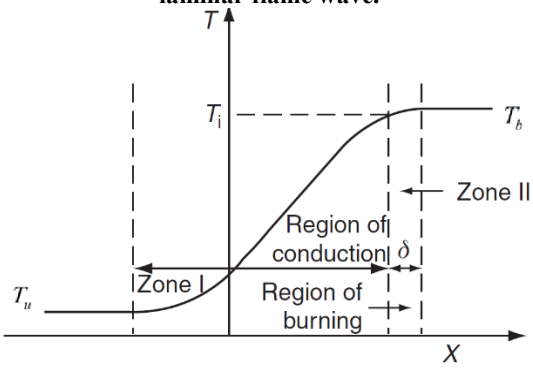

Source: GLASSMAN and YETTER (2008)

In Figure 2-5 T is temperature, and the subscripts $u, b,$ and i mean unburned mixture, burned mixture and ignition, respectively. δ is the reaction zone thickness.

Mallard and Le Chatelier stated that heat conducted from zone II is equal to that necessary to raise the unburned gases to the ignition temperature (the boundary between zones I and II). If it is assumed that the slope of the temperature curve is linear. The enthalpy balance then becomes:

$$\dot{m}c_p\left(T_i - T_u\right) = k\frac{\left(T_b - T_i\right)}{\delta}A \tag{2.14}$$

$\dot{m}$ is the mass rate of the unburned gas mixture, which is admitted to be constant, c_p is the specific heat at constant pressure, k the thermal conductivity, and A is the cross-sectional area, taken as unity.

Since the problem as described is fundamentally one-dimensional, and because the unburned gases enter normal to the wave, this velocity is by definition, the laminar flame speed. Then the mass flux in Equation (2.14) is:

$$\dot{m} = \rho_u S_L A \tag{2.15}$$

Substituting Equation (2.15) in Equation (2.14), the expression for the flame speed obtained by Mallard and Le Chatelier is found:

$$S_L = \frac{k\left(T_b - T_i\right)}{\rho_u c_p\left(T_i - T_u\right)}\frac{1}{\delta} \tag{2.16}$$

Unfortunately, in this expression δ is not known; therefore, a better representation is required. Since δ is the reaction zone thickness, it is possible to relate δ to S_L . The total rate of mass per unit area entering the reaction zone must be the mass rate of consumption in that zone for the steady flow problem being considered. This consideration yields the expression:

$$\rho_u S_L A = \dot{\omega} \delta A \tag{2.17}$$

where $\dot{\omega}$ specifies the reaction rate in terms of concentration (in grams per cubic centimeter) per unit time. Equation (2.16) for flame speed then becomes:

$$S_L = \sqrt{\frac{k(T_b - T_i)}{\rho_u c_p (T_i - T_u)} \frac{\dot{\omega}}{\rho_u}} \tag{2.18}$$

This expression indicates that laminar flame speed is proportional to the square root of the product between the thermic diffusivity and the reaction rate and to the difference of temperatures between the burned gas mixture and the ignition temperature. The burned gas mixture temperature can also be interpreted as the adiabatic flame temperature.

The Mallard and Le Chatelier model clearly shows that the mechanism that promotes the displacement of the flame is the heating of the reactants by heat conduction from the region of burning. If the adiabatic flame temperature is increased, so is the heat transfer rate, and by consequence the flame speed. Therefore, the laminar flame speed is expected to be higher for equivalence ratios near stoichiometry, where the adiabatic flame temperature is also higher.

2.2.2 Spalding's Model

A more recent model was developed by Spalding (1979) and further explored by Turns (1996). Spalding's model is restrictive, and does not provide predictive results with enough quality to be compared with experimental data. However it reveals and facilitates the understanding of factors that influence the flame speed, and it includes mass transfer, which adds more similarity to the real physics of the problem.

The model developed by Spalding begins with a set of hyphotesis:

a. Unidimensional problem; constant cross-sectional area; Steady state.
b. Kinetic and potential energy, friction, and radiation are neglected.
c. Pressure is constant

d. Mass diffusion is considered binary and modelled by Fick's Law; Heat diffusion is modelled by Fourier's Law.

e. The Lewis Number (Le) defined as:

$$Le = \frac{\alpha_T}{D} = \frac{k}{\rho c_p D} \tag{2.19}$$

is equal 1. α_T is thermal diffusivity and D is mass diffusivity.

f. The specific heat of each chemical species is equal among each other, and equal to the mixture.

g. Fuel and oxidizer react in a single step reaction forming products, following the exothermic reaction:

$$f + \nu O \rightarrow (1+\nu)P \tag{2.20}$$

where f is the fuel, O the oxidizer, P the product, and ν the mass ratio of oxidizer and fuel.

h. All fuel is consumed in the flame.

i. Temperature distribution in the flame is linear.

The control volume and boundary conditions are represented by Figure 2-6.

Figure 2-6 – Control volume and boundary conditions for the Spalding's model for flame speed

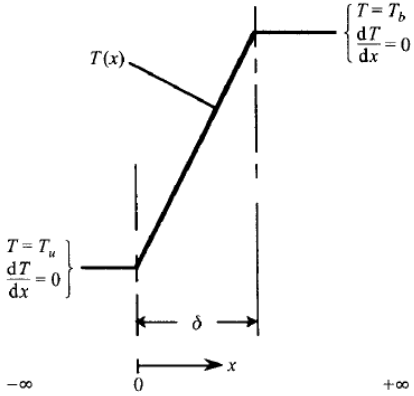

Source: TURNS (1996)

The boundary conditions are:

$$\begin{aligned} T\left(x\to-\infty\right)&=T_u\\ \frac{dT}{dx}\left(x\to-\infty\right)&=0\\ T\left(x\to+\infty\right)&=T_b\\ \frac{dT}{dx}\left(x\to+\infty\right)&=0 \end{aligned} \tag{2.21}$$

Then, the mass conservation equations for the fuel, oxidizer and product are:

$$\dot{m}''\frac{\partial Y_f}{\partial x}-\frac{\partial}{\partial x}\left(\rho D\frac{\partial Y_f}{\partial x}\right)=\dot{\omega} \tag{2.22}$$

$$\dot{m}''\frac{\partial Y_O}{\partial x}-\frac{\partial}{\partial x}\left(\rho D\frac{\partial Y_O}{\partial x}\right)=\nu\dot{\omega} \tag{2.23}$$

$$\dot{m}''\frac{\partial Y_P}{\partial x}-\frac{\partial}{\partial x}\left(\rho D\frac{\partial Y_P}{\partial x}\right)=-\left(\nu+1\right)\dot{\omega} \tag{2.24}$$

where $\dot{m}''$ is the mass flow rate per area unit, Y_f, Y_O, Y_P are the mass fractions of fuel oxidizer and products.

The energy conservation equation, where the condition of unitary Lewis number is already imposed is:

$$\dot{m}''\frac{\partial T}{\partial x}-\frac{1}{c_p}\frac{\partial}{\partial x}\left(k\frac{\partial T}{\partial x}\right)=-\frac{\dot{\omega}\Delta h_c}{c_p} \tag{2.25}$$

Δh_c is the heat of combustion of the fuel and can be represented by:

$$\Delta h_c=\left(\nu+1\right)c_p\left(T_b-T_u\right) \tag{2.26}$$

The Equation (2.15) from the Mallard-Le Chatelier's deduction is also valid here:

$$S_L=\frac{\dot{m}''}{\rho_u} \tag{2.27}$$

Using Equations (2.22), (2.23), (2.24), (2.25), (2.26), (2.27) and the boudary conditions (2.21). The solution for the laminar flame speed is determined:

$$S_L = \sqrt{-2\alpha_T (\nu+1)\frac{\bar{\dot{\omega}}}{\rho_u}} \tag{2.28}$$

$$\delta = \sqrt{\frac{-2\alpha_T \rho_u}{\bar{\dot{\omega}}(\nu+1)}} \tag{2.29}$$

$$\delta = \frac{2\alpha_T}{S_L} \tag{2.30}$$

where $\bar{\dot{\omega}}$ is the mean reaction rate, defined as:

$$\bar{\dot{\omega}} = \frac{1}{(T_b - T_u)} \int_{T_u}^{T_b} \dot{\omega} dT \tag{2.31}$$

Just as Equation (2.18), Equation (2.28) shows clearly which thermophysical and thermochemical properties influence the laminar flame speed. It is important to highlight the proportionally inverse relation between flame speed and flame thickness.

The equations presented in both models are sufficient to qualitatively predict the behavior of the flame speed in many practical cases, but they do not predict with precision enough its value, due to difficulties in calculating the reaction rate for example. Therefore, experimental analysis is extremely helpful to further understand the role that the thermodynamic properties play in the laminar flame speed. The following section is about classical experiments and results obtained with methane flames, which represents the behavior of the laminar flame speed for most hydrocarbons.

2.2.3 Governing elements of flame speed

In section 2.2.1 the influence of the equivalence ratio on the laminar flame speed was briefly discussed. Beginning with a lean mixture, the laminar flame speed increases as the amount of fuel in relation to oxidizer increases, since there is a larger amount of fuel being oxidized which increases the adiabatic flame temperature and the reaction rate. As the equivalence ratio increases so does the flame speed to a maximum value at a equivalence ratio around 1,1; this is also the point of maximum adiabatic flame temperature. Then for richer mixtures the laminar flame speed decreases.

The Figure 2-7 shows experimental data by different authors for methane at 300 K and 100 kPa plotting laminar flame speed versus equivalence ratio.

Figure 2-7 – Influence of equivalence ratio on laminar flame speed.

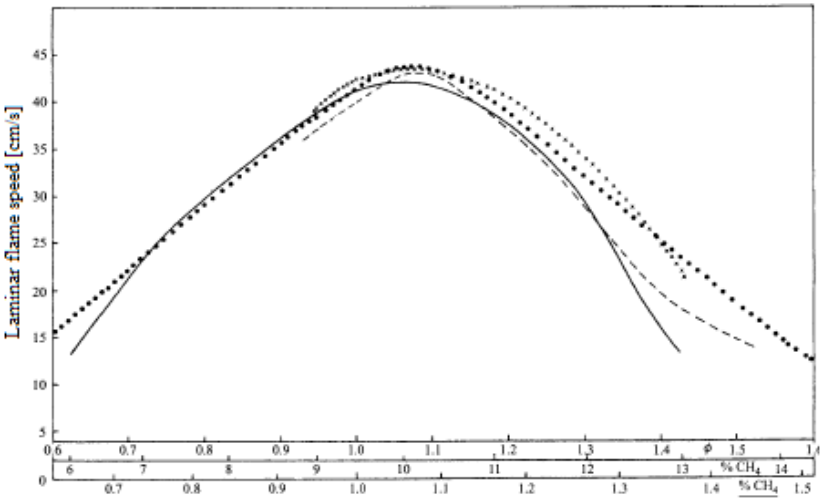

Source: TURNS (1996).

Temperature is perhaps the thermodynamic property that influences the flame speed the most. Some of the reasons were already explored, as the influence of the adiabatic flame temperature. Analyzing equation (2.31), it can be inferred that increasing the unburned gas temperature will increase the mean reaction rate, which will in turn increase the flame speed. It is also known that the temperature influences exponentially the rate of reaction, it is often modeled as presented by TURNS (1996):

$$\dot{\omega} = -k[f][O] \tag{2.32}$$

Where k is the rate coefficient, expressed by the empirical Arrhenius form:

$$k = A\exp(-E_A/R_uT) \tag{2.33}$$

therefore it is expected also an exponential form dependence between flame speed and temperature.

In Equation (2.33), A is a constant termed pre-exponential factor, E_A is the activation energy, and R_u the universal gas constant. In Equation (2.32), $[f]$ and $[O]$ are the volumetric molar concentration of fuel and oxidizer.

The expected relation between both variables is indeed observed in experiments as presented in Figure 2-8.

Figure 2-8 - Influence of unburnt mixture temperature on laminar flame speed.

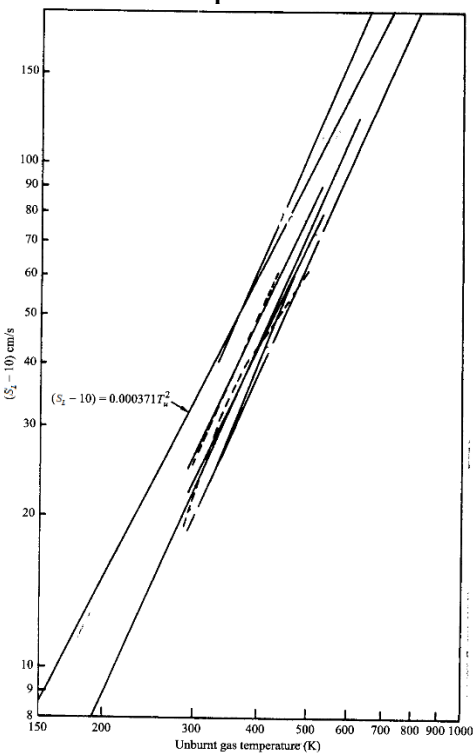

Source: TURNS (1996).

Pressure is also of great importance. As the initial pressure of the unburned gases is increased, from a fluid mechanics point of view, the momentum that the flame must overcome in order to continue propagation also increases, therefore the flame speed is expected to decrease. Also the pressure influences the density of the unburned mixture, and as it can be observed by analyzing the equations of the previous section, an increase of the unburned mixture density results in a decrease of the laminar flame speed.

Experiments developed by Bradley and Andrews (1972) with methane flames in a CVR demonstrate this negative dependence of the flame speed regarding initial pressure increase, as shown in Figure 2-9.

Figure 2-9 - Influence of unburnt mixture temperature on laminar flame speed.

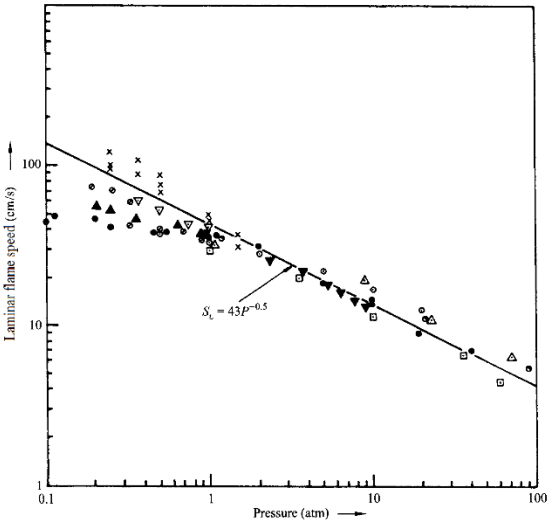

Source: TURNS (1996).

Other variables, that are relevant to this work, and affect flame development are the Lewis number of the unburned mixture and the stretch rate, discussion about this features may be found in the Appendix A .

The control of these parameters is of essential importance if the objective is to measure laminar flame speed.

It is of great interest to relate, by means of empirical formulations, the relation among these three variables and the laminar flame speed.

2.2.4 Empiric formulations for flame speed modeling

With the evolution of experiments, measurements of laminar flame speed became more precise, and more suitable to explore new conditions, at unprecedented temperatures and pressure levels, including evaluations for liquid fuels with high evaporation temperatures. A great amount of data was obtained thus enabling the proposal of empirical formulations.

Metghalchi and Keck (1980), developed a series of experiments and proposed flame speed correlations., One of their expressions, which presented a remarkable agreement with results and has wide application to this day is the Equation (2.34):

$$S_L = S_{L0}\left(\frac{T}{T_0}\right)^{\alpha}\left(\frac{P}{P_0}\right)^{\beta}\left(1-2{,}1Y_{dil}\right) \qquad (2.34)$$

where the subscript 0 refers to a reference state, usually 298 K and 1 atm. The exponents α and β are adjusted by linear regression of experimental curves, and are expressed as linear or quadratic functions of the equivalence ratio. S_{L0} is the laminar flame speed measured in the reference conditions, expressed as polynomial function of the equivalence ratio. Y_{dil} is the mass fraction of diluent in the fuel-air mixture.

Therefore, by using this expression, it is possible to calculate the laminar flame speed in any condition of temperature, pressure and equivalence ratio, as far as the experiments are valid.

A great number of researchers have published works were some form of the Equation (2.34) is used. It is worth mentioning the recent works of: BROUSTAIL, SEERSB, *et al.* (2013); BRADLEY, LAWES and MANSOUR (2009); KONNOV, MEUWISSEN and GOEY (2011); LIAO, JIANG, *et al.* (2007); MANNAA, MANSOUR, *et al.* (2015); SILEGHEM, ALEKSEEV, *et al.* (2013).

2.3 FLAME SPEED MEASUREMENTS

There are several methods to evaluate flame speed. The experimental configurations are usually divided in two groups: stationary flames and moving flames. The former group comprises experiments where, as the name suggests, the flame is stationary to a reference point, the laboratory, and in the latter group the flame moves in relation to the reference point, which is usually the ignition point.

These groups may be further divided in six experiments categories: Conical stationary flames, counter flow method, flat flame method, flames in tubes, soap bubble method, and constant volume explosion, the latter being employed in this study. The Figure 2-10 illustrates the different methods

Figure 2-10 – Categorization of flame speed measurement experiments.

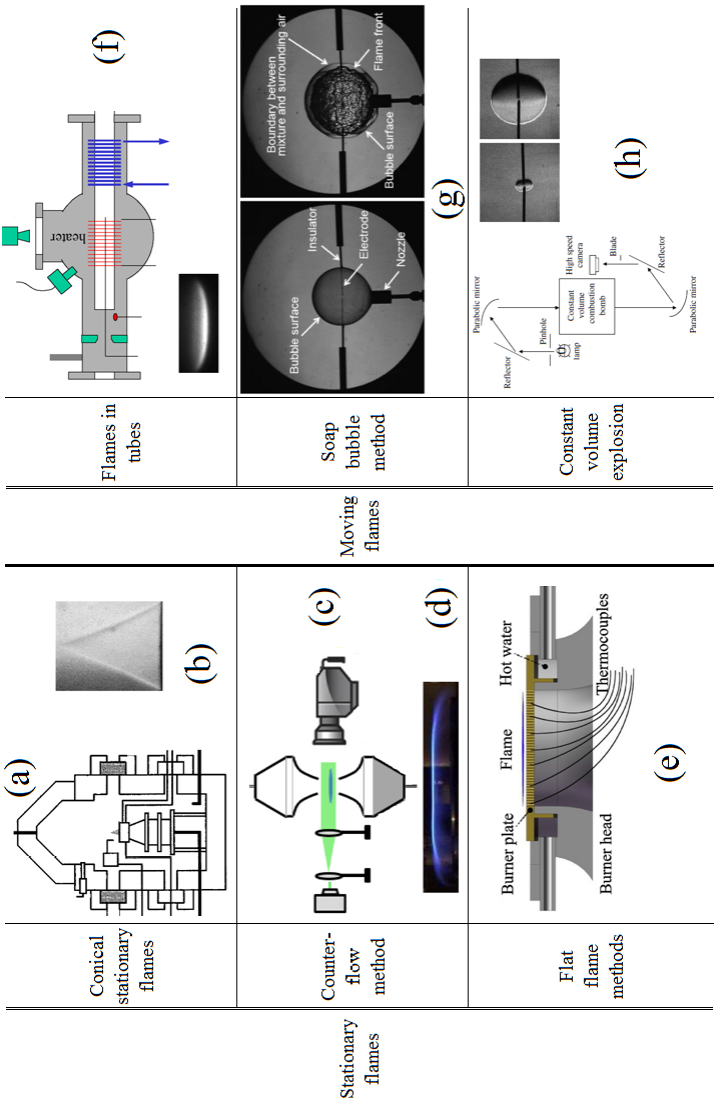

Source: (a) KOBAYASHI, TAMURA, *et al.* (1996); (b) QIN, KOBAYASHI and (2000); (c) VELOO, WANG, *et al.* (2010); (d) NIEMANN, SESHADRI and WILLIAMS (2014); (e) WANG, WENG, *et al.* (2015); (f) KIM, KATAOKA, *et al.* (2005); (g) KIM, MOGI and DOBASHI (2013); (h) LIAO, JIANG, *et al.* (2007).

In a succinct explanation, each method can be described as follows.

In conical stationary flames gas burns at the mouth of a tube, and the shape of the Bunsen cone is recorded and measured.

The counter flow method consists in stabilizing a planar flame between two nozzles, one delivering fuel-air mixture while the other provides inert gas flow, the axial flow velocities are measured and related to the laminar flame speed.

The flat flame method consists of placing either a porous metal disk or a series of small tubes at the exit of the larger flow tube, thus establishing suitable conditions for flat flames. The flame diameter is measured, and the area is divided by the volume flow rate of unburned gas, by doing so the laminar flame speed is determined. GLASSMAN and YETTER (2008).

In the flames in tubes method, a gas mixture is placed in a horizontal tube opened at one end; then the mixture is ignited at the open end of the tube. The rate of progress of the flame into the unburned gas is the flame speed.

The soap bubble method consists of a gas mixture contained in a soap bubble and ignited at the center by a spark so that a spherical flame spreads radially through the mixture. Because the gas is enclosed in a soap film, the pressure remains constant. The growth of the flame front along the radius is followed by photographic means. GLASSMAN and YETTER (2008).

In the constant volume explosion method a premixed mixture of fuel and air fills a spherical or cylindrical vessel and is ignited by a spark at the center of the vessel. The evolution of the flame front is observed as well as the pressure rise. The flame speed may be calculated through thermodynamic considerations about the pressure curve or by acquisitions of images of the flame radius evolution. The second method is used in this work.

The design of the reactor was mainly based in previous works developed by BRADLEY and HUNDY (1971), METGHALCHI and KECK (1980) and EISAZADEH-FAR (2010). The following section describes in detail these three works.

2.4 CONSTANT VOLUME REACTOR

The choice of the constant volume reactor among the several other experiments is based on the fact that the CVR is the most versatile one. It makes possible measurements of the fluid dynamics of the flame, like transition to turbulence, corrugated and wrinkled regimen. Studies of flammability limits, minimal ignition energy, critical radius for flame

propagation and detonation are also possible. Laminar flame speed may be determined by either pressure curve acquisition or optical measurements.

Detailed description of the reactor used is in the materials and methods section of this work. For further information on the literature review of the three works described in the following section, the reader may refer to the work of Hartmann (2014), the author wrote a master's dissertation on the mechanical, electrical and data acquisition design of the CVR used to perform the measurements.

2.4.1 Bradley and Hundy (1971) – Leeds University

Bradley and Hundy developed a pioneer work with laminar flame speed measurements and constant volume reactors at Leeds University in 1971. The researchers designed a cast steel cylindrical reactor with 304.8 mm in diameter and 304.8 mm in length. The reactor was equipped with two rectangular glass windows, with 158.75 mm x 107.95 mm, which allow the visualization of the reactor's interior.

Ignition was promoted by capacitor discharge through electrodes with a 0.635 mm distance. Pressure acquisition is made by a pressure sensor mounted perpendicular to the vessel's walls. The reactor was also equipped with a thermocouple and a hot wire anemometer. Oscilloscopes were used to record pressure sensor, thermocouple and anemometer data.

Flame visualization was made using reflexive plate interferometer, similar to the Schlieren method. Images were recorded using a Fastax rotating-prism high speed camera.

2.4.2 Metghalchi and Keck (1980) – MIT

In 1980 Metghalchi and Keck developed at the Massachusetts Institute of Technology a constant volume reactor for high temperatures and pressures.

The experimental apparatus consisted of a spherical reactor with inner radius of 76.2 mm, and was projected to support pressures up to 70 MPa. Ignition system used a capacitive discharge system and ordinary automotive spark plugs, where stainless steel electrodes were coupled so that the spark could be generated in the center of the reactor.

The reactor was placed inside an electric oven and could be heated up to 500 K. Both gaseous and liquid fuels could be tried. The pressure acquisition was made with a Kistler® piezoelectric pressure sensor. The time of flame arrival to the reactor walls was measured by ionization probes located in three positions over the reactor perimeter.

The Figure 2-11 shows a schematic diagram of the reactor developed by Metghalchi and Keck.

Figure 2-11 - Schematic diagram of the reactor developed by Metghalchi and Keck.

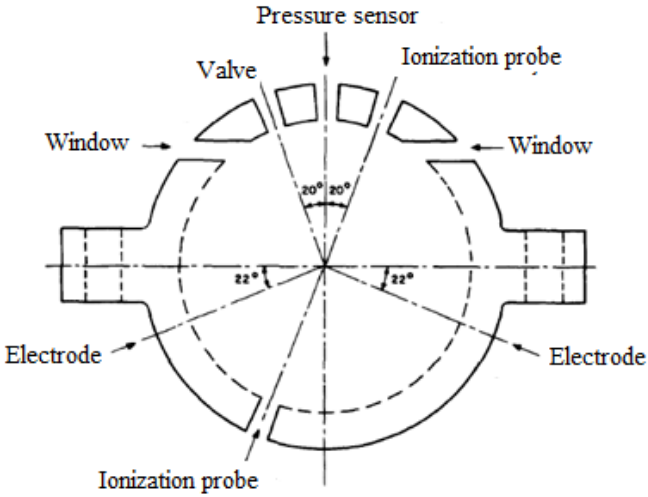

Source: METGHALCHI and KECK (1980)

2.4.3 Eisazadeh-Far (2010) - Northeastern University

The reactor developed in the Northeastern University is a square cylindrical SAE4140 steel vessel with inner diameter and length of 133.35 mm. The reactor has two silica windows, and is designed to support pressures up to 43 MPa and temperatures up to 500 K.

Visualization of the flame is made possible using the "Z-type" Schlieren, which consists of an arrangement of two spherical mirrors with a 152.4 mm diameter and a 1524 mm focal distance, a punctual light source and a high-speed camera, with a 40000 frames per second acquisition rate. The Figure 2-12 is a picture of the experimental apparatus used by Eisazadeh-Far (2010).

Figure 2-12 - Experimental apparatus used by Eisazadeh-Far (2010).

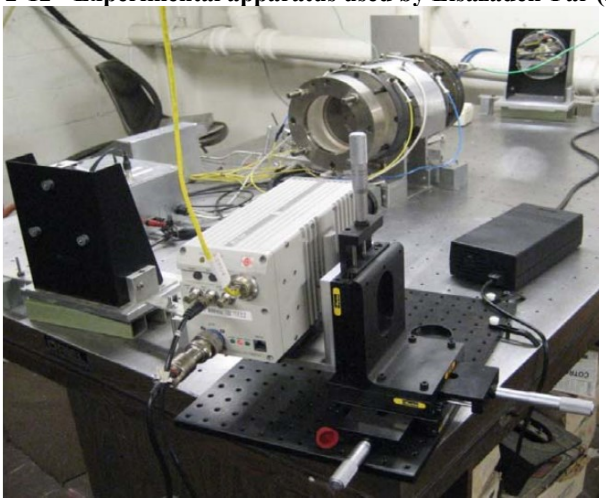

Source: EISAZADEH-FAR (2010)

The CVR in this work uses the Schlieren method to acquire flame images in a very similar arrangement of the one designed by EISAZADEH-FAR (2010). The section that follows is a report about the main features, concepts and operation of the Schlieren method.

2.4.4 The Schlieren optic method

Schlieren is a widely used method to "visualize phenomena in transparent media". SETTLES (2001). This technique makes it possible to detect the disturbances, like local variations of density, that alter light propagation through the air, or any other transparent medium.

The fundamental principle of the technique is the fact that light slows upon interacting with matter. The refractive index $n = c_0/c$ of a transparent medium indicates this change, where c is the light speed in the medium and c_0 is the speed of light in vacuum, 3.10^8 m/s.

According to Settles (2001); for air and other gases there is a simple linear relationship between the refractive index and the gas density ρ :

$$n - 1 = k\rho \tag{2.35}$$

k is the Gladstone-Dale coefficient, and is about 0,23 cm^3/g for air at standard conditions.

Settles (2001) exemplifies that air at 0°C and 1 bar pressure has n = 1.000292 when trans-illuminated by light from the Sodium-D spectral line. Helium, with n = 1.000035, is distinctly refractive upon mixing with air, despite what appears to be only a minor difference in n. Alcohol vapor, at around n = 1.0008, differs enough from air that its evaporation from an alcoholic drink is clearly visible to Schlieren and shadowgraph equipment.

The refractivity $(n-1)$ of a gas, depends upon gas composition, temperature and density, and the wavelength of illumination. The flame changes temperature, composition, pressure, velocity and density of the gas mixture, and all these changes are detected by Schlieren.

Settles (2001) summarizes the basics of the Schlieren imaging. It helps to begin as simply as possible with two lenses, geometric optics and a point light source.

Figure 2-13 – Diagram of a simple Schlieren system.

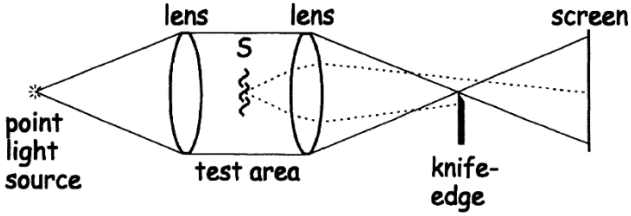

Source: SETTLES (2001).

As shown in Figure 2-13, the beam from a "point" source is collimated by a lens, and a second lens refocuses the beam to an image of a point source. From there, the beam proceeds to a viewing screen where a real inverted image of the test area is formed. At this point the optical system is merely a projector, imaging opaque objects in the test area as silhouettes on the screen. Transparent Schlieren objects are not imaged at all until a knife-edge is added at the focus of the second lens. In practice, this knife-edge is usually just an ordinary razor blade.

As the knife-edge advances toward the focal point, nothing happens until it rather suddenly blocks the image of the light source, causing the screen to go dark.

Let the knife-edge be positioned just prior to blocking the image of the source point. If we now add Schlieren object S to the test area, it bends light rays away from their original paths. Despite this, however, the second lens focuses the ray from each point in S to a corresponding point in the screen image. Two such rays are shown in Figure 2-13, one bent upward, the other downward. Both refracted rays miss the focus of the optical system. The upward-deflected ray brightens a point on the screen, but the downward-

deflected ray hits the knife-edge. Its corresponding image point is dark against a bright background. For this particular point of the Schlieren object, the phase difference causing a vertical gradient in the test area is converted to an amplitude difference, and the invisible is made visible.

Generalizing from this example of individual rays, a finite Schlieren object refracts many such rays in many directions. All downward components of these ray deflections are blocked by the knife-edge, painting at least a partial picture of the Schlieren object on the screen in shadows on a bright background. This is - in basic physical terms - the essence of the Schlieren effect.

A word about the orientation of the knife-edge: here shown horizontal, it detects only vertical components in the Schlieren object. That is, a simple knife-edge affects only those ray refractions with components perpendicular to it. Refractions parallel to the edge, move rays along it but not across it, so there is no change in cutoff or in screen illuminance. Schlieren with purely horizontal gradients remains invisible despite the presence of the knife-edge.

Settles (2001) sais that two Schlieren images are needed to completely portray a Schlieren object: one with a horizontal and one with a vertical knife-edge. In practice, a single knife-edge judiciously oriented is often good enough. To illustrate this, three actual Schlieren images of the same phenomenon with different cutoffs are shown in Figure 2-14. These images were obtained by Schlieren photographs of the turbulent flame and mixing phenomena of an oxy-acetylene torch.

Figure 2-14 – Differences of knife-edge positions and forms in Schlieren imaging: (a) Circular knife-edge; (b) Vertical knife-edge; (c) Horizontal knife-edge.

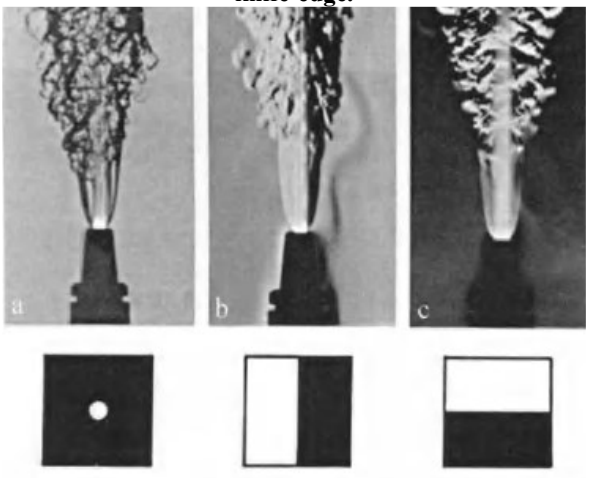

Source: SETTLES (2001).

The basic arrangement presented in Figure 2-13 is different from practical cases, there is a great variability of sets using different lenses, and also mirrors. Mirrors systems are reliable and cheap since satisfactory quality can be achieved with simpler manufacturing techniques in comparison with lenses. SETTLES (2001).

By far the most popular mirror system arrangement is the "Z-Type". SETTLES (2001). The method uses two oppositely-tilted, on-axis mirrors. The combination of a diverging illuminator beam, an opposite converging analyzer beam, and a parallel beam between the two mirrors suggests the letter z, whence the name. The Figure 2-15 is a representation of the features in the arrangement.

In Figure 2-15 the lamp represents a punctual divergent light source positioned in the focal point of the parabolic mirror 1. Since the light source is at the focal point, the divergent light rays emitted are reflected as parallel rays by the mirror. The mirror is tilted by an angle of θ_1. The now parallel light rays collide with a second parabolic mirror, also tilted θ_2, now the parallel light rays converge, the knife-edge is positioned in the focal point of the parabolic mirror. The camera that records the image is positioned behind the knife-edge.

Figure 2-15 – Representation of a typical Z-type Schlieren arrangement.

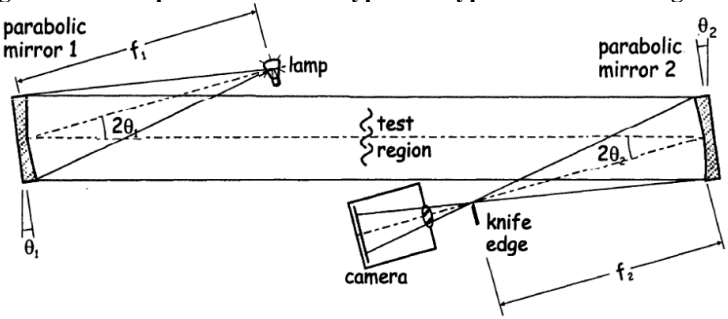

Source: SETTLES (2001).

Although the Z-type Schlieren presents some advantages, the fact that the mirrors are tilted off their optical axes generates some aberrations that must be dealt with. Settles (2001) states that there are two off-axis aberrations: coma and astigmatism. If either is allowed to get out of hand, then there results uneven Schlieren-image illuminance even when the test area is Schlieren-free.

By definition., SETTLES (2001). coma occurs when the direction of light reflected from a mirror depends on the position of the point of reflection. This is a consequence of tilting the Schlieren field mirrors off their optical axes. In result, beginning with a point light source, a comatic optical system spreads the point focus into a line. Different annular zones of the mirror-face focus at different points along this line with different spot sizes. The point focus becomes smeared into a region of flare with a bright core at one end: a "comet," whence the name. This effect is repernted in Figure 2-16.

Figure 2-16 – Coma aberration representation.

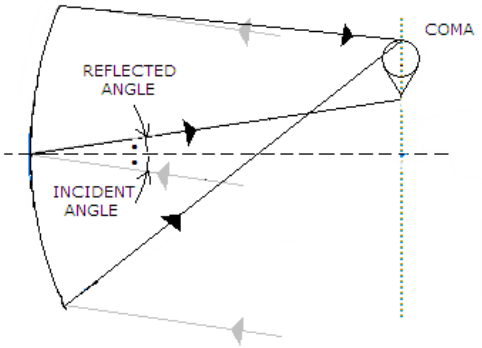

This aberration grows in proportion to the offset angle θ, for a given θ. SETTLES (2001). It is thus minimized by keeping θ small and using long-focal-length mirrors. There are other reasons to do this as well, but fortunately, since coma is generated at both Schlieren field mirrors, it is possible to cancel its overall effect by tilting the mirrors at equal angles $\left(\theta_2 = \theta_1\right)$ in opposite directions from the central optical axis, forming a "z." One must use identical mirrors, of course, and all optical elements must be centered in a common plane: the plane of the page in Figure 2-15. Therefore the z-type Schlieren arrangement is not susceptible to coma if the mirrors are perfectly and identically figured, and are arranged carefully as just described.

Unlike coma, astigmatism cannot be eliminated from the z-type Schlieren or any off-axis mirror system. The word literally means non-paint-like, or failure to focus a point to a point. It arises from differences in path length along the optical centerline and the mirror periphery. Due to finite off-axis angles θ_1 and θ_2, a point light source is imaged as two short lines at right angles to one another and spaced apart a small distance along the optical axis. Even though θ_1 and θ_2 are small and large focus mirrors are used, some astigmatism is always present thus one must endure it.

Astigmatism smears or spreads the elemental source images from various points of the test area along two short lines near the focus of the second mirror. The second of these, called the sagittal focus. Here the spreading is horizontal, i.e. in the plane of the Schlieren system. If we apply a horizontal knife-edge, then despite the smearing, all elemental source images are equally cut off. Uniform screen illuminance thus results and visible astigmatism errors are avoided. Figure 2-17 represents the astigmatism aberration.

Figure 2-17 - Astigmatism aberration representation.

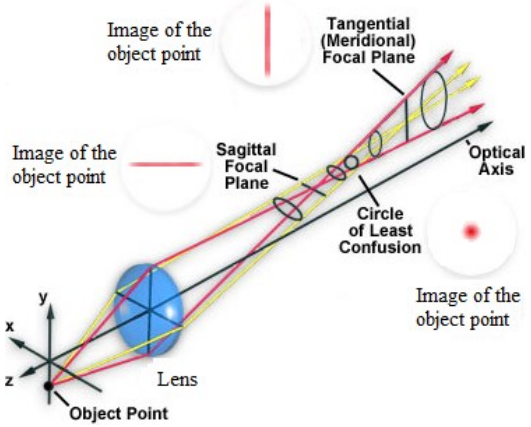

Source: adapted from NIKON (2015).

In order to avoid astigmatism in the picture above, a horizontal knife-edge should be positioned in the sagittal focal plane, and the camera lens in the circle of least confusion, between the meridional focal plane and the sagittal focal plane.

To this point in the literature review, we have covered the central definitions needed to understand the ground features of combustion. It was been explained the physics behind the phenomenon, and how to obtain data in order to measure it, the next step is: how to interpret the data captured by the experiment.

2.4.5 Optic Method

It was discussed in Section 2.1.4 that the propagation velocity captured by the camera, by means of the Schlieren method is equal to the stretched flame speed in relation to the burned mixture. Let's remind Equation (2.8):

$$\frac{dr_f}{dt} = S_{n,b} \tag{2.36}$$

To obtain the unstretched flame speed in relation to the burned mixture, it is necessary to use models to correlate $S_{L,b}$, $S_{n,b}$ and the stretch rate κ.

The methodology is divided in two models, the first considers that flame stretch correlates linearly with flame speed, the second considers this correlation to be non-linear. The linear model is more extensively used in

literature given that it was derived earlier but also because in most cases it models the experimental data with great accuracy. The second model was developed later in order to best model the cases where the first lacked accuracy, or just in order to explore if the difference between methods was representative. The advantage of the latter is its better agreement with smaller radius flames, with a larger stretch rate, but for flames with smaller stretch rate, (e.g. radius bigger than 15 mm) in most cases, the difference between methods is usually negligible.

The linear method is used in the works of: GU, HAQ, *et al.*); KELLEY, LIU, *et al.* (2011); KWON, HASSAN and FAETH (2000); LIAO, JIANG, *et al.* (2007); BRADLEY, HICKS, *et al.* (1998) and BRADLEY, LAWES and MANSOUR (2009). The non-linear method is adopted in the works of: MIAO and LIU (2014); BROUSTAIL, SEERSB, *et al.* (2013); BEECKMANN, CAI and PITSCH (2014); HALTER, TAHTOUH and MOUNAÏM-ROUSSELLE (2010) and KELLEY, JOMAAS and LAW (2009).

The linear method relates 'stretched flame speed' in relation to the burned mixture to the 'unstretched flame speed' in relation to the burned mixture and stretch rate by means of the expression:

$$S_{n,b} = L_b \kappa + S_{L,b} \tag{2.37}$$

where L_b , the inclination of the curve, is the Markstein length of the burned mixture.

The non linear method relates the same physical variables using the expression:

$$\left(\frac{S_{n,b}}{S_{L,b}}\right)^2 \ln\left(\frac{S_{n,b}}{S_{L,b}}\right)^2 = -2\frac{L_b \kappa}{S_{L,b}} \tag{2.38}$$

Once the unstretched flame speed in relation to the burned mixture is established by either method, one simply falls back to Equation (2.11):

$$S_L = \frac{S_{L,b}}{E} \tag{2.39}$$

and the unstretched flame speed in relation to the unburned mixture is determined.

Given these explanations regarding the experiments employed to measure flame speed and the optical diagnostic of such flames, one must now discuss the impact of the fuel in the measurements. In the next section a review of flame speed measurements of the fuels studied in this work is presented as well as a brief discussion about advantages and disadvantages in their utilization.

2.5 FUELS AND BIOFUELS

2.5.1 Gasoline and surrogates

The main objective of this work is to measure laminar flame speed of hydrocarbon fuels that simulate the behavior of gasoline. For conventional liquid fuels like gasoline, it is not possible to represent the complex oxidation chemistry with a chemical kinetic model. Since gasoline is a complex mixture of hundreds of hydrocarbons, and because of the varying composition , surrogate mixtures must be used in experiments and calculations.

The term surrogate refers to a simpler representation of a fully blended fuel. The simplest surrogate fuels consist of single components, e.g., the use of iso-octane as a gasoline surrogate. Binary blends of n-heptane and iso-octane, the primary reference fuels for octane ratings, also find widespread use as convenient surrogates. Ternary and larger surrogates are commonly used to investigate the effects of chemical composition on internal combustion engine (ICE) efficiency and emissions. With a suitable number of components, it is also possible to model a fuel's physical properties (for example, its distillation characteristics). PITZ, CERNANSKY, *et al.* (2007).

In order to determine the best composition for a surrogate fuel, one needs to specify and understand how the surrogate fuel will be used. Specifically, one needs to decide which combustion or fuel metric must be predicted accurately when using a surrogate fuel model. These quantities are referred to as “targets”. Example targets for surrogate fuels include fuel properties (chemical composition, C/H ratio, density, evaporation characteristics), engine characteristics (combustion phasing, bulk burn duration, emissions), and laboratory data (flow reactor concentration histories, flame speeds, ignition delays, etc.). PITZ, CERNANSKY, *et al.* (2007).

Research teams from Lawrence Livermore National Laboratory, Drexel University, Princeton University, University of Southern California, ExxonMobil Research and Engineering, National Institute of Standards and Technology and Stanford University, Pitz, Cernansky, *et al.* (2007), suggested that three hydrocarbons species are very important in compositions of gasoline surrogates: the linear alkane n-heptane, the highly branched iso-octane, given that they are the primary reference fuel components, and toluene, which is usually the most abundant aromatic in gasoline. In this work, a binary gasoline surrogate comprising iso-octane and n-heptane is investigated considering the flame speed as a target.

A great number of researchers have already studied the flame speed of n-heptane and iso-octane, for various temperatures, pressures and equivalence ratios. Table 2-1 shows a brief review of such works including

fuels, experimental method , and the conditions of temperature, pressure and equivalence ratio studied.

Table 2-1 – Literature review on n-heptane and iso-octane flame speeds measurements.

Authors	*Fuels*	*Method*	*Temperature [K]*	*Pressure [MPa]*	*φ*
GÜLDER (1984)	iso-octane; ethanol	CVR	250-600	0.1	0.75-1.4
BRADLEY, HICKS, *et al.* (1998)	iso-octane; n-heptane	CVR	358-450	0.1-1	0.8-1.3
DAVIS and LAW (1998)	iso-octane; n-heptane	Counterf low	298	0.1	0.6-1.7
HUANG, SUNG and ENG (2006)	iso-octane; n-heptane; exaust gas	Counterf low	298	0.1	0.7-1.4
SMALLBONE, LIU, *et al.* (2009)	n-heptane	Counterf low	350	0.1-0.2	0.7-1.5
VAN LIPZIG, NILSSON, *et al.* (2011)	iso-octane; n-heptane; ethanol	Heat flux	298-338	0.1	0.6-1.3
BROUSTAIL, SEERSB, *et al.* (2013)	iso-octane; ethanol; buthanol	CVR	400	0.1-10	0.8-1.4
KELLEY, LIU, *et al.* (2011)	iso-octane	Counterf low	350	0.1-1	0.8-1.6
VAREA, MODICA, *et al.* (2012)	methane; iso-octane; ethanol	CVR	298-373	0.1-0.5	0.6-1.5
SILEGHEM, ALEKSEEV, *et al.* (2013)	iso-octane; n-heptane; toluene; gasoline	Heat flux	298-358	0.1	0.7-1.3
DIRRENBERGER, GLAUDE, *et al.* (2014)	iso-octane; n-heptane; toluene; ethanol; gasoline	Heat flux	298-398	0.1	0.7-1.5

RAU, HARTL, *et al.* (2015)	iso-octane; ethanol	Heat flux	298-399	0.1	0.7-1.4

2.5.2 Biofuels

Ethanol, as already pointed out, is the most utilized biofuel in blends with gasoline in the world. The Table 2-2 shows, in volume fraction, the quatity of ethanol in gasoline sold worldwide.

Table 2-2 – Content of ethanol in gasoline worldwide. Volume fraction.

Country	*Ethanol blends*
Austria	5%, 85%
Brazil	25%, 27%, 100%
Canada	5%
Germany	5%, 10%, 85%
USA	17%, 24%, 85%
Japan	3%

Source: RAU, HARTL, *et al.* (2015).

In comparison to gasoline Pagliuso (2010) argues that short carbon chain alcohols tend to produce more power due to the following factors:

- Lower stoichiometric air–fuel ratio: due to their intramolecular oxygen content, alcohols demand less oxygen for complete combustion. This leads to lower stoichiometric air–fuel ratios when compared to gasoline, which means a higher specific energy, i.e., the amount of energy that can be generated per kg of inducted air. In the other hand, engines fueled with them tend to show higher volumetric fuel consumption.
- Higher latent heat of vaporization: alcohols have a substantially higher latent heat of vaporization than gasoline due to the hydrogen bonds of the OH group. This enables a high evaporative charge cooling that increases volumetric efficiency. Also, by reducing the initial charge temperature, the knock limit can be expanded, allowing for further improvements in power. Furthermore, the reduction of charge temperature means that less compression work is needed, again benefiting, cycle efficiency and power.
- Higher octane rating: the higher octane rating of ethanol enables higher compression ratios to be used with optimum spark advance, a fact that improves both full-load performance and efficiency.

- Higher laminar flame speed: Alcohols offer significantly higher burning velocities than non-oxygenated hydrocarbons, allowing more efficient power development due to the reduction of negative work (less ignition advance is needed for the same angle of peak pressure). This fact also gives them the ability to burn at rich mixture strengths, which coupled with their high latent heat of vaporization yields further increase in volumetric efficiency.
- Mole ratio of products to reactants: the combustion of alcohols generates a larger volume of combustion products, which allows the development of higher cylinder pressures and potentially higher power output.

Researchers have already reported flame speed measurements of ethanol, in various temperatures, pressures and equivalence ratios. Table 2-3 shows a brief review of such works including fuels, experimental methods, and the conditions of temperature, pressure and equivalence ratio studied.

Table 2-3 – Literature review on ethanol flame speeds measurements.

Authors	*Fuels*	*Method*	*Temperature [K]*	*Pressure [MPa]*	*φ*
LIAO, JIANG, *et al.* (2007)	ethanol	CVR	358-550	0.1	0.7-1.4
BRADLEY, LAWES and MANSOUR (2009)	ethanol	CVR	300-393	0.1-1.4	0.7-1.5
VELOO, WANG, *et al.* (2010)	methanol; ethanol; n-butanol	Counterf low	343	0.1	0.7-1.5
KONNOV, MEUWISSEN and GOEY (2011)	ethanol	Heat flux	298-358	0.1	0.65-1.55
VAN LIPZIG, NILSSON, *et al.* (2011)	iso-octane; n-heptane; ethanol	Heat flux	298-338	0.1	0.6-1.3
VAREA, MODICA, *et al.* (2012)	methane; iso-octane; ethanol	CVR	298-373	0.1-0.5	0.6-1.5
DIRRENBERGER, GLAUDE, *et al.* (2014)	iso-octane; n-heptane; toluene; ethanol; gasoline	Heat flux	298-373	0.1	0.7-1.5
RAU, HARTL, *et al.* (2015)	iso-octane; ethanol	Heat flux	298-399	0.1	0.7-1.4

This section concludes the literature review. Now most aspects that concerns the measurements made in this work have been discussed. In the next section the materials and methods used in the measurements are enlightened.

3 MATERIALS AND METHODS

This chapter describes the experimental apparatus in detail, and the method employed to measure flame speeds.

This description can also be found in the previous work of Hartmann (2014), where the CVR was mounted to work with gaseous fuels. Here, to experiment with liquid fuels some adaptations are made.

3.1 EXPERIMENTAL APPARATUS

The set of equipments used are distributed in six groups: (i) the constant volume reactor; (ii) filling system; (iii) evacuation system; (iv) data acquisition and sensors system; (v) ignition system; (vi) optical system.

3.1.1 Constant volume reactor

The CVR is designed to obtain images and pressure data of the combustion process. It consists of two hemispheres with clearance to fit quartz cylinders (windows), joined together to form a 150 mm radius sphere. The total volume of the CVR is calculated using 3D modelling and is 14.8 L.

The windows are quartz cylinders with 190 mm in diameter and 50 mm thickness. They are mounted one in each hemisphere, and are concentric and parallel to each other. Figure 3-1 shows an exploded view od the CVR's main componets.

Figure 3-1 – Exploded view of the CVR's main components.

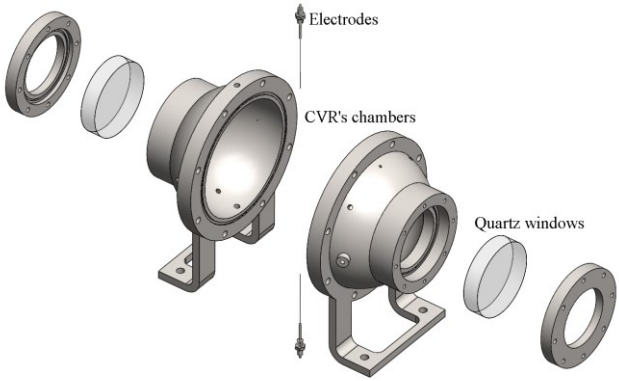

The hemispheres have holes for positioning one thermocouple, dynamic pressure sensor, injection septum, spark plugs, and filling/emptying

system. The type K thermocouple is inserted inside the CVR, the tip of the thermocouple is 75 mm from the center, to measure the unburned mixture temperature prior to ignition. The pressure sensor is located at the wall of the reactor, to measure pressure evolution during combustion. The spark plugs where adapted from common spark ignition engine plugs, a copper wire with 1 mm diameter is welded to prolong the plugs, so they meet at the center of the reactor, with a 2 mm gap, also the tips of the copper wire are machined to form a needle like ending. The injection septum is mounted in the wall of the reactor; a syringe with a 90 mm needle is used to inject fuel.

The hemispheres are joined together by 8 M14 bolts, and each quartz window is positioned by fixation flanges and 8 M12 bolts. O-rigs are used in all joins.

The CVR is also equipped with a heating system, which is composed by a copper-nickel 3 mm diameter and 20 m length wire that involves the reactor and has a maximum heating power of 900 W. Also two 250 W lamps are mounted to the windows to accelerate the heating process, totalizing 1400 W of heating power. Due to the O-rings temperature resistance, the maximum temperature inside the reactor is 135 ºC. Three thermocouples measure temperature in different points in the outer wall of the CVR, in order to provide information and control the heating system.

3.1.2 Filling system

The filling system comprises of two subsystems: the air and the fuel systems.

The air filling system is a mount of 3/8 inches stainless steel tubes, four ball valves, one needle valve, and two pressure sensors. A compression pump supplies the system with 900 kPa compressed air, depending on the initial pressure required for the test, one can choose the pressure sensor accordingly, from 1 to 200 kPa with an uncertainty of 0.2 kPa. As determined by Hartmann (2014) or form 200 to 1100 kPa. The Figure 3-2 shows a scheme of the air filling system. The ball valve and the needle valve near the air flow entrance are used to control the air pressure that fill the reactor, and the ball valve near the reactor is used to isolate the reactor from the filling system when the explosion occurs.

Figure 3-2 – Air filling system schematic.

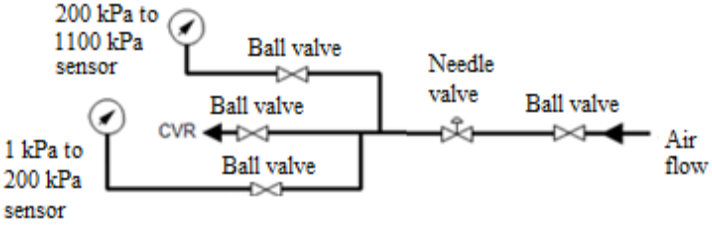

Source: Adapted from HARTMANN (2014).

To fill the reactor with the desired fuel volume, a balance and a syringe are used, a septum allows the injection of the fuel in the reactor, and isolates the reactor interior. The balance measures a maximum of 200 g with an uncertainty of ±0.0002 g. With these two systems the user can fill the reactor with the calculated values of fuel and air, to meet the specified equivalence ratio, with an acceptable uncertainty. The uncertainty calculations for the equivalence ratio can be found in the later sections.

3.1.3 Evacuation system

The evacuation system is mounted with 3/8 inches stainless steel tubes, three ball valves and a vacuum pump.

The vacuum pump can reach a minimum pressure of 0.2 mPa and a maximum flow of 6.2 m^3/h. The low pressure allows the injected fuel to evaporate inside the reactor, and provides cleaning between experiments.

The tube system is mounted to allow the gases inside the reactor to be evacuated by the vacuum pump or directly to the atmosphere. The Figure 3-3 shows a scheme of this mounting.

Figure 3-3 - Evacuation system schematic.

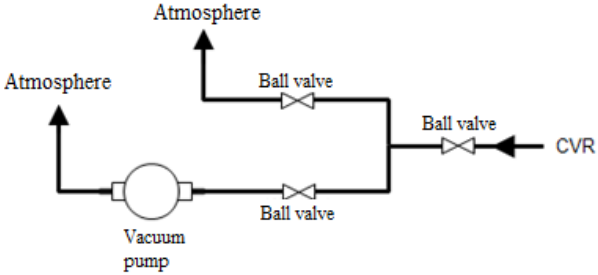

Source: Adapted from HARTMANN (2014).

3.1.4 Data acquisition and sensors system

The data obtained by the measurements made by the thermocouples and static pressure sensors is read by a *National Instruments*® data acquisition system, which communicates with a notebook through USB plug.

The data acquisition system has three modules. One with four isolated channels that acquire analogical electric potential difference, in the range ±10 V, at an acquisition rate of 1 MHz (million samples per second), 16 bits resolution, entrance impedance of 1 GΩ, and a maximum uncertainty of 0.003 V, this module is used to acquire data from the two static pressure sensors in the evacuation and filling systems, the dynamic pressure sensor, and the current sensor. The second module has 16 thermocouples channels with an acquisition rate of 75 Hz, and is used to acquire temperature data from the thermocouple inside the reactor and the three thermocouples of the heating system. The last module has 32 channels of digital input and output, with 7 μs of response time, and is used to control the ignition system.

To measure the pressure evolution inside the reactor while the combustion occurs a Kistler® piezoelectric pressure sensor model 6041BS31 is mounted to the reactor inner wall. The sensor communicates with a Kistler® charge amplifier model 5018A, which in turn communicates to the data acquisition system. This pressure information is utilized only as a complementary data to aid in the optical method, as it will be discussed later.

The four thermocouples are all type K, with a measuring range of -200 to 1200 °C.

3.1.5 Ignition system

The ignition is controlled by an electrical system developed in the previous work of Hartmann (2014). The principal features of the system are: an automotive battery of 12 ±2 V to supply power to the system, a transformer from 12 V to 220 V, a capacitor of 115 μF and an automotive coil with a 1:60 ratio. It is possible to vary the electric potential difference that charges the capacitor from 0 to 220 V thus controlling the energy that it can discharge, from 0 to 2 J. The energy deposited by the spark affects the development of the flame up to a radius of 10 mm but does not affects the flame speed if it is measured just beyond this point, as it is demonstrated by the experiments of Kelley, Jomaas and Law (2009), and also corroborated in this work, a more detailed discussion of this feature may be found in APPENDIX A. In order to minimize any of these effects and adopt a constant pattern, the energy discharged by the capacitor is set to 300 mJ in all experiments.

3.1.6 Optical system

As already pointed out the optical system adopted is a Z-type Schlieren. The system was acquired from *Edmund Optics*® and is composed by two spherical mirrors with 152.4 mm in diameter and a focal point distance of 1524 mm with λ/8 precision, a punctual light source (5 mm LED lamp), and a cutting edge.

The image acquisition is made by a IDT® high speed digital camera model Y4-S2. The acquisition rate varies according with the resolution utilized, the resolution of 256x256 pixels enables a maximal of 17700 frames per second. The rate utilized is 10000 FPS, the same rate of the pressure sensor acquisition, that facilitates the relation of the data acquired by both systems and also provides very good number of images that supports reduction of the associated uncertainties.

The Figure 3-4 shows the dimensions of the optical system, and the Figure 3-5 shows a photo of the actual optical system assembled.

Figure 3-4 - Dimensions of the optical system

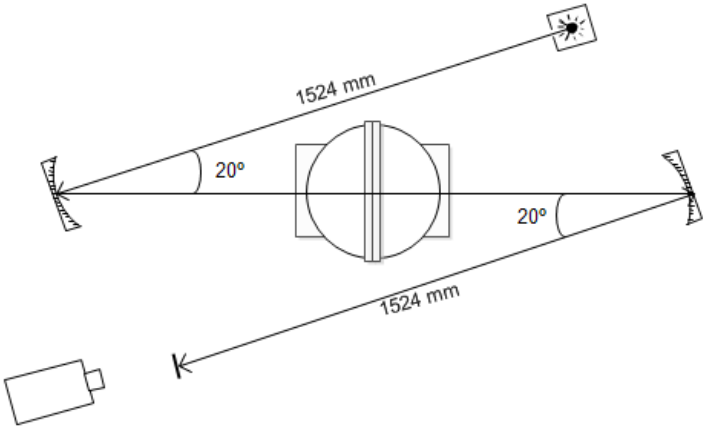

Source: Adapted from HARTMANN (2014).

Figure 3-5 – Optical system photo. 1- punctual light source; 2 and 4- spherical mirrors; 3- CVR; 5- cutting edge; 6- camera.

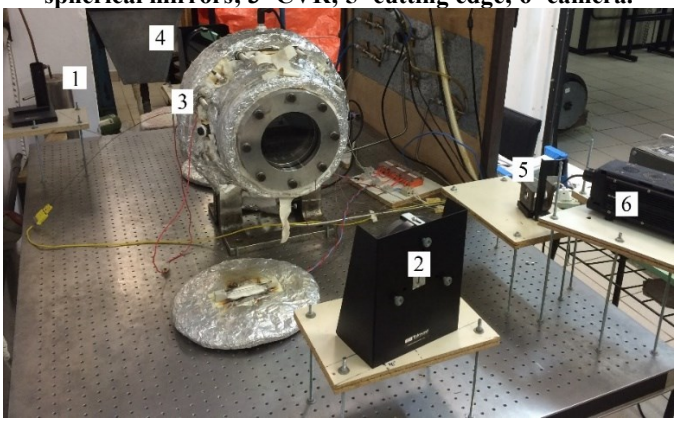

3.2 EXPERIMENTAL PROCEDURE

Each experiment must follow the same exact procedure, this is fundamental in order to diminish flaws and enhance repeatability. Figure 3-6 shows the experimental apparatus that need to be managed in each experiment.

A document listing each action the operator must do in sequence in order to perform a series of experiments follows next to the Figure 3-6.

Figure 3-6 – Experimental apparatus.

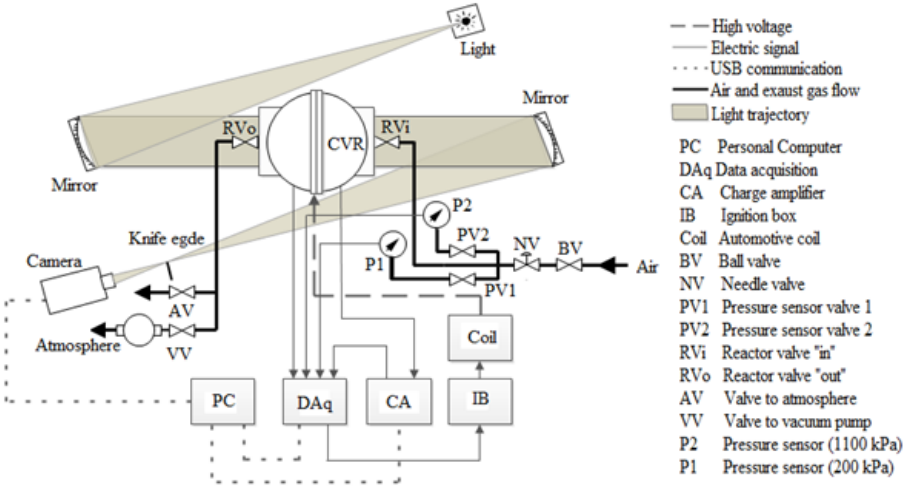

3.2.1 Step-by-step experimental procedure

The experiment procedure follows 4 procedures: initialization, filling, ignition, and emptying.

In the initialization the experimenter must set the parameters of the experiment, such as: fuel to be tested, initial temperature and pressure. In the filling procedure, the reactor is filled with the desired amount of fuel and air, at the designated temperature and pressure. In the ignition procedure, the mixture is ignited and the pressure and radius data are acquired. Finally in the emptying procedure the reactor is emptied and prepared for a new experiment.

In Appendix C a detailed step-by-step experimental procedure is presented

Any operator that follows the steps thoroughly is capable of acquiring data, in order to calculate the unstretched laminar flame speed, of the determined air-fuel mixture, at the initial conditions of equivalence ratio, pressure, and temperature.

3.3 METHOD TO CALCULATE THE LAMINAR FLAME SPEED

One of the objectives of this work is to study the dependence of the laminar flame speed regarding the equivalence ratio.

Instruments do not directly measure the equivalence ratio, contrarily from the initial pressure and temperature, it is calculated with information collected by the measurements. In the next section this calculation is explained.

3.3.1 Equivalence ratio

For every experiment there is an ideal equivalence ratio set by the experimenter. Since the equivalence ratio calculation mathod depends on the measured data of initial total pressure (unburned mixture pressure p_u), injected fuel mass, and initial temperature (unburned mixture temperature T_u). The ideal equivalence ratio is never the real equivalence ratio of the mixture in the reactor, it needs to be recalculated.

The assumptions made to determine the ideal mass of fuel and, after, the real equivalence ratio are:

1. The fuel evaporates completely.
2. All gases behave as ideal gases and are modeled by the ideal gas law equation of state.

3. The fuel composition is represented by the simplified molecular formula: $C_{N_C} H_{N_H} O_{N_O}$.

then, the mass of fuel and the mixture equivalence ratio relate trough the equation:

$$\frac{p_u MM_f V_{CVR}}{m_f R_u T_u} = \left(N_C + \frac{N_H}{4} - \frac{N_O}{2} \right) \frac{1}{x_{O_2} \phi} + 1 \qquad (3.1)$$

m_f is the mass of fuel, V_{CVR} is the CVR volume and x_{O_2} is the oxygen molar fraction in air.

First the experimenter must assign the ideal values of all variables in Equation (3.1), except for m_f, to obtain its value. After the fuel-air mixture is injected and the temperature is stabilized, the software assigns the measured values to all variables, except for ϕ, and the real value for the equivalence ratio is determined.

Data from each experiment is recorded by the "CVR.vi" program in two files, the first file, a .xls file, contains: Date and time of the experiment, fuel used, initial temperature, mass of fuel, total initial pressure, the real equivalence ratio, and finally data of pressure versus time measured by the dynamic transducer in the wall of the reactor.

The second file is a video of the flame development, recorded by the high speed camera at 10000 FPS. This file is converted by the "Video Analysis.vi" program in a .xls file. The program, also developed in the work of Hartmann (2014), recognizes the radius of the flame in each frame of the video creating the .xls file that relates flame radius versus time. Uncertainty related to this measurement is +/- 0.5 mm as determined by Hartmann (2014).

The data the .xls files, must be processed in order to calculate the flame speed of the mixture in question. The method used, subject to this work, is the optic method already discussed in the sections 2.1.4 and 2.4.5.

The next section will present some results and examples of the calculations that are made to obtain the flame speed and other physical characteristics of the flame.

3.3.2 Flame speed calculation example

The experiment exemplified here presents the initial conditions expressed in

Table 3-1

Table 3-1 – Initial parameters of example experiment.

Date:	26/03/2015
Time:	15:46:20
Fuel:	Iso-Octane
Equivalence ratio:	1.002
Initial pressure [kPa]:	100.1
Initial temperature [K]:	398.3
Full syringe [g]:	0.8471
Empty syringe [g]:	-0.0008
Injected mass [g]:	0.8479

The data of pressure and flame radius (r_f) is presented in the Figure 3-7.

Figure 3-7 – Pressure and flame radius data.

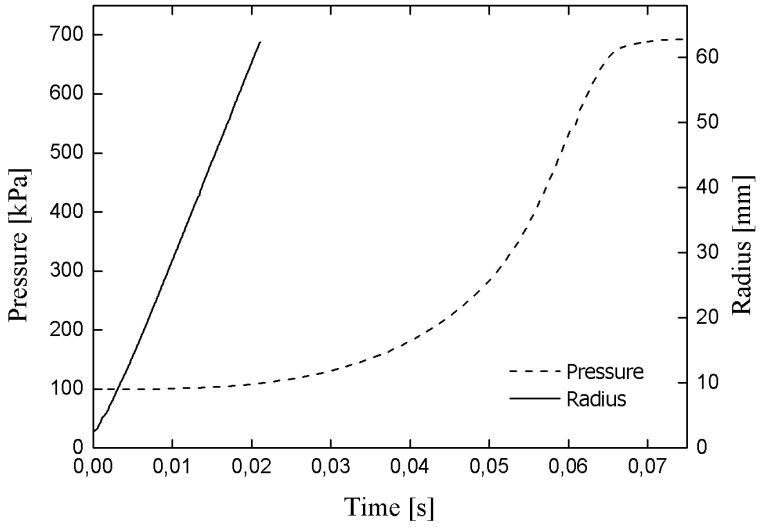

By deriving r_f in relation to time, the stretched flame speed in relation to the burned mixture $(S_{n,b})$ is determined, as it is denoted in Equation (2.8). And it is also possible to determine the stretch rate using Equation (2.13). At this point it is useful to remind Equation (2.37):

$$S_{n,b} = L_b \kappa + S_{L,b} \tag{3.2}$$

By plotting the stretch rate in the x-axis and the stretched flame speed in the y-axis, and adding a linear fit, then the inclination of the line gives the value of L_b and the intercept; the value of $S_{L,b}$.

Figure 3-8 – Stretched flame speed versus strech rate.

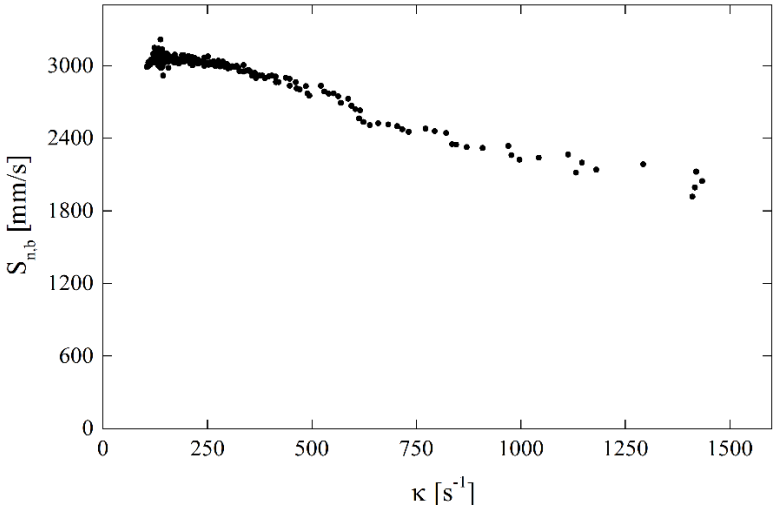

In order to perform the fitting correctly, some considerations must be made. As it is shown in the work of Kelley, Jomaas and Law (2009) and also investigated in this work, spark energy affects the flame propagation until the flame is around 10 mm in radius, for the ignition energy used. Furthermore, observing the Figure 3-7, it is possible to affirm that the pressure starts to rise when the flame is around 35 mm in radius, thus affecting the flame development.

In fact, a pattern is observed in every experiment: when the flame is 30 mm in radius the pressure in the reactor is 1 kPa (1%) above the initial pressure.

Therefore, two boundaries for the curve fitting are established: the initial radius must be above 8 mm and the final radius must be below 40 mm, then it is possible to guarantee that the radius of the flame used to determine the flame speed is unaffected by the energy of the spark or the pressure rise. Respecting these boundaries, linear regression is made.

In this example the radius range chosen for the fitting is $8 < r_f < 35$ mm, as it is shown in Figure 3-9.

Figure 3-9 – Selected data for linear regression.

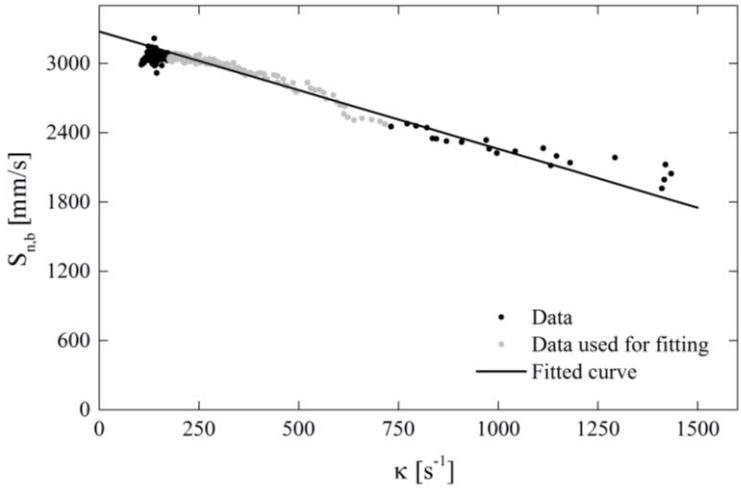

Results of the linear regression parameters are presented in Table 3-2, where u is the standard uncertainty of the parameter:

Table 3-2 – Results of the linear regression parameters.

$S_{L,b}$ [mm/s]:	3276.4
L_b [mm]:	-1.017
$u_{S_{L,b}}$:	10.81
u_{L_b} :	0.029
R^2:	0.9399
Number of points:	96

At this point the only feature left to determine the laminar flame speed is the expansion factor.

The expansion factor is calculated using the software ChemKin-PRO®. In the software, the expansion factor is calculated using the equilibrium reactor model, the model calculates the adiabatic flame temperature, radical species that might occur in the flame, as well as stable

reactants, products and its properties. The ChemKin-PRO® equilibrium reactor employs the STANJAN library of routines in it's solution method, all that is required is thermodynamic data for all species in each phase REACTION DESIGN (2008).

The thermodynamic data is the database found in the chemical kinetic mechanism developed by Mehl, Pitz, *et al.* (2011).

The results of the equilibrium calculation in this example is exposed in Table 3-3:

Table 3-3 – Results and inputs of the equilibrium calculation.

Initial temperature [K]:	398.15
Equilibrium temperature [K]:	2325.72
Initial specific volume [cm^3/g]:	1093.54
Equilibrium specific volume [cm^3/g]:	6837.03
Expansion factor:	6.25

Assuming that the burned gas mixture is at the equilibrium temperature (adiabatic flame temperature). The expansion factor is calculated simply by dividing the equilibrium specific volume by initial specific volume.

Finally, the unstretched laminar flame speed in relation to the unburned mixture is determined by dividing $S_{L,b}$ by the expansion factor. In this example the value found is: $S_L = 52.40$ cm/s.

Since all results elapse from measurements, and every measurement is subject to uncertainties, to calculate them is imperative. It is also vital to determine which measurement needs improvement in order to enhance the quality of the results. The next chapter treats about the uncertainty of the measurements and its propagation over the results.

3.3.3 Determination of uncertainties

The uncertainty of measurements affects the uncertainty of the variables calculated by these measurements, that are denominated indirectly measured variables. Albaetazzi Jr. and Sousa (2008) presents a general equation to estimate the uncertainty propagation:

$$u^2(G)=\sum_{i=1}^{n}\left(\frac{\partial f}{\partial X_i}\right)^2 u^2(X_i)+2\sum_{i=1}^{n-1}\sum_{j=i+1}^{n}\frac{\partial f}{\partial X_i}\frac{\partial f}{\partial X_j}u(X_i)u(X_j)r(X_i,X_j) \tag{3.3}$$

G is the variable to be determined by indirect measurement, $u(X)$ is the standard uncertainty of the variable X, f is the function that relates the indirect measured variable and the measured variables. $r(X_i,X_j)$ is the estimative of the correlation coefficient of the measurement of the variables X_i and X_j.

Table 3-4 shows the values and uncertainties of the variables in the example of section 3.3.2. Details about uncertainty calculation are found in the Appendix B

Table 3-4 – Variables relevant to flame speed determination and corresponding uncertainties.

Initial pressure [kPa]:	100.1±0.2
Initial temperature [K]:	398±1
Injected mass [g]:	0.8479±0.0004
$S_{L,b}$ [mm/s]:	3276±11
L_b [mm]:	-1.01±0.03
Expansion factor:	6.25±0.01
Equivalence ratio:	1.002±0.008
S_L [cm/s]:	52.4±0.9

3.4 COMPOSITION OF THE SURROGATE

Table 2-2 shows that the gasoline commercialized in Brazil has a composition of 27 % of ethanol, in the gas stations it is sold after the name of Common Gasoline, or Gasoline C. Gasoline without the addition of ethanol is referred to by the name of Gasoline A. In this work, “Gasoline A” refers to the “pure” gasoline without a addition of ethanol, and “Gasoline C” refers to the gasoline A with addition of 27% in volume of ethanol, as it is sold commercially. The terms “Surrogate A” and “Surrogate C” refer to the surrogates developed to emulate flame speed of gasoline A and gasoline C respectively.

As already pointed out, the surrogate of gasoline A (surrogate A) studied in this work is composed by two hydrocarbon species: n-heptane and iso-octane. After experiments of flame speed determination with h-heptane, iso-octane and gasoline A, the composition of surrogate A is determined using the system of equations:

$$x_{C_7H_{16}} S_{L,C_7H_{16}} + x_{C_8H_{18}} S_{L,C_8H_{18}} = S_{L,GasA} \tag{3.4}$$

$$x_{C_7H_{16}} + x_{C_8H_{18}} = 1 \tag{3.5}$$

where x is molar fraction, and the subscripts C_7H_{16}, C_8H_{18} and $GasA$, refer to n-heptane, iso-octane and gasoline A respectively.

Equations (3.4) and (3.5) are solved together, for every equivalence ratio and temperature, and an average of the results is taken as the final composition for surrogate A. This composition is found to be: 68% of iso-octane and 32% of n-heptane in molar fraction. In volume fraction this composition is: 66% iso-octane and 34% n-heptane.

Gasoline C is produced by adding 27% in volume of ethanol to gasoline A, therefore the surrogate C follows the same method, it is produced by adding 27% in volume of ethanol to surrogate A. This mixture results in a composition for surrogate C of: 30% iso-octane, 19% n-heptane and 51% of ethanol in molar fraction, or 48% iso-octane, 25% n-heptane and 27% of ethanol in volume fraction.

This concludes the section 3: Materials and Methods. In the next section, the results of the performed experiments is presented and discussed.

4 RESULTS

The images sequence produced by the video recorded by the high speed camera is the most important data acquired to calculated laminar flame speed using the method explored in this work. Figure 4-1 shows a sequence of images, for three different equivalence ratios of a n-heptane spherical flame propagating in the CVR's chamber. The first three lines correspond to the same time steps, and the last line the same radius, the columns are each equivalence ratio.

The results are categorized by fuel, in each chapter, named after the fuel. The following results are presented:

1) Flame speed versus equivalence ratio:
   a) Measurements with uncertainty bars.
   b) Comparison with other works.
   c) Fitting curves of the measured values.
2) Flame speed versus unburned mixture temperature:
   a) Measurements.
   b) Fitting curves of the measured values.
3) Temperature dependence parameter versus equivalence ratio:
   a) Measurements with uncertainty bars.
   b) Comparison with other works.
   c) Fitting curves of the measured values.
   d) Global fitting curve.
4) Deviation in percentage of the flame speed measured values from the flame speed calculated values using the global fitting curve versus normalized equivalence ratio.

Figure 4-1– Spherical flame evolution. N-heptane at T_u= 398 K.

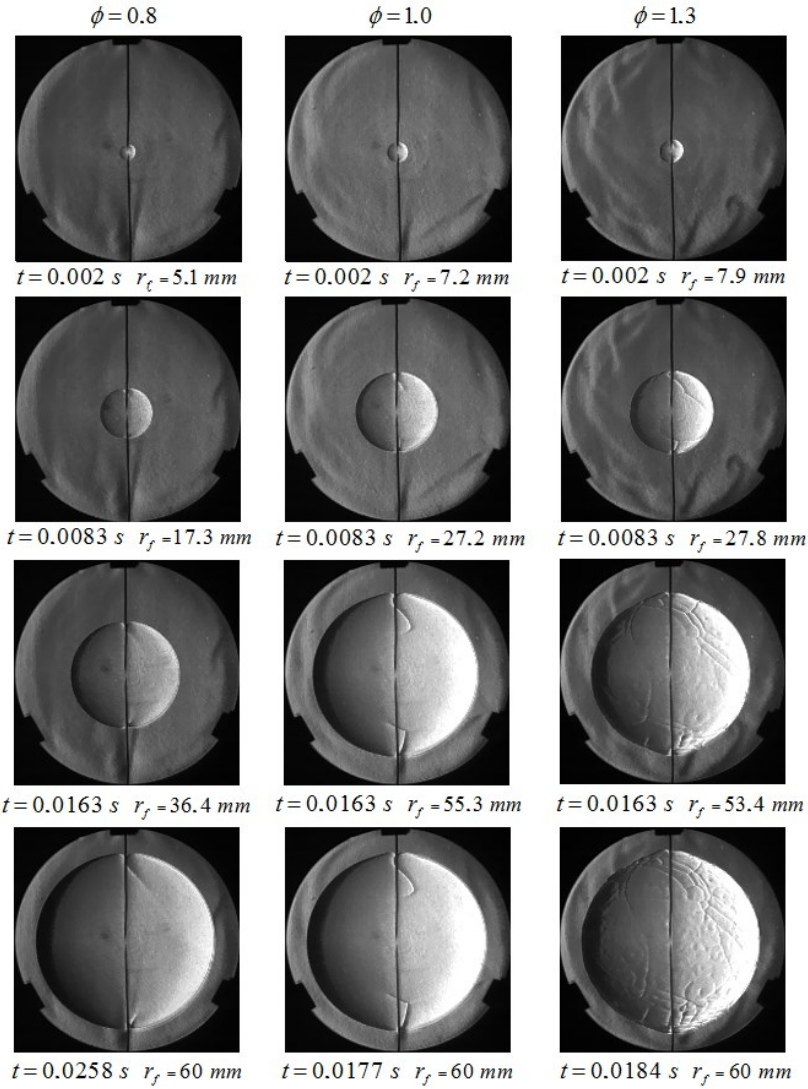

Two types of fitting curve to relate flame speed and equivalence ratio are calculated, the first; a third degree polynomial:

$$S_L(\phi) = a + b\phi + c\phi^2 + d\phi^3 \qquad (4.1)$$

The second fitting curve is the form proposed by GÜLDER (1984):

$$S_L(\phi) = \omega \phi^{\eta} \exp\left[-\xi(\phi - \sigma)^2\right] \tag{4.2}$$

The polynomial function is recommended for interpolation of the values, due to its better fitting, on the other hand, this function yields non physical values for equivalences ratios values that are not in tested range, if extrapolation of the equivalence ratio is needed it is highly recommended to use the exponential equation, due to its stability. Figure 4-2 presents a comparison of the extrapolation of both fitting curves, for the fittings data of n-heptane unburned mixture temperature of 298 K and equivalence ratio of 1 are used.

Figure 4-2 – Comparison for extrapolation of the third degree and exponential fitting curves for laminar flame speed as a function of equivalence ratio.

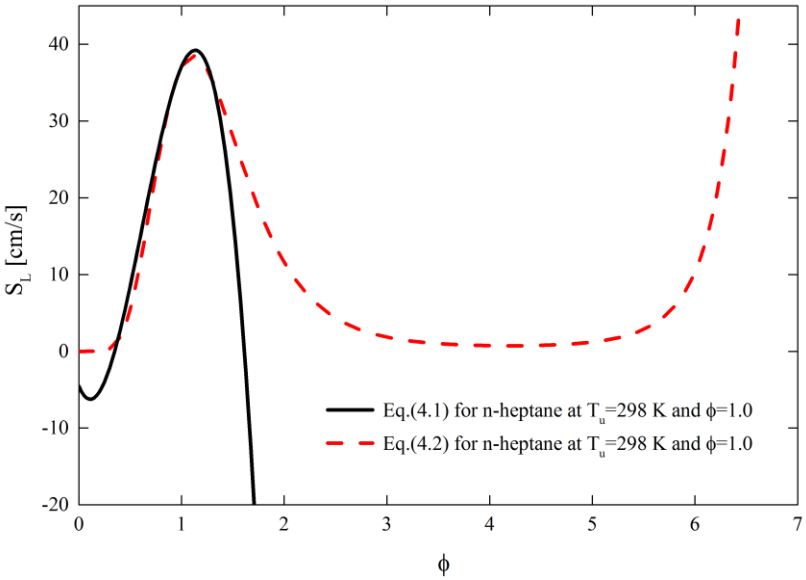

Equation (4.2) is interesting because differently from Equation (4.1), it does not produce negative values for flame speed for extrapolated lean or rich values of equivalence ratio.

The fitting curve that relates flame speed and unburned mixture is an adaption of Equation (2.34):

$$S_L\left(T_u\right) = S_{L,0}\left(\frac{T_u}{T_0}\right)^{\alpha} \tag{4.3}$$

where T_0 is the reference temperature of 398 K, and $S_{L,0}$, is the reference laminar flame speed calculated using Equation (4.1), with the equivalence ratio concerned.

The temperature dependence parameter is the α factor in Equation (4.3), its dependence with equivalence ratio is modeled by a quadratic curve:

$$\alpha(\phi) = e + f\phi + g\phi^2 \tag{4.4}$$

Finally, a global fitting curve which allows calculating laminar flame speed in any equivalence ratio and unburned mixture temperature is derived by compiling Equation (4.1), Equation (4.3) and Equation (4.4):

$$S_L\left(\phi, T_u\right) = S_{L,0}\left(\frac{T_u}{T_0}\right)^{e+f\phi+g\phi^2} \tag{4.5}$$

where $S_{L,0}$ is Equation (4.1) at the reference temperature.

For information about the method used by each author, it is recommended to recur to Table 2-1 and Table 2-3.

It fits to highlight that there is a minimum unburned mixture temperature for which it is possible to completely evaporate the fuel. The results of n-heptane at 298 K make this evident. The laminar flame speed at equivalence ratio greater than 1.3 are larger (5%) than the literature, and values do not follow the same tendency as the literature and other temperatures, this is evidence of lack of evaporation.

A second limitation is that for equivalence ratios larger than 1.4 when the flame is around 30 mm, its surface starts to wrinkle, and then it is no longer possible to affirm that it is a laminar flame. This is observed in all tested substances except for ethanol. Figure 4-3 illustrates this observation.

Figure 4-3 – Comparison of wrinkle in flames. T_u = 398 K; ϕ = 1.4 r_f = 50 mm. (a) n-hepthane; (b) gasoline A; (c) iso-octane; (d) ethanol.

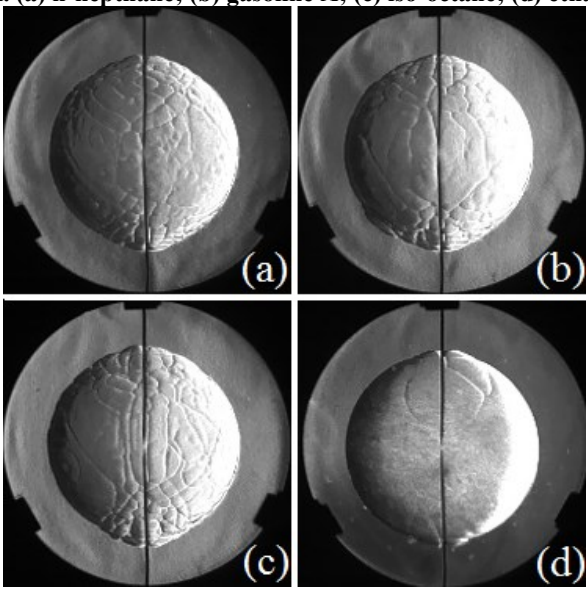

4.1 N-HEPTANE

Laminar flame speed of n-heptane is investigated in five temperature levels: 298 K, 323 K, 348 K, 373 K and 398 K are evaluated. In each temperature level, six equivalence ratio levels: 0.8; 0.9; 1.0; 1.1; 1.2 and 1.3.

Results of laminar flame speed versus equivalence ratio in each temperature level are presented in Figure 4-4; Figure 4-5; Figure 4-6; Figure 4-7 and Figure 4-8. For information about the method used by each author, it is recommended to recur to Table 2-1 and Table 2-3.

Figure 4-4 – Results of laminar flame speed of n-heptane versus equivalence ratio at 298 K.

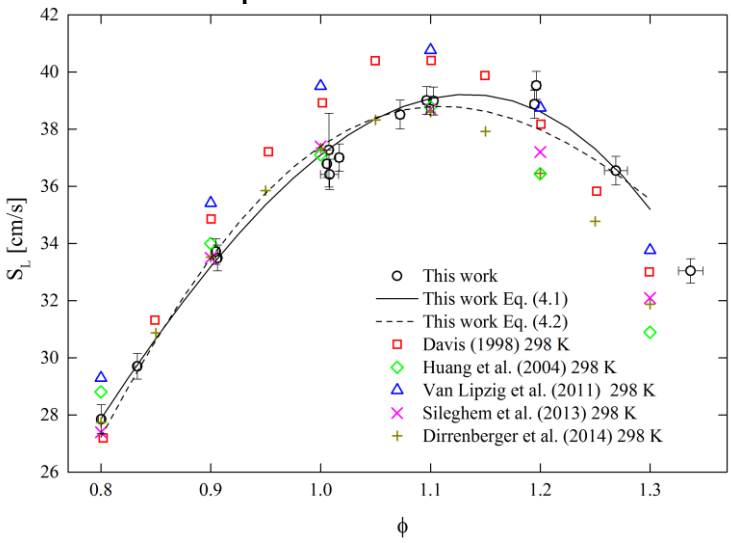

Figure 4-5 – Results of laminar flame speed of n-heptane versus equivalence ratio at 323 K.

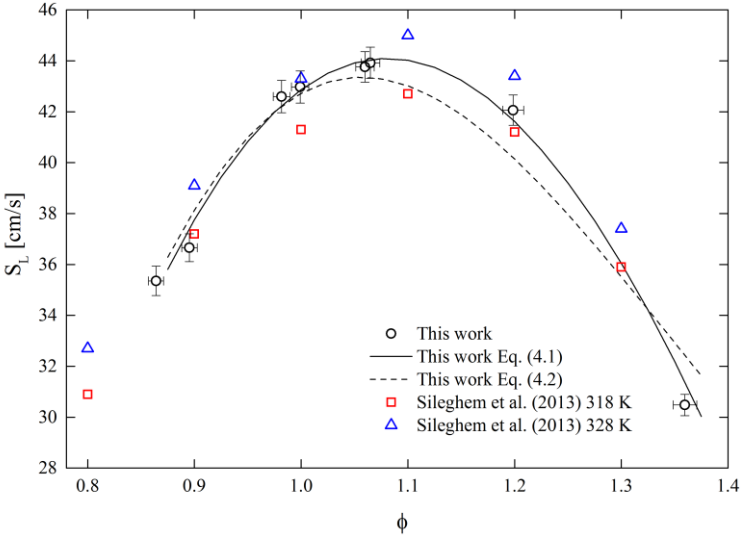

Figure 4-6– Results of laminar flame speed of n-heptane versus equivalence ratio at 348 K. Other references measured at different temperatures.

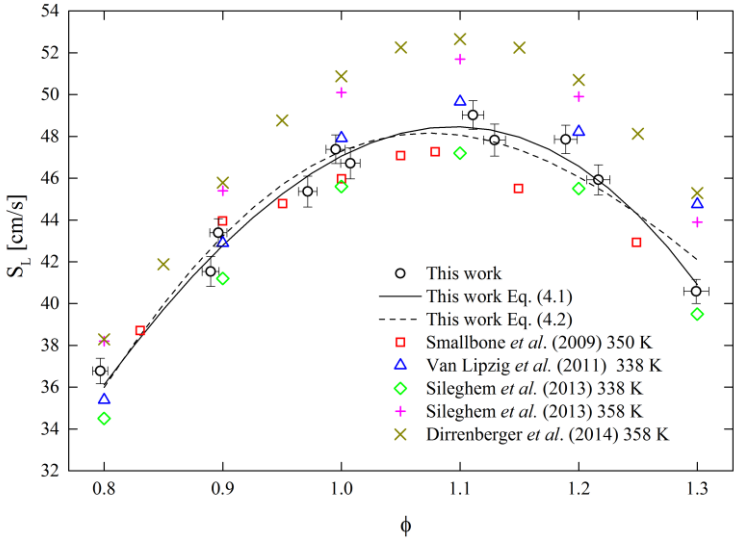

Figure 4-7– Results of laminar flame speed of n-heptane versus equivalence ratio at 373K.

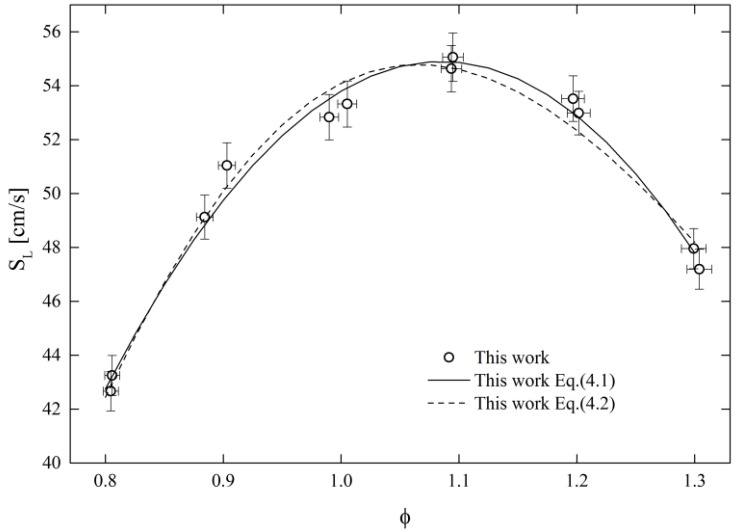

Figure 4-8– Results of laminar flame speed of n-heptane versus equivalence ratio at 398 K.

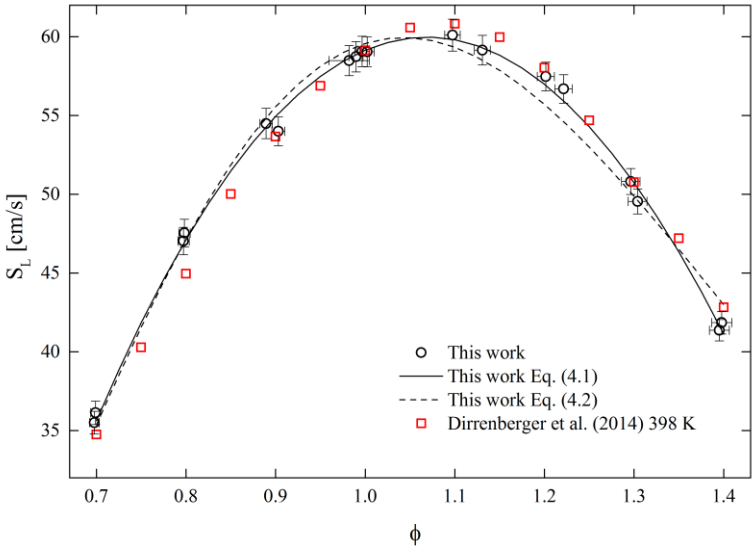

In Figure 4-4 the laminar flame speed measured for n-heptane at 298 K agrees well with the compared data, even though the large differences among the results found in the literature which for this case is at maximum 10%, all results present a similar tendency. For rich mixtures, the measured data differs form the tendency presented by the literature, that suggests lack of evaporation of the fuel. This is not observed in Figure 4-5 to 4-8, in these figures, the measured values follows the same tendency of the literature, it can be concluded that evaporation occurred without problems for the 323, 348, 373 and 398 K temperature steps. Furthermore, the values measured agreed very well for the literature found. In Figure 4-5 no other flame speed data with the same unburned mixture temperature was found, therefore the compared data at 323 K are compared with 318 K and 328 K, and the measured values are in between the compared data, where they where expected to be. In Figure 4-6 one can observe the large dispersion of experimental results (from 51 to 46 cm/s at ϕ =1), that is due to the fact that different temperatures are compared, the measured data follows the tendency and presents the expected results. For the temperature of 373 K in Figure 4-7 no other work with data at similar temperatures is found. For the last temperature step of 398 K great agreement with the literature is found, with differences at maximum 3%.

Experimental uncertainty of the literature data, when given, is of the same order of the measured data of this work.

Each point in the laminar flame speed versus equivalence ratio figures, in this section and the following sections, corresponds to a single experiment, a total of 345 experiments are presented in this work.

The parameters of Equation (4.1) and Equation (4.2) are described in Table 4-1 and Table 4-2 respectively.

Table 4-1 – Parameters of Equation (4.1) for n-heptane.

Temperature [K]	*a*	*b*	*c*	*d*
298	-4.53	-32.13	158.89	-85.12
323	-252.81	627.47	-398.57	66.79
348	-48.97	87.14	84.63	-75.75
373	-112.58	298.13	-122.80	-8.95
398	-152.59	409.35	-207.74	10.13

Table 4-2– Parameters of Equation (4.2) for n-heptane.

Temperature [K]	ω	η	ξ	σ
298	3.077E-07	9.386	-1.012	5.288
323	3.711E-08	17.257	-3.346	3.497
348	8.941E-11	8.498	-0.592	7.751
373	3.683E-06	8.878	-1.088	4.894
398	8.665E-11	8.625	-0.636	7.548

In Figure 4-4; Figure 4-5; Figure 4-6; Figure 4-7 and Figure 4-8, are also plotted the fittings of Equation (4.1) and Equation (4.2). For the cubic fittings the results were good, the R^2 parameter for Equation (4.1) is 0.98 and for the exponential fitting the R^2 parameter is 0.95 for Equation (4.2) in all five cases.

To determine the temperature dependence parameter, it is necessary to plot flame speed against unburned mixture temperature for each equivalence ratio. Figure 4-9 demonstrate this dependence for the six levels of equivalence ratio, the lines are the fitted equations using Equation (4.3), and the figures are the measured data.

Figure 4-9 – Laminar flame speed versus unburned mixture temperature.

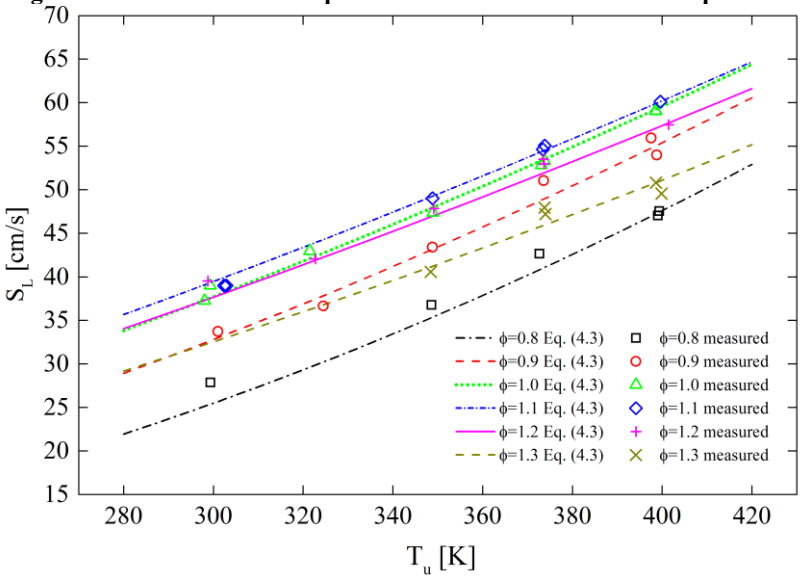

In Figure 4-9, the slope of each curve corresponds to the temperature dependence parameter for each equivalence ratio. The dispersion of the data varies for each curve significantly; for the worst case (ϕ =0.8) the adjusted R^2 is 0.88 with a standard deviation of 0,11, and the best case (ϕ =1.1) the values are 0.99 and 0.04 for adjusted R^2 and standard deviation respectively. The parameters of Equation (4.3) are presented in Table 4-3. These parameters can be substituted in Equation (4.3), then it is possible to extrapolate or interpolate for any desired value of unburned mixture temperature for a selected equivalence ratio, although extrapolation may result in values of unknown uncertainty, because there is scarce data in literature regarding comparison of this extrapolation to higher tempeartures and actual measured values.

Table 4-3 – Parameters of Equation (4.3) for n-heptane.

ϕ	$S_{L,398K}$ *[cm/s]*	α
0.8	47.1	1.777
0.9	54.9	1.752
1	59.1	1.585
1.1	59.8	1.486

1.2	56.9	1.473
1.3	50.7	1.560

The temperature dependence parameter varies with the equivalence ratio as can be inferred by Figure 4-9, this is illustrated by Figure 4-10 as well as Equation (4.4). The standard deviation of each value from the fitted curve, Equation (4.3), is plotted as an uncertainty bar.

Figure 4-10 – Temperature dependence parameter versus equivalence ratio for n-heptane.

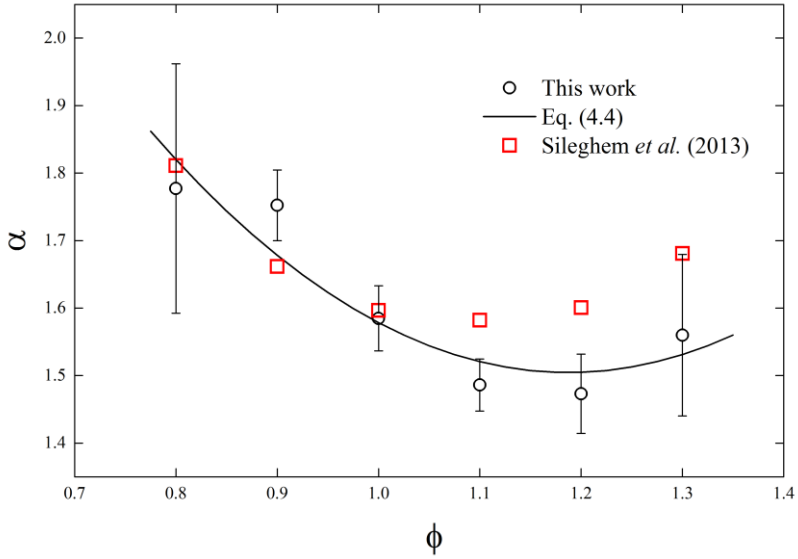

The values for the temperature dependence parameter vary over an average of 1.61. The difference form the average is of the same degree as the uncertainty of the value, therefore using the average value and assuming that the temperature dependence parameter is constant regarding the equivalence ratio may be a better solution, depending on the problem. This discussion is addressed at the end of the section.

The global fitting equation for n-heptane is:

$$S_L\left(\phi,T_u\right)=\left(-152.59+409.35\phi-207.74\phi^2+10.13\phi^3\right)\left(\frac{T_u}{398}\right)^{4.47-4.99\phi+2.10\phi^2} \quad (4.6)$$

Equation (4.6) allows calculating laminar flame speed as a function of equivalence ratio and unburned mixture temperature. Note that the third degree polynomial function (Equation (4.1)) may be substituted by Equation (4.2). The consequences of this substitution are the same already pointed out at the beginning of the section, worse representation of the interpolated data but better characterization of extrapolated data. Also the exponent of the temperature, the second degree polynomial function, is the function that models the temperature dependence parameter, it may be substituted by the average of the data, implications of this substitution are explored in the next paragraphs and in Table 4-4.

It is very important to characterize the deviation from the measured data that results from the use of Equation (4.6). Deviation in percentage of the flame speed measured values from the flame speed calculated values using the global fitting curve is illustrated by Figure 4-11.

Figure 4-11 - Deviation in percentage of the flame speed measured values from the flame speed calculated values using the global fitting curve versus normalized equivalence ratio for n-heptane.

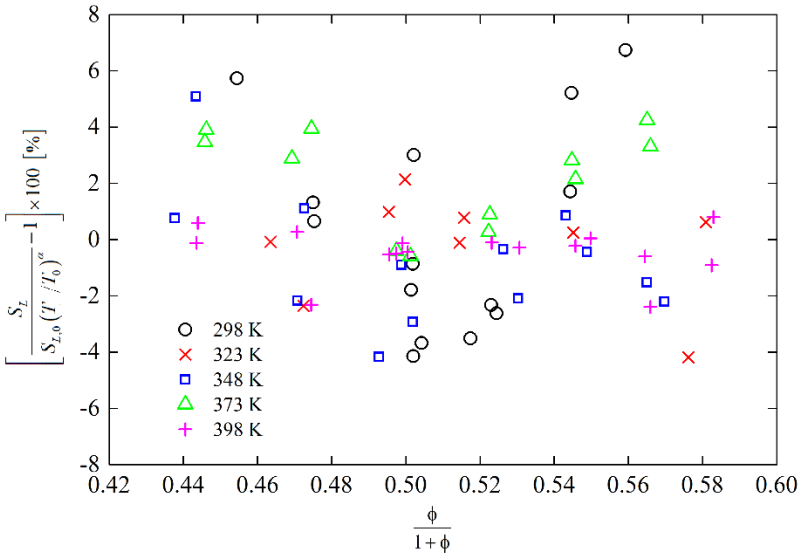

By analyzing Figure 4-11 it is possible to affirm that the use of Equation (4.6) will result in a deviation of utmost +/- 5% from the actual value for the laminar flame speed of n-heptane.

The utilization of a quadratic function for the temperature dependence parameter may result in not physically applicable values, if

extrapolation is needed. Since the values do not vary significantly, an average can be used. Table 4-4, shows the differences for utilizing the average or the quadratic function for the temperature dependence parameter. Δ is the average of the deviation in percentage of the flame speed measured values from the flame speed calculated values using the global fitting curve and quadratic equation for the temperature dependence parameter. ε is the average of the deviation in percentage of the flame speed measured values from the flame speed calculated values using the global fitting curve and average for the temperature dependence parameter. σ is the standard deviation of the values from which the averages are calculated.

Table 4-4 - Differences for utilizing the average or the quadratic function for the temperature dependence parameter.

Fuel	$\bar{\alpha}$	Δ ***[%]***	σ_{Δ} ***[%]***	ε ***[%]***	σ_{ε} ***[%]***
iso-Octane	1,66	-0,25	1,77	0,26	1,96
n-Heptane	1,61	-0,31	2,10	-0,18	2,95
Ethanol	1,57	0,10	1,60	0,12	1,72
Gasoline A	1,69	-0,01	2,06	0,17	1,74
Surrogate A	1,72	-0,07	0,68	-0,13	1,09
Gasoline C	1,89	-0,38	0,83	-0,37	0,93
Surrogate C	1,89	-0,19	0,98	-0,23	0,98

4.2 ISO-OCTANE

Laminar flame speed of iso-octane is investigated in five temperature levels: 298 K, 323 K, 348 K, 373 K and 398 K. In each temperature level, six equivalence ratio levels: 0.8; 0.9; 1.0; 1.1; 1.2 and 1.3.

Results of laminar flame speed versus equivalence ratio in each temperature level are presented in Figure 4-12; Figure 4-13; Figure 4-14; Figure 4-15 and Figure 4-16.

Figure 4-12 – Results of laminar flame speed of iso-octane versus equivalence ratio at 298 K.

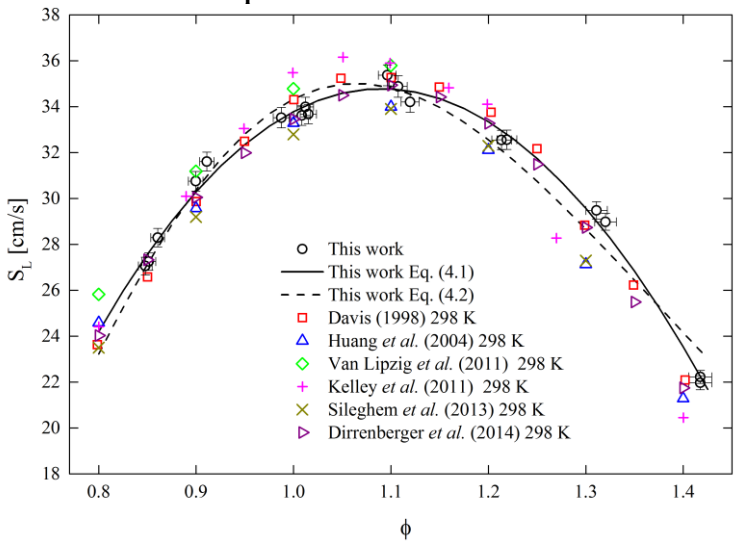

Figure 4-13 – Results of laminar flame speed of iso-octane versus equivalence ratio at 323 K.

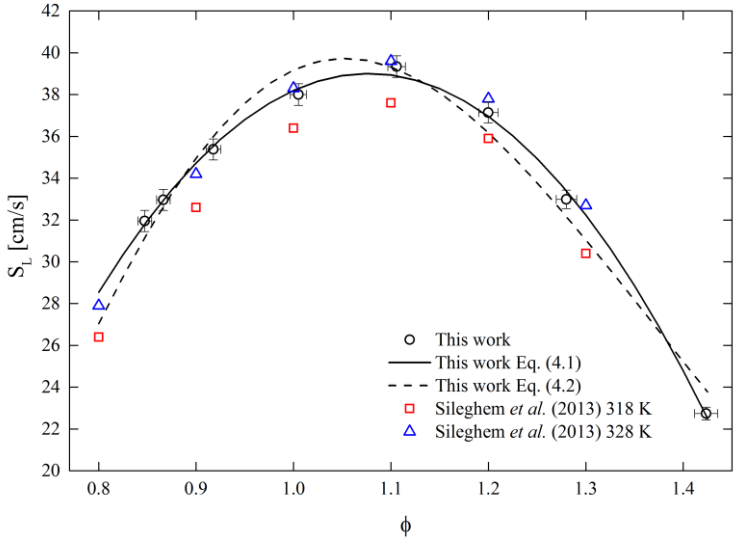

Figure 4-14– Results of laminar flame speed of iso-octane versus equivalence ratio at 348 K.

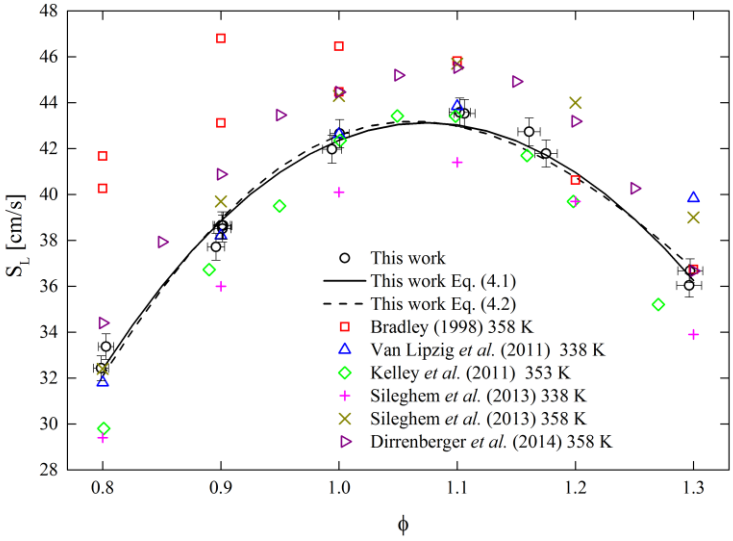

Figure 4-15– Results of laminar flame speed of iso-octane versus equivalence ratio at 373K.

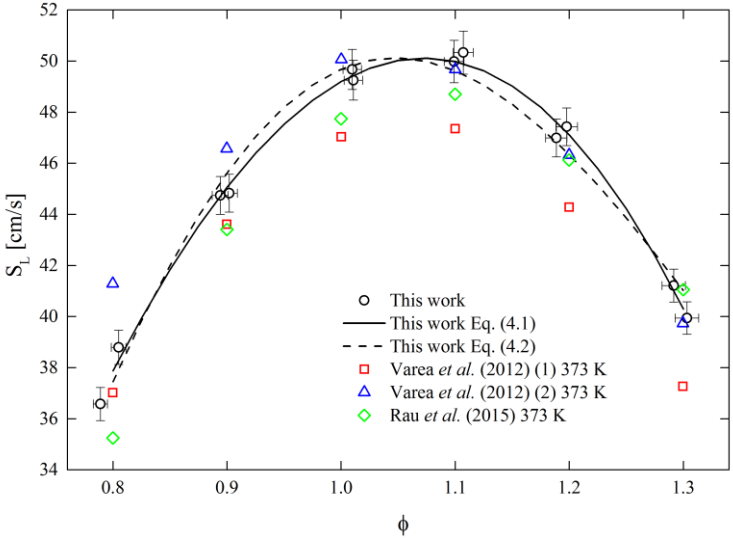

Figure 4-16– Results of laminar flame speed of iso-octane versus equivalence ratio at 398 K.

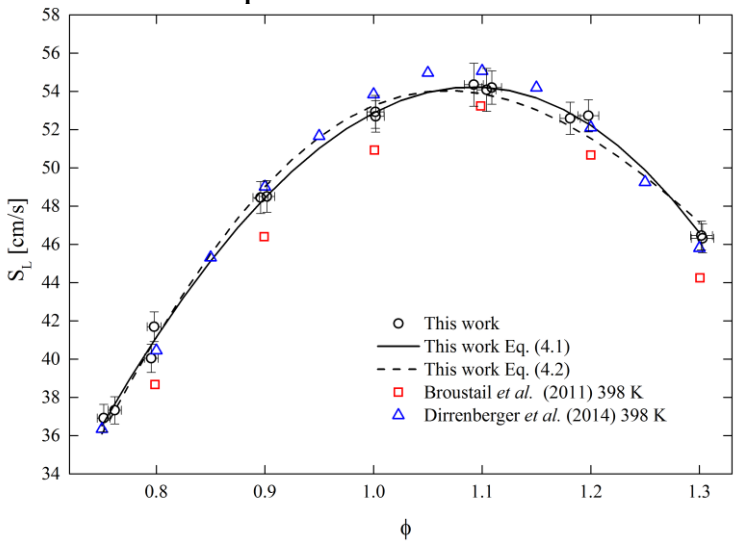

As an overall conclusion by analyzing Figure 4-12; Figure 4-13; Figure 4-14; Figure 4-15 and Figure 4-16, similarly to the results of n-heptane, this measured data of iso-octane also agrees well with the results of the literature, their variation with equivalence ratio and temperature are coherent, and this validates the results as reliable. In Figure 4-12 the calculated values fall between all compared data, the literature results spread over a narrow range, from 33 to 35 cm/s for ϕ =1, the measured value in this point is 33,8 cm/s, for the rich mixtures of ϕ >1.3, the flame speed calculated is greater than the literature's. This is possibly due to lack of evaporation, as it is not observed in higher temperatures. For the 323 K initial temperature the measured data is compared to data acquired at 318 and 328 K, and the results fall in between the literature, this is represented in Figure 4-12. The Figure 4-14 compares the measured values at 348 K with literature values at 338 K and 358 K, these data show a wider variation among the literature's results, but the values found in this work are coherent with the literature and the other temperatures measured, this conclusion extends to the data calculated at 373 K presented in Figure 4-15. In the 398 K temperature, the values agree with the literature with a difference of 4% at maximum.

The parameters of Equation (4.1) and Equation (4.2) are described in Table 4-5 and Table 4-6 respectively.

Table 4-5– Parameters of Equation (4.1) for iso-octane.

Temperature [K]	*a*	*b*	*c*	*d*
298	-127.87	314.99	-167.31	13.98
323	-118.51	291.81	-134.56	-0.55
348	-138.57	359.17	-196.21	17.98
373	-93.49	210.33	-17.68	-49.96
398	-88.73	211.26	-27.06	-42.59

Table 4-6– Parameters of Equation (4.2) for iso-octane.

Temperature [K]	ω	η	ξ	σ
298	3.32E-09	15.71	-2.47	4.06
323	9.30E-14	13.48	-1.24	6.21
348	4.86E-09	9.93	-0.98	5.84
373	1.15E-09	10.80	-1.11	5.70
398	4.85E-08	8.75	-0.83	6.01

In Figure 4-12; Figure 4-13; Figure 4-14; Figure 4-15 and Figure 4-16, are also plotted the fittings of Equation (4.1) and Equation (4.2). For all fittings the results were good, the R^2 parameter for Equation (4.1) is 0.98 and 0.95 for Equation (4.2) in all five cases.

Figure 4-17, as Figure 4-9 demonstrates the dependence between flame speed and unburned mixture temperature, for the six levels of equivalence ratio, the lines are the fitted equations using Equation (4.3) and the figures are the measured data.

Figure 4-17 – Laminar flame speed versus unburned mixture temperature for iso-octane.

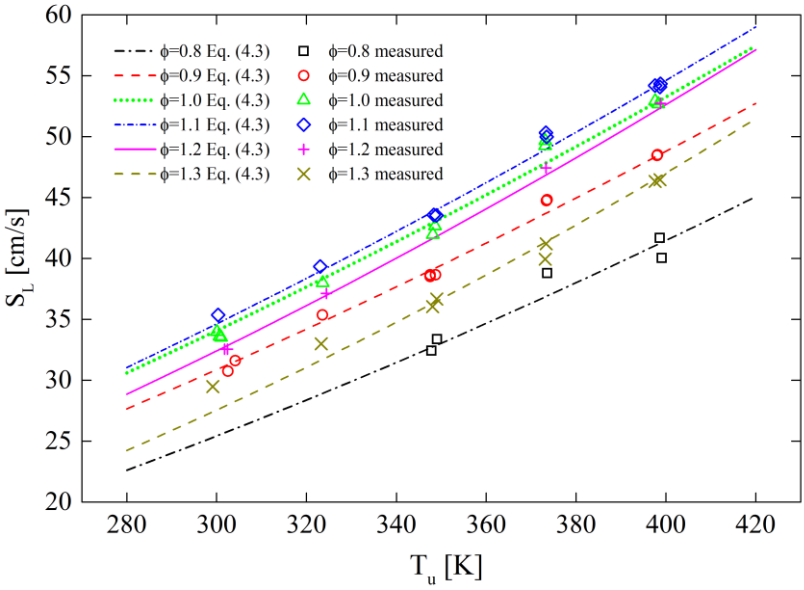

In Figure 4-17, the conclusions are similar to the n-heptane case, the slope of each curve corresponds to the temperature dependence parameter for each equivalence ratio. The dispersion of the data varies for each curve significantly; for the worst case (ϕ =0.8) the adjusted R^2 is 0.92 with a standard deviation of 0,08, and the best case (ϕ =1.2) the values are 0.99 and 0.04 for adjusted R^2 and standard deviation respectively. The parameters of Equation (4.3) are presented in Table 4-7. As it was previously highlighted, these parameters can be substituted in Equation (4.3), then it is possible to extrapolate or interpolate for any desired value of unburned mixture temperature for a selected equivalence ratio.

Table 4-7 – Parameters of Equation (4.3) for iso-octane.

ϕ	$S_{L,398K}$ *[cm/s]*	α
0.8	41.2	1.717
0.9	48.4	1.565
1	52.9	1.547
1.1	54.2	1.599
1.2	52.2	1.698
1.3	46.6	1.845

The temperature dependence parameter varies with the equivalence ratio as can be inferred by Figure 4-17, this is illustrated by Figure 4-18 as well as Equation (4.4). The standard deviation of each value from the fitted curve, Equation (4.3), is plotted as an uncertainty bar.

Figure 4-18 – Temperature dependence parameter versus equivalence ratio for iso-octane.

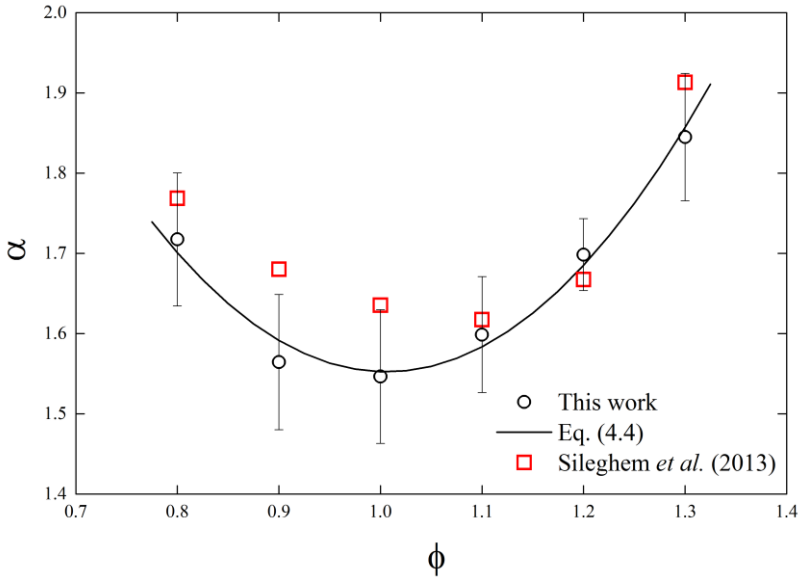

The values for the dependence parameter vary over an average of 1.66. The difference form the average is of the same degree as the uncertainty of the value as in the case of n-heptane, therefore using the average value and assume that the temperature dependence parameter it constant regarding the equivalence ratio may be a better solution, depending on the problem.

The global fitting equation for iso-octane is:

$$S_L(\phi, T_u) = \left(-88.73 + 211.26\phi - 27.06\phi^2 - 42.59\phi^3\right)\left(\frac{T_u}{398}\right)^{5.11-7.07\phi+3.51\phi^2} \quad (4.7)$$

Equation (4.7) be changed as described in the n-heptane case, the exponential equation may be used in place of the third degree polynomial function and the average of the temperature dependence parameter may

substitute the second degree polynomial function. The consequences of these are the same as in the n-heptane case.

Deviation in percentage of the flame speed measured values from the flame speed calculated values using the global fitting curve is illustrated by Figure 4-19.

Figure 4-19 - Deviation in percentage of the flame speed measured values from the flame speed calculated values using the global fitting curve versus normalized equivalence ratio for iso-octane.

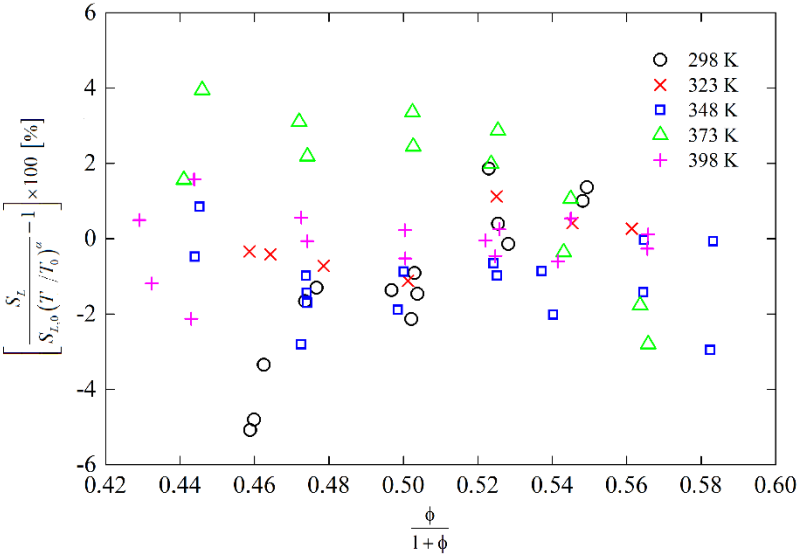

By analyzing Figure 4-19 it is possible to affirm that the use of Equation (4.6) will result in a deviation of utmost +/- 4% from the actual value for the laminar flame speed of iso-octane.

4.3 ETHANOL

Laminar flame speed of ethanol is investigated in three temperature levels: 348 K, 373 K and 398 K. In each temperature level, six equivalence ratio levels: 0.8; 0.9; 1.0; 1.1; 1.2 and 1.3.

Results of laminar flame speed versus equivalence ratio in each temperature level are presented in Figure 4-20; Figure 4-21, and Figure 4-22.

Figure 4-20– Results of laminar flame speed of ethanol versus equivalence ratio at 348 K.

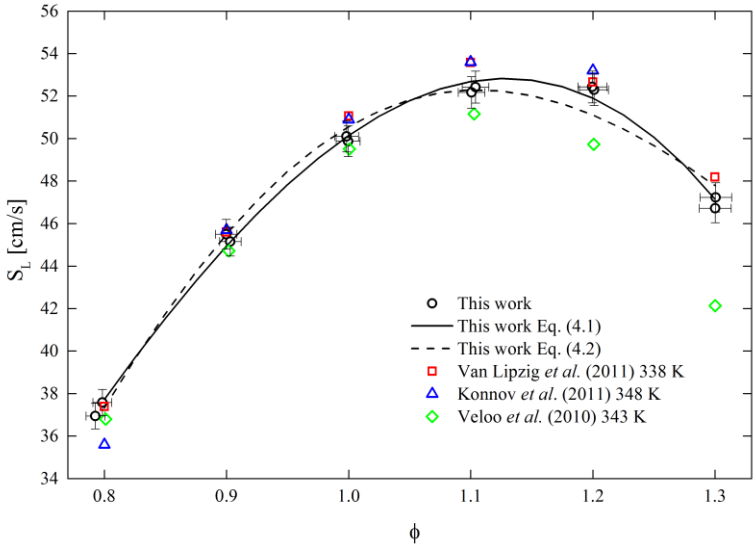

Figure 4-21– Results of laminar flame speed of ethanol versus equivalence ratio at 373K.

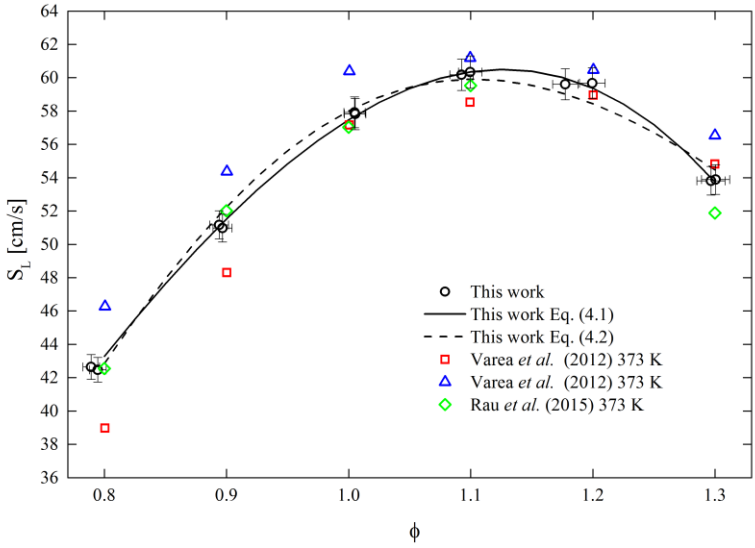

Figure 4-22– Results of laminar flame speed of ethanol versus equivalence ratio at 398 K.

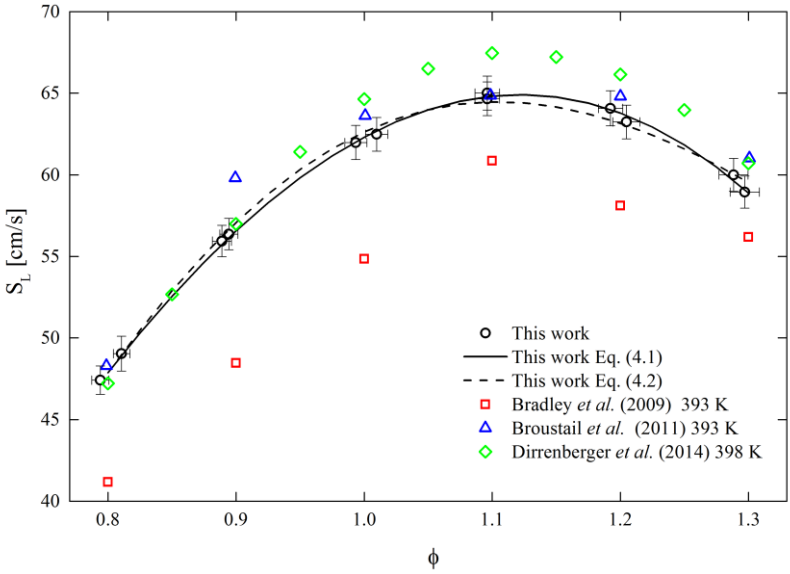

For ethanol only three temperatures steps are probed, this is due to evaporation difficulties at lower temperatures. The conclusion of the results presented in Figure 4-20; Figure 4-21, and

Figure 4-22, is the same for the n-heptane and iso-octane cases, the agreement with the literature data is good, the difference is at average 3 %, which is smaller than the difference among the literature values, that in some cases are as high as 7 %. All cases follow the same tendency in the variation of flame speed with temperature, and these results validate the values as reliable.

The parameters of Equation (4.1) and Equation (4.2) are described in Table 4-8 and Table 4-9 respectively.

Table 4-8– Parameters of Equation (4.1) for ethanol.

Temperature [K]	*a*	*b*	*c*	*d*
348	-13.77	-21.06	194.07	-109.09
373	-11.44	-37.86	237.05	-130.28
398	-90.10	211.55	-7.70	-51.44

Table 4-9– Parameters of Equation (4.2) for ethanol.

Temperature [K]	ω	η	ξ	σ
348	1.76E-07	8.86	-0.86	5.75
373	5.93E-08	8.82	-0.81	6.07
398	1.12E-05	8.22	-0.94	5.07

In Figure 4-20; Figure 4-21, and

Figure 4-22, are also plotted the fittings of Equation (4.1) and Equation (4.2). For all fittings the results were good, the R^2 parameter for Equation (4.1) is 0.98 and 0.95 for Equation (4.2) in all three cases.

Figure 4-23 demonstrate the dependence between flame speed and unburned mixture temperature, for six levels of equivalence ratio, the lines are the fitted equations using Equation (4.3) and the figures are the measured data.

Figure 4-23 – Laminar flame speed versus unburned mixture temperature for ethanol.

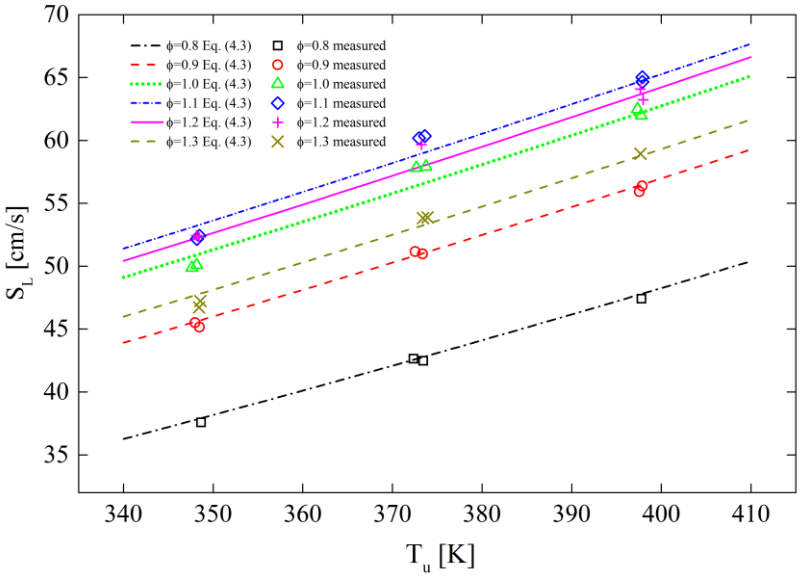

In Figure 4-23 the dispersion of the data varies for each curve significantly; for the worst case (ϕ =1.2) the adjusted R^2 is 0.95 with a standard deviation of 0,13, and the best case (ϕ =0.8) the values are 0.99 and

0.06 for adjusted R^2 and standard deviation respectively. The parameters of Equation (4.3) are presented in Table 4-10.

Table 4-10 – Parameters of Equation (4.3) for ethanol.

ϕ	$S_{L,398K}$ *[cm/s]*	α
0.8	47.9	1.724
0.9	56.6	1.650
1	62.3	1.534
1.1	64.8	1.445
1.2	63.8	1.439
1.3	58.9	1.600

The temperature dependence parameter varies with the equivalence ratio as can be inferred by Figure 4-23, this is illustrated by Figure 4-24 as well as Equation (4.4). The standard deviation of each value from the fitted curve, Equation (4.3), is plotted as an uncertainty bar.

Figure 4-24 – Temperature dependence parameter versus equivalence ratio for ethanol.

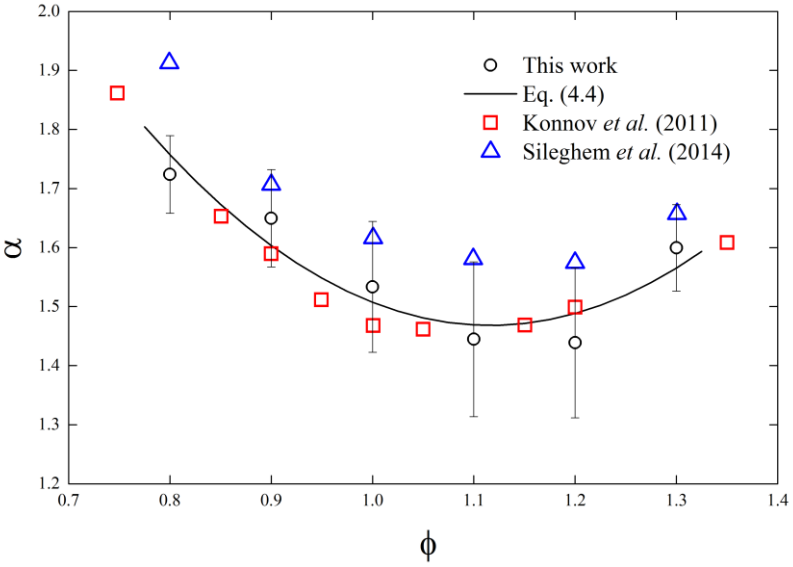

The values for the dependence parameter vary over an average of 1.57. The difference form the average is of the same degree as the uncertainty of the value as in the case of n-heptane, therefore using the average value and assume that the temperature dependence parameter it constant regarding the equivalence ratio may be a better solution, depending on the problem.

The global fitting equation for ethanol is:

$$S_L\left(\phi,T_u\right)=\left(-90.10+211.55\phi-7.70\phi^2-51.44\phi^3\right)\left(\frac{T_u}{398}\right)^{5.06-6.44\phi+2.88\phi^2} \tag{4.8}$$

Equation (4.8) may be changed as described in the n-heptane and iso-octane cases, the exponential equation may be used in place of the third degree polynomial function and the average of the temperature dependence parameter may substitute the second degree polynomial function. The consequences of these are the same as in the previous cases.

Deviation in percentage of the flame speed measured values from the flame speed calculated values using the global fitting curve is illustrated by Figure 4-25.

Figure 4-25 - Deviation in percentage of the flame speed measured values from the flame speed calculated values using the global fitting curve versus normalized equivalence ratio for ethanol.

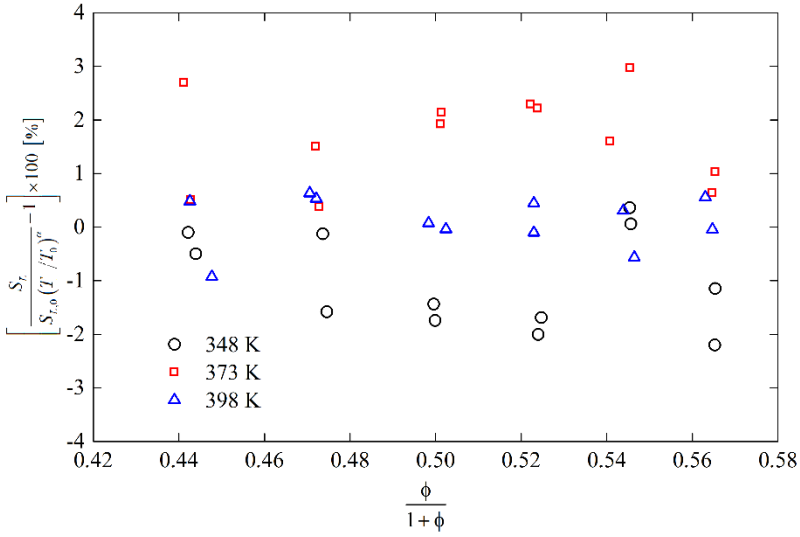

By analyzing Figure 4-25 it is possible to affirm that the use of Equation (4.6) will result in a deviation of utmost +/- 3 % from the actual value for the laminar flame speed of ethanol.

4.4 GASOLINE A AND SURROGATE A

Laminar flame speed of gasoline A and surrogate A are investigated in three temperature levels: 373 K, 398 K and 408 K. In each temperature level, six equivalence ratio levels: 0.8; 0.9; 1.0; 1.1; 1.2 and 1.3.

Results of laminar flame speed versus equivalence ratio in each temperature level are presented in Figure 4-26; Figure 4-27, and Figure 4-28.

Figure 4-26– Results of laminar flame speed of gasoline A and surrogate A versus equivalence ratio at 373 K.

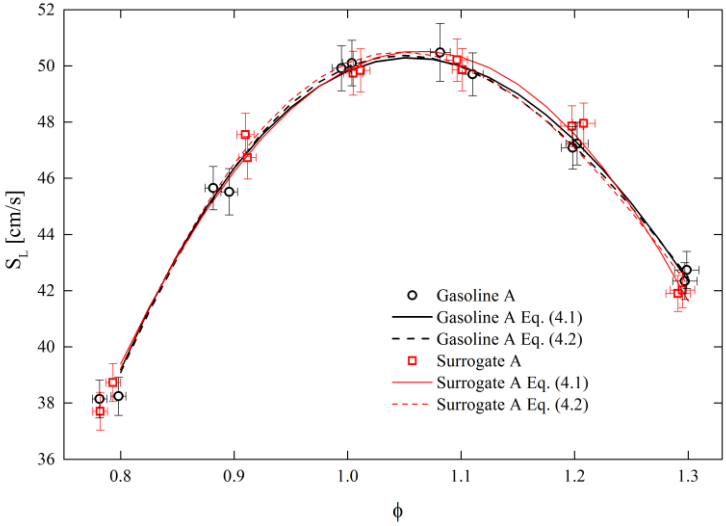

Figure 4-27– Results of laminar flame speed of gasoline A and surrogate A versus equivalence ratio at 398 K.

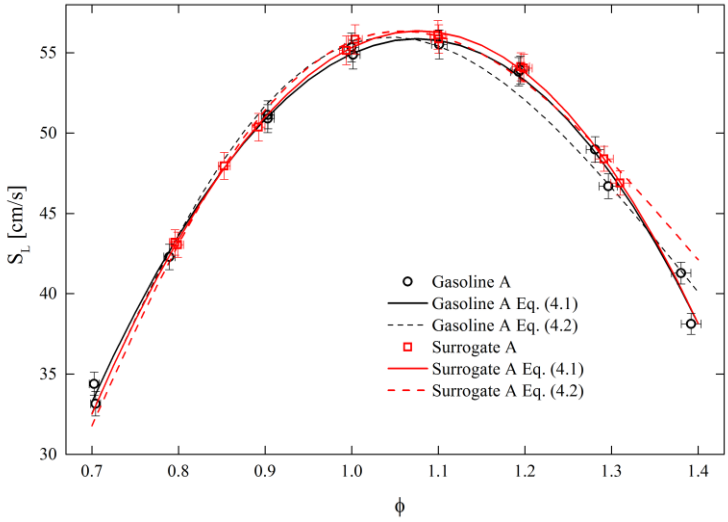

Figure 4-28– Results of laminar flame speed of gasoline A and surrogate A versus equivalence ratio at 408 K.

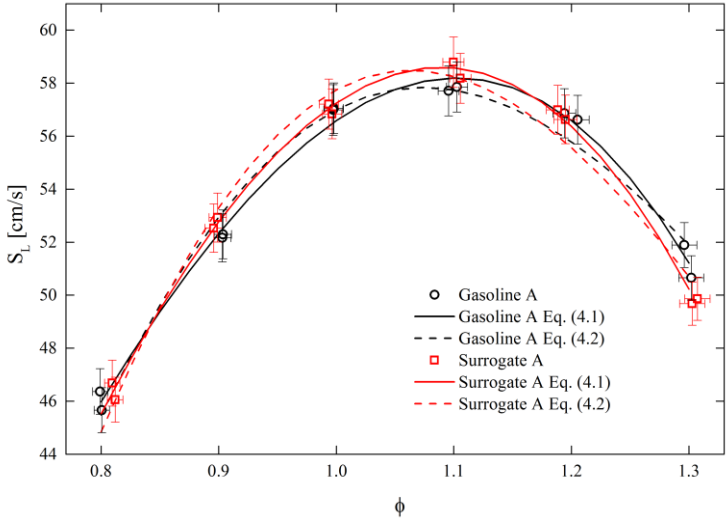

Compared to the substances already studied, gasolines are very different, as already pointed out, gasolines are a blend of a great number of different hydrocarbons, aromatics, linear and ramified hydrocarbons represent the most common species found in gasolines, this results in a higher vapor pressure. These aspects limited the test temperatures to a minimum of 373 K due to evaporation difficulties. Comparison with the literature is not made in the gasoline A or C cases, there is very few data, and they vary over a wide range, due to different composition of gasoline, the data is not reliable for comparison. The data presented in Figure 4-26; Figure 4-27, and Figure 4-28 is supported by the results of the pure substances cases, as their values are reliable, then it leads to the conclusion that the results of gasoline A and surrogate A are also reliable. Comparing the evolution of the laminar flame speed values over the equivalence ratio range, of the three temperatures, point of maximum is the same, for both gasoline A and surrogate A, and present the same tendency, this coherence is expected.

The results presented in Figure 4-26; Figure 4-27, and Figure 4-28 also lead to the conclusion that the surrogate A composition is adequate to model the laminar flame speed of gasoline A, as the difference between the experimental values is never greater then 2 %.

The parameters of Equation (4.1) and Equation (4.2) are described in Table 4-11 and Table 4-12 respectively, for gasoline A.

Table 4-11– Parameters of Equation (4.1) for gasoline A.

Temperature [K]	***a***	***b***	***c***	***d***
373	-206.01	569.05	-388.03	74.81
398	-120.66	315.37	-128.56	-11.21
408	-13.84	18.06	144.93	-92.56

Table 4-12– Parameters of Equation (4.2) for gasoline A.

Temperature [K]	ω	η	ξ	σ
373	4.08E-08	9.33	-0.97	5.65
398	4.54E-11	8.76	-0.64	7.59
408	1.93E-06	7.49	-0.73	5.86

Parameters of Equation (4.1) and Equation (4.2) are described in Table 4-13 and Table 4-14 respectively, for surrogate A.

Table 4-13– Parameters of Equation (4.1) for surrogate A.

Temperature [K]	*a*	*b*	*c*	*d*
373	-131.29	342.75	-162.41	0.82
398	-128.41	329.43	-134.07	-11.62
408	-65.02	149.81	37.50	-65.03

Table 4-14– Parameters of Equation (4.2) for surrogate A.

Temperature [K]	ω	η	ξ	σ
373	1.19E-10	8.85	-0.68	7.29
398	4.99E-08	9.33	-0.96	5.67
408	8.55E-08	8.86	-0.88	5.81

In Figure 4-26; Figure 4-27, and Figure 4-28 are also plotted the fittings of Equation (4.1) and Equation (4.2) for gasoline and surrogate A. For all fittings the results were good, the R^2 parameter for Equation (4.1) is 0.99 and 0.94 for Equation (4.2) in all three cases for gasoline and surrogate A.

Figure 4-29 and Figure 4-30, for gasoline A and surrogate A respectively, demonstrate the dependence between flame speed and unburned mixture temperature, for six levels of equivalence ratio, the lines are the fitted equations using Equation (4.3).

Figure 4-29 – Laminar flame speed versus unburned mixture temperature for gasoline A.

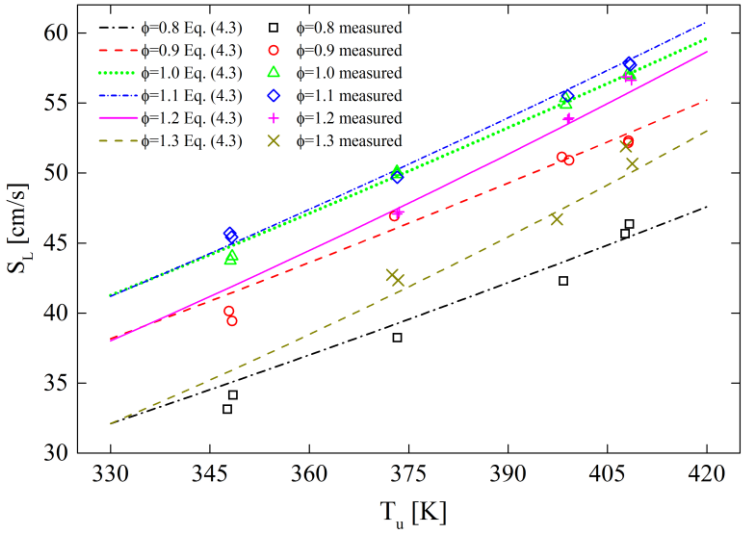

Figure 4-30– Laminar flame speed versus unburned mixture temperature for surrogate A.

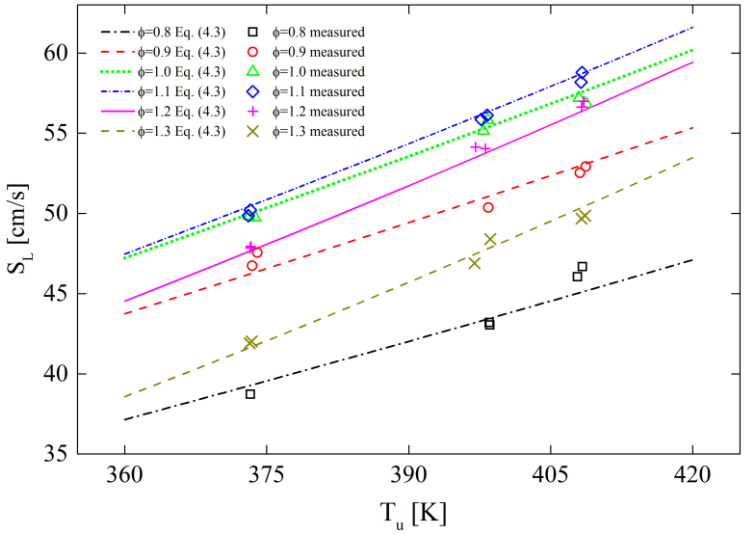

In Figure 4-29 and Figure 4-30, the slope of each curve corresponds to the temperature dependence parameter for each equivalence ratio. The dispersion of the data varies for each curve significantly; for the worst case of gasoline A in Figure 4-29 (ϕ =0.8) the adjusted R^2 is 0.97 with a standard deviation of 0,12, and the best case (ϕ =1.1) the values are 0.99 and 0.01 for adjusted R^2 and standard deviation respectively; for the worst case of surrogate A in Figure 4-30 (ϕ =0.8) the adjusted R^2 is 0.96 with a standard deviation of 0,12, and the best case (ϕ =1.1) the values are 0.99 and 0.01 for adjusted R^2 and standard deviation respectively. The parameters of Equation (4.3) are presented in Table 4-15 and Table 4-16 for gasoline A and surrogate A, respectively. These parameters can be substituted in Equation (4.3), then it is possible to extrapolate or interpolate for any desired value of unburned mixture temperature for a selected equivalence ratio.

Table 4-15 – Parameters of Equation (4.3) for gasoline A.

ϕ	$S_{L,398\,K}$ *[cm/s]*	α
0.8	43.6	1.730
0.9	50.9	1.385
1	54.9	1.460
1.1	55.8	1.691
1.2	53.3	1.925
1.3	47.4	1.986

Table 4-16 – Parameters of Equation (4.3) for surrogate A.

ϕ	$S_{L,398\,K}$ *[cm/s]*	α
0.8	43.4	1.562
0.9	51.0	1.492
1	55.3	1.564
1.1	56.3	1.708
1.2	53.8	1.893
1.3	47.8	2.103

The temperature dependence parameter varies with the equivalence ratio as can be inferred by Figure 4-29 and Figure 4-30, this is illustrated by Figure 4-31 as well as Equation (4.4). The standard deviation of each value from the fitted curve, Equation (4.3), is plotted as an uncertainty bar.

Figure 4-31 – Temperature dependence parameter versus equivalence ratio for gasoline A and surrogate A.

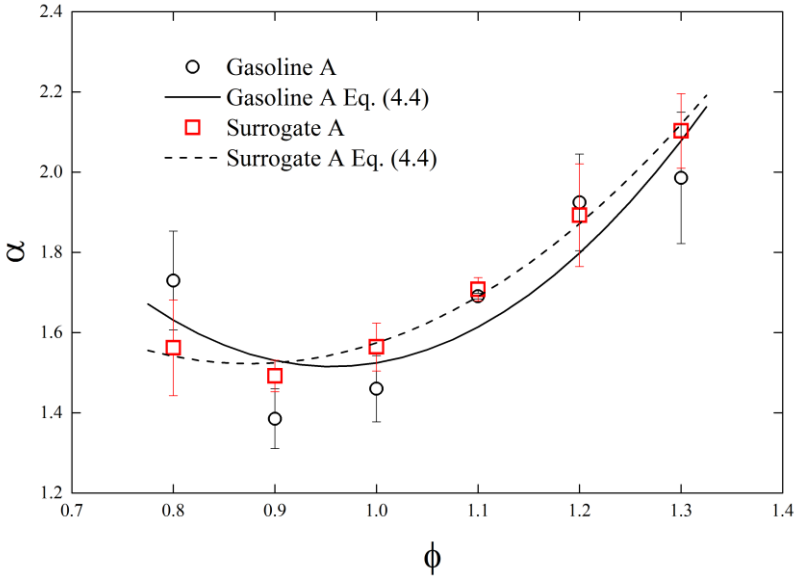

The great agreement of the laminar flame speed of the surrogate A and gasoline A extends to the temperature dependence parameter, the difference of each value is never greater than the standard deviation.

The values for the dependence parameter vary over an average of 1.70 for gasoline A and 1,72 for surrogate A. As suggested in the previous cases substitution of the quadratic function by the average value may be done observing the consequences already pointed out in the previous fuels cases.

The global fitting equation for gasoline A is:

$$S_L\left(\phi,T_u\right)=\left(-120.66+315.37\phi-128.56\phi^2-11.21\phi^3\right)\left(\frac{T_u}{398}\right)^{5.87-9.10\phi+4.76\phi^2} \tag{4.9}$$

The global fitting equation for surrogate A is:

$$S_L\left(\phi,T_u\right)=\left(-128.41+329.43\phi-134.07\phi^2-11.62\phi^3\right)\left(\frac{T_u}{398}\right)^{4.05-5.78\phi+3.30\phi^2} \tag{4.10}$$

Equation (4.9) and (4.10) may be changed as described in the previous cases, the exponential equation may be used in place of the third degree polynomial function and the average of the temperature dependence parameter may substitute the second degree polynomial function. The consequences of these are the same as in the previous cases

Deviation in percentage of the flame speed measured values from the flame speed calculated values using the global fitting curve is illustrated by Figure 4-32 and Figure 4-33, for gasoline A and surrogate A respectively.

Figure 4-32 - Deviation in percentage of the flame speed measured values from the flame speed calculated values using the global fitting curve versus normalized equivalence ratio for gasoline A.

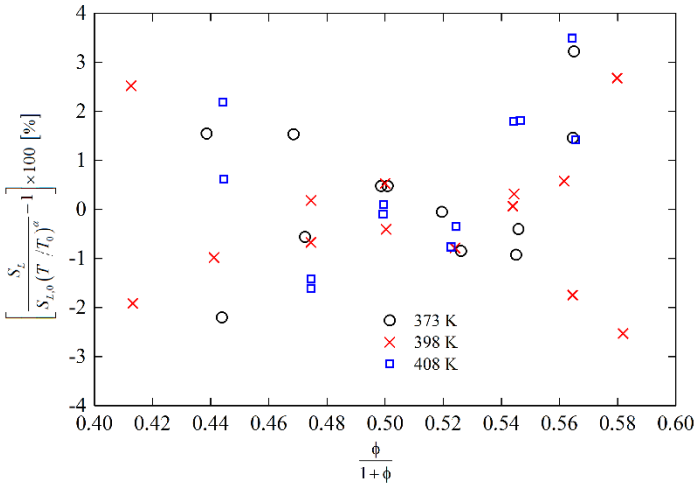

Figure 4-33 - Deviation in percentage of the flame speed measured values from the flame speed calculated values using the global fitting curve versus normalized equivalence ratio for surrogate A.

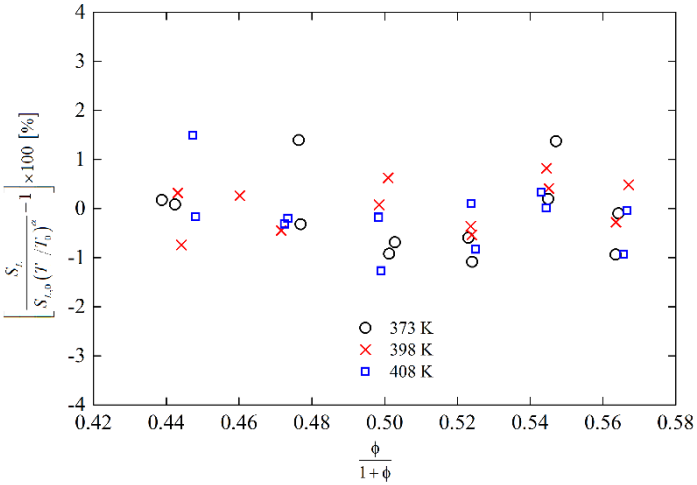

By analyzing Figure 4-32 and Figure 4-33 it is possible to affirm that the use of Equation (4.9) will result in a deviation of utmost +/- 3 % from the actual value for the laminar flame speed of gasoline A, and +/- 2% for surrogate A.

4.5 GASOLINE C AND SURROGATE C

Laminar flame speed of gasoline C and surrogate C are investigated in three temperature levels: 373 K, 398 K and 408 K. In each temperature level, six equivalence ratio levels: 0.8; 0.9; 1.0; 1.1; 1.2 and 1.3.

Results of laminar flame speed versus equivalence ratio in each temperature level are presented in Figure 4-34; Figure 4-35, and Figure 4-36.

Figure 4-34– Results of laminar flame speed of gasoline C and surrogate C versus equivalence ratio at 373 K.

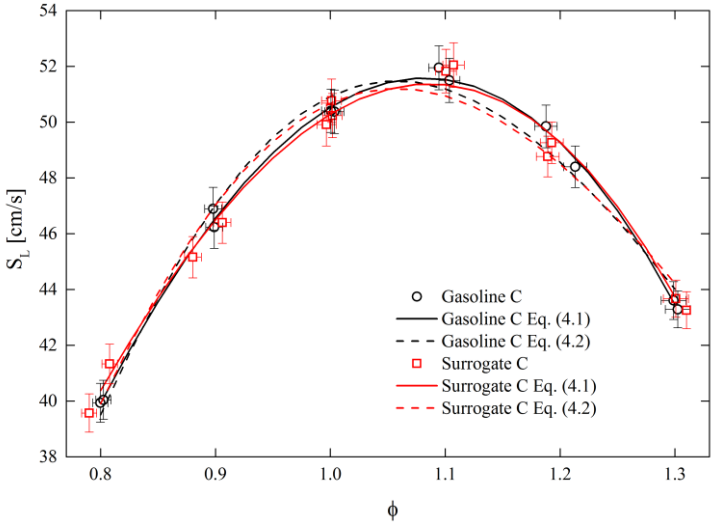

Figure 4-35– Results of laminar flame speed of gasoline C and surrogate C versus equivalence ratio at 398 K.

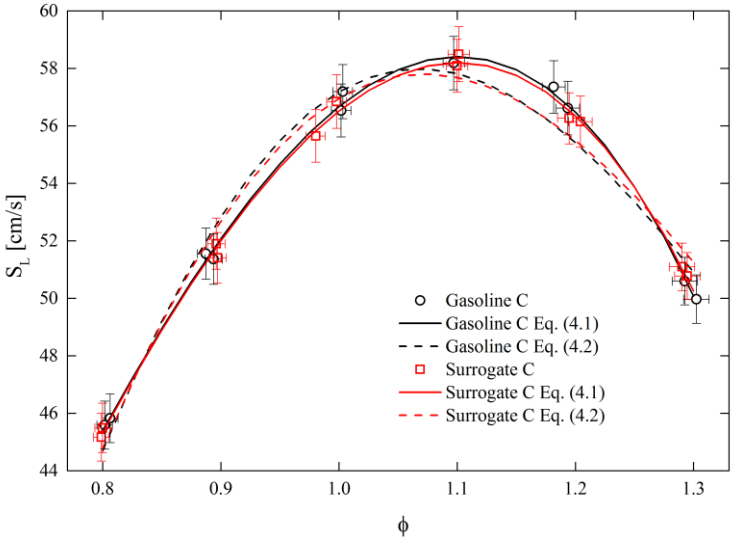

Figure 4-36– Results of laminar flame speed of gasoline C and surrogate C versus equivalence ratio at 408 K.

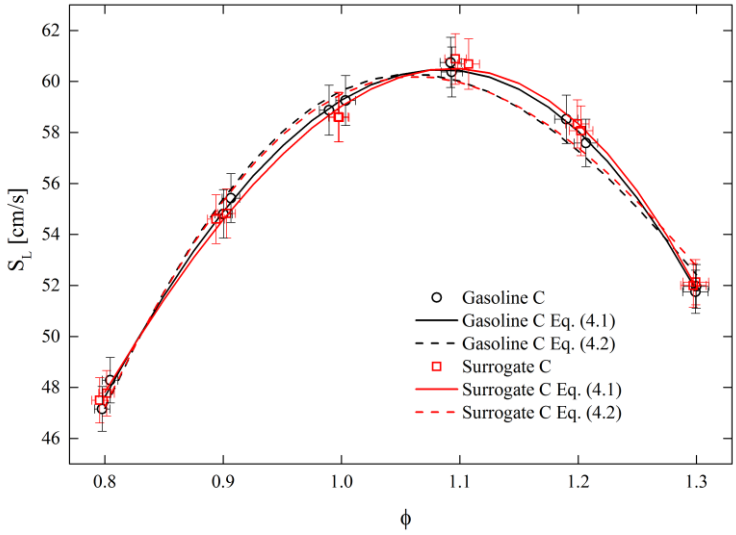

The results presented in Figure 4-34; Figure 4-35, and Figure 4-36, lead to the same conclusions as the gasoline and surrogate A case, the difference between each measured value of gasoline C and surrogate C in never greater than 2 % that validates the surrogate C as a very good model for the laminar flame speed of gasoline C.

The parameters of Equation (4.1) and Equation (4.2) are described in Table 4-11 and Table 4-12 respectively, for gasoline C.

Table 4-17– Parameters of Equation (4.1) for gasoline C.

Temperature [K]	*a*	*b*	*c*	*d*
373	-74.88	177.20	-3.47	-48.32
398	13.24	-79.05	255.40	-132.92
408	-76.28	189.40	-0.34	-53.52

Table 4-18– Parameters of Equation (4.2) for gasoline C.

Temperature [K]	ω	η	ξ	σ
373	3.02E-08	9.15	-0.90	5.85
398	1.37E-07	8.36	-0.79	6.00
408	1.52E-07	8.28	-0.79	6.00

Parameters of Equation (4.1) and Equation (4.2) are described in Table 4-13 and Table 4-14 respectively, for surrogate C.

Table 4-19– Parameters of Equation (4.1) for surrogate C.

Temperature [K]	*a*	*b*	*c*	*d*
373	-47.00	105.80	55.43	-63.94
398	-1.37	-32.63	206.75	-116.23
408	-11.64	1.87	177.61	-108.80

Table 4-20– Parameters of Equation (4.2) for surrogate C.

Temperature [K]	ω	η	ξ	σ
373	1.17E-07	8.61	-0.85	5.82
398	2.89E-07	8.00	-0.75	6.04
408	2.56E-07	8.01	-0.76	6.05

In Figure 4-34; Figure 4-35, and Figure 4-36 are also plotted the fittings of Equation (4.1) and Equation (4.2) for gasoline and surrogate C. For all fittings the results were good, the R^2 parameter for Equation (4.1) is 0.99 and 0.94 for Equation (4.2) in all three cases for gasoline and surrogate C.

Figure 4-37 and Figure 4-38, for gasoline C and surrogate C respectively, demonstrate the dependence between flame speed and unburned mixture temperature, for six levels of equivalence ratio, the lines are the fitted equations using Equation (4.3).

Figure 4-37 – Laminar flame speed versus unburned mixture temperature for gasoline C.

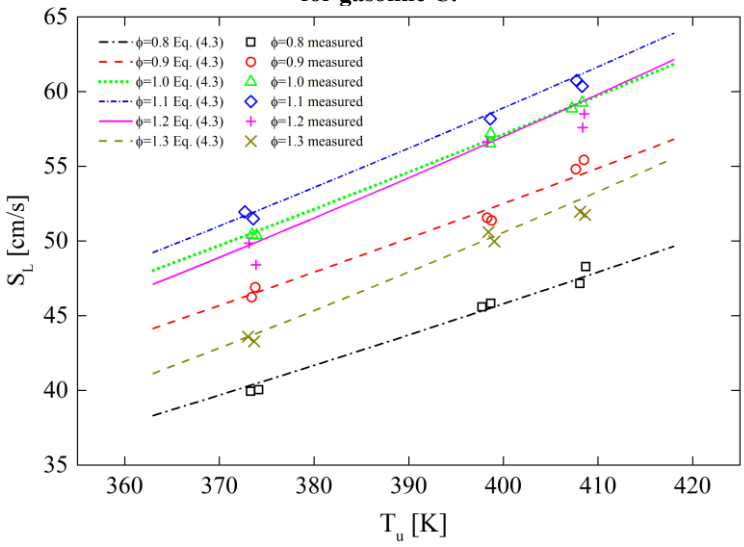

Figure 4-38– Laminar flame speed versus unburned mixture temperature for surrogate C.

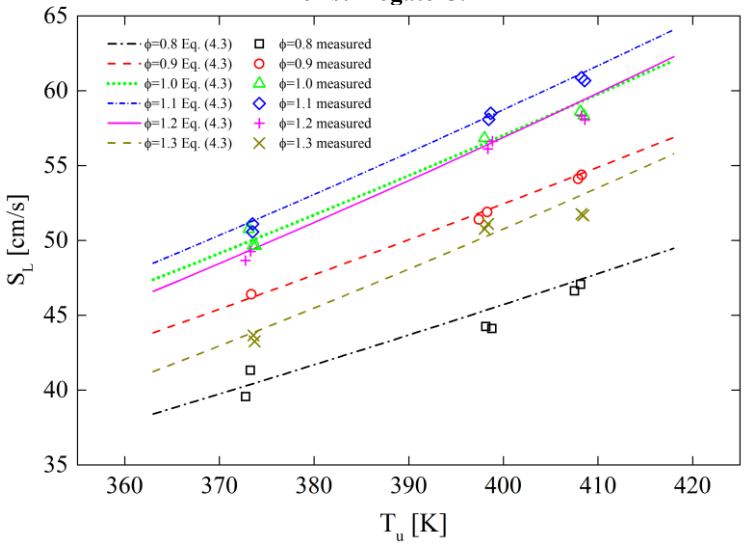

In Figure 4-37 and Figure 4-38, the slope of each curve corresponds to the temperature dependence parameter for each equivalence ratio. The dispersion of the data varies for each curve significantly; for the worst case of gasoline C in Figure 4-37 (ϕ =1.3) the adjusted R^2 is 0.95 with a standard deviation of 0,20, and the best case (ϕ =1.0) the values are 0.99 and 0.01 for adjusted R^2 and standard deviation respectively; for the worst case of surrogate C in Figure 4-38 (ϕ =1.2) the adjusted R^2 is 0.95 with a standard deviation of 0,17, and the best case (ϕ =1.0) the values are 0.99 and 0.01 for adjusted R^2 and standard deviation respectively. The parameters of Equation (4.3) are presented in Table 4-21 and Table 4-22 for gasoline C and surrogate C, respectively. These parameters can be substituted in Equation (4.3), then it is possible to extrapolate or interpolate for any desired value of unburned mixture temperature for a selected equivalence ratio, although extrapolation for temperatures far from 700 K, because there is scarce data in literature regarding comparison of this extrapolation and actual measured values.

Table 4-21 – Parameters of Equation (4.3) for gasoline C.

ϕ	$S_{L,398K}$ *[cm/s]*	α
0.8	45.4	1.974
0.9	52.1	1.791
1	56.7	1.774
1.1	58.4	1.836
1.2	56.5	1.933
1.3	50.1	2.042

Table 4-22 – Parameters of Equation (4.3) for surrogate C.

ϕ	$S_{L,398K}$ *[cm/s]*	α
0.8	45.3	1.848
0.9	52.0	1.761
1	56.5	1.793
1.1	58.2	1.870
1.2	56.3	1.951
1.3	50.3	2.130

The temperature dependence parameter varies with the equivalence ratio, this is illustrated by Figure 4-39 as well as Equation (4.4).

Figure 4-39 – Temperature dependence parameter versus equivalence ratio for gasoline C and surrogate C.

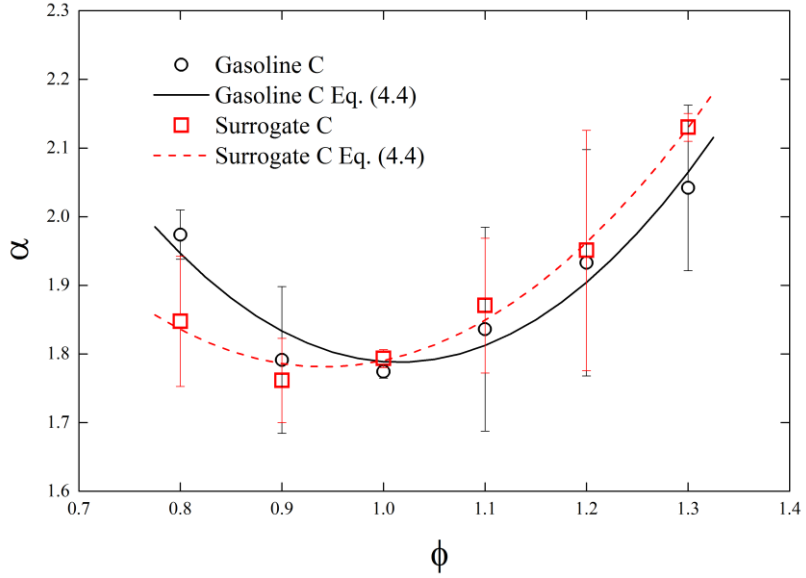

The great agreement of the laminar flame speed of the surrogate C and gasoline C extends to the temperature dependence parameter, the difference of each value is never greater than the standard deviation.

The values for the dependence parameter vary over an average of 1.89 for gasoline C and 1,89 for surrogate C. As suggested in the previous cases substitution of the quadratic function by the average value may be done observing the consequences already pointed out in the previous fuels cases.

The global fitting equation for gasoline C is:

$$S_L\left(\phi,T_u\right)=\left(13.24-79.05\phi+255.40\phi^2-132.92\phi^3\right)\left(\frac{T_u}{398}\right)^{5.31-6.93\phi+3.42\phi^2} \tag{4.11}$$

The global fitting equation for surrogate C is:

$$S_L(\phi,T_u)=\left(-1.37-32.63\phi+206.75\phi^2-116.23\phi^3\right)\left(\frac{T_u}{398}\right)^{1.69-0.20\phi+0.43\phi^2} \quad (4.12)$$

Equation (4.11) and (4.12) may be changed as described in the previous cases, the exponential equation may be used in place of the third degree polynomial function and the average of the temperature dependence parameter may substitute the second degree polynomial function. The consequences of these are the same as in the previous cases.

Deviation in percentage of the flame speed measured values from the flame speed calculated values using the global fitting curve is illustrated by Figure 4-40 and Figure 4-41, for gasoline C and surrogate C respectively.

Figure 4-40 - Deviation in percentage of the flame speed measured values from the flame speed calculated values using the global fitting curve versus normalized equivalence ratio for gasoline C.

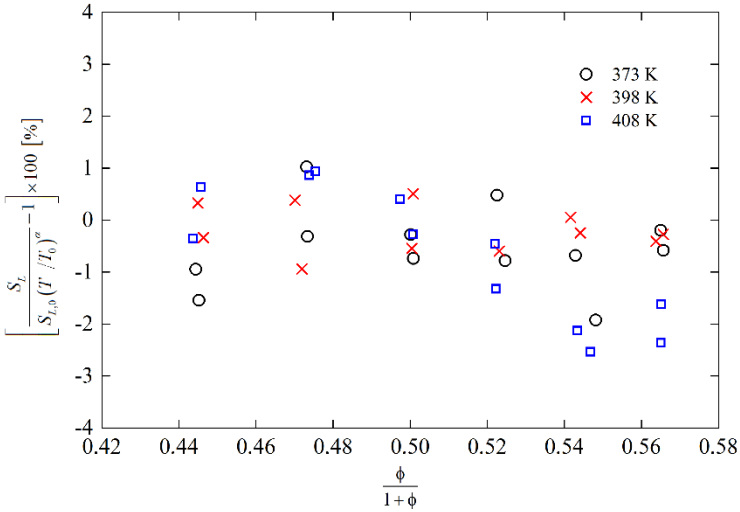

Figure 4-41 - Deviation in percentage of the flame speed measured values from the flame speed calculated values using the global fitting curve versus normalized equivalence ratio for surrogate C.

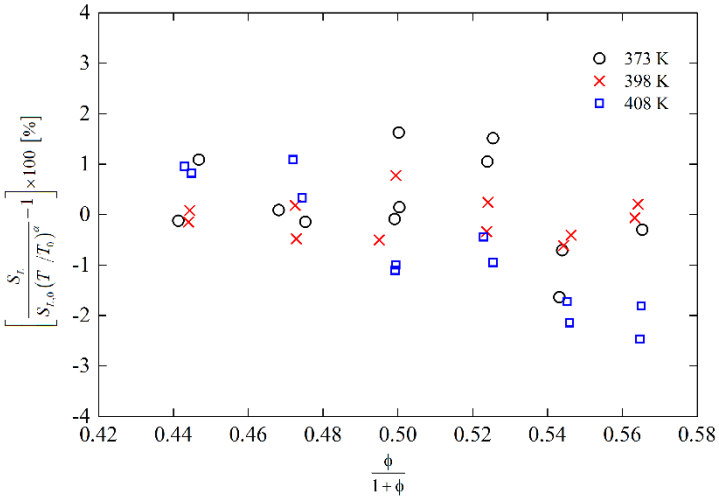

By analyzing Figure 4-40 and Figure 4-41 it is possible to affirm that the use of Equation (4.9) will result in a deviation of utmost +/- 2 % from the actual value for the laminar flame speed of gasoline C and surrogate C.

Finally it is very useful to compare the flame speed of all fuels tested ate a same temperature level versus the equivalence ratio. Figure 4-42 shows this comparison, the lines for each fuel are the cubic fitting curve ate 398 K. In the figure it is possible to preview some of the conclusions presented in the next section and also some results already discussed in this section.

The curve of the laminar flame speed of ethanol is higher than all other fuels tested, and also presents a maximum value slightly dislocated to a richer mixture of equivalence ratio of around 1.12. N-heptane presents the second higher flame speed, and iso-octane is the presents the slower flame speed for the tested fuels, both fuels present the maximum point of flame speed at equivalence ratio of around 1.05 as it is also the case of gasoline and surrogate A. Gasoline and surrogate A present flame speed just above iso-octane's. The addition of 27 % of ethanol to the gasoline and to the surrogate results in a higher flame speed, but not as high as n-heptane's, also it is possible to perceive the addition of ethanol by analyzing the curve peak which is slightly dislocated to a richer mixture (1.1), just as is also the ethanol curve.

Figure 4-42 – Comparison of laminar flame speed versus equivalence ratio of all tested fuels at 398 K.

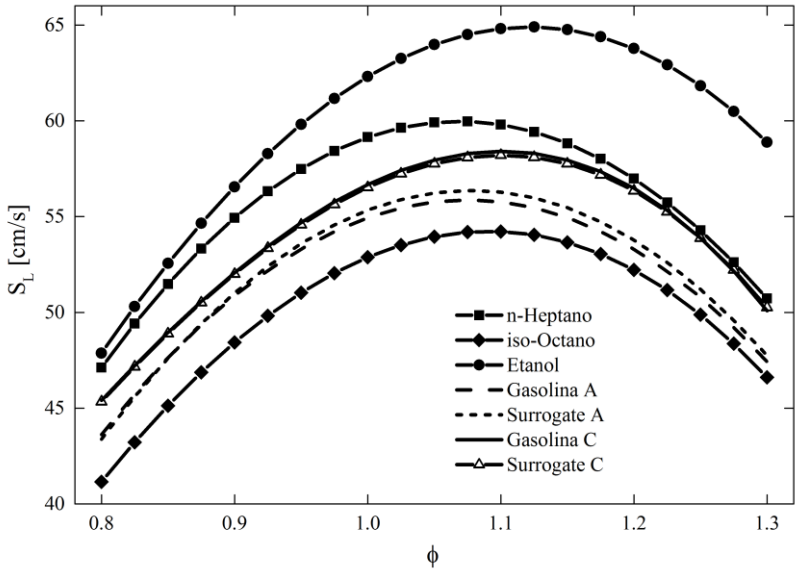

5 CONCLUSIONS

In this work, the laminar flame speeds of ethanol, iso-octane, n-heptane, gasoline, gasoline with 27% ethanol in volume, two surrogates for the gasoline and the gasoline with ethanol, in mixture with dry air were measured at 100 kPa, temperature range from 298 K to 408 K, and equivalence ratio from 0.6 to 1.4. The measurements were made in a constant volume reactor equipped with a high-speed camera (10000 FPS), for the visualization of the spherically expanding flame front propagation using the Schlieren method. Unstretched laminar flame speed was obtained through extrapolation using a linear relation between flame stretch rate and flame propagation velocity.

The main conclusions of the work are:

1. The results of laminar flame speed for the three pure substances (n-heptane, iso-octane and ethanol) are in accordance to the values found in literature. The values measured here differ up to 10 % when compared with values obtained from different sources. The good agreement with the literature validates the equipment and method.
2. The measurements were limited in the lower temperature and in the richer side by the minimum initial temperature needed to evaporate the fuel. The results for n-heptane at 298 K make this evident. The laminar flame speed at equivalence ratio greater than 1.3 are larger (5%) than the literature, and the values do not follow the same tendency as the literature at other temperatures. This disagreement suggests lack of evaporation in the experiments conducted in the rich side, at lower temperature.
3. A second limitation of the method is found at equivalence ratios larger than 1.4 when the flame radius is around 30 mm. Experiments show that the flame surface starts to wrinkle due to thermo-diffusive instability and the propagation of the flame front deviates from that of a laminar flame. This is observed in all tested fuels except for ethanol.
4. The laminar flame speed measured for the surrogates differ by, at most, 2 % when compared to the measurements for the commercial gasolines. The hypothesis of formulating the surrogate using the mole fraction to average the laminar flame speed for the pure components provided a good approximation, since the difference between the laminar flame speed of the surrogate and the corresponding gasoline is never greater than 2%.
5. Despite the fact that the surrogates emulate with precision the laminar flame speed of gasoline, the composition is not indicated for other purposes besides flame speed simulations, since the surrogates lack and aromatic substance. Aromatics are a very representative substance of gasoline, composing up to 40 % in volume, and in order to emulate further features related to its combustion an aromatic must be included.

The lack of an aromatic on the surrogates composition did not impaired the results because the laminar flame speed of most aromatics such as toluene is very close to the laminar flame speed of the gasoline itself as it can be observed in the work of Dirrenberger, Glaude, *et al.* (2014).

6. Ethanol addition to gasoline produces an augmentation of the laminar flame speed and dislocates the maximum point to a slightly richer value of equivalence ratio. The addition of 27 % of ethanol dislocates the maximum point of laminar flame speed from approximately 1.05 to 1.10 and accelerates approximately 3.5 % at the maximum point.
7. Both curves used to curve fit the measurements (third degree polynomial and exponential function) presented good agreement with the measurements. The third degree curve presents a better fitting, with an adjusted R^2 of 0.98 in average for all curves, against an adjusted R^2 of 0.94 for the exponential function.
8. The use of the global fitting curve is recommended to obtain values for laminar flame speed in conditions that are not measured. The deviation in percentage for the calculated values using the global fitting curve from the measured values is at maximum 4%. However, extrapolations far from the range measured are not recommended, since the curve fits may deviate in an unknown way. In this sense, the use of the exponential function by Goulder is safer for extrapolation.
9. The temperature dependence parameter is in good agreement with the literature. The uncertainty related to its determination is large, being around 10 % of the value. Therefore, a larger set of experiments is suggested to determine a value with a smaller uncertainty.
10. Gasoline C presented a larger temperature dependence for lean mixtures than Gasoline A. At lean mixtures, the temperature dependence of ethanol is greater than gasoline A, while for rich mixtures, there is an inversion, the temperature dependence of gasoline A is greater than ethanol. At rich mixtures the difference between the temperature dependence of gasoline A and C decreases and is equal for equivalence ratio of 1.3. This leads to conclude that the addition of ethanol affects temperature dependence at the equivalence ratio when ethanol's α is greater than the substance it is being added to.
11. Although a quadratic function best describes the dependence of the temperature exponent with the equivalence ratio, a constant value can be used for both gasolines providing essentially the same standard deviation when the values predicted by the curve fit is compared to the measurements.

In order to improve the quality of the results obtained and to better understand the features of the flame established in the CVR's chamber the following suggestions for subsequent research are listed:

1. Perform new calculations of the laminar flame speed, assuming a non-linear function to obtain the non-stretched flame speed in relation to the unburned.
2. Obtain the elementary composition of the test fuels by means of a proper test, instead of their standard average values.
3. Perform new calculations of the expansion factor utilizing the elementary composition of the fuels ant their lower heating value.
4. Perform experiments in other temperature steps in order to reduce uncertainty of the temperature dependence parameter.
5. Perform tests to determine the pressure dependence parameter.

BIBLIOGRAPHIC REFERENCE

ALBERTAZZI JR., A.; SOUSA, A. R. D. **Fundamentos de Metrologia Científica e Industrial**. 1ª. ed. Barueri: Manole, v. 1, 2008. ISBN 405.

ANFAVEA. http://www.anfavea.com.br/tabelas2007/autoveiculos/tabela10_producao.pdf, 2014. Access in: 20 oct. 2014.

BEECKMANN, J.; CAI, L.; PITSCH, H. Experimental investigation of the laminar burning velocities of methanol, ethanol, n-propanol, and n-butanol at high pressure. **Fuel**, v. 117, p. 340-350, 2014.

BRADLEY, D. et al. The measurements of laminar burning velocities and markstein numbers for iso-octane-air and iso-octane-n-heptane-air at elevated temperatures and pressures in an explosion bomb. **Combustion and flame**, n. 115, p. 126-144, 1998.

BRADLEY, D.; ANDREWS, G. E. The Burning Velocity of Methane-Air Mixtures. **Combustion and Flame**, 1972. 275-288.

BRADLEY, D.; HUNDY, G. F. **Burning velocities of methane-air mixtures using hot-wire anemometers in closed-vessel explosions**. [S.l.]: [s.n.], 1971. ISBN Symposium (International) on Combustion, Volume 13, 1971, Páginas 575-583.

BRADLEY, D.; LAWES, M.; MANSOUR, M. S. Explosion bomb measurements of ethanol–air laminar gaseous flame characteristics at pressures up to 1.4 MPa. **Combustion and Flame**, v. 156, p. 1462-1470, 2009.

Brazilian Energy Balance 2014. Empresa de Pesquisa Energética. Rio de Janeiro, p. 288. 2014.

BROUSTAIL, G. et al. Experimental determination of laminar burning velocity for butanol and ethanol iso-octane blends. **Fuel**, v. 90, p. 1-6, 2013.

DAVIS, S. G.; LAW, C. K. Laminar flame speeds and oxidation kinetics of iso-octane-air and n-heptane-air flames. **International Symposium on Combustion**, v. 27, p. 521-527, 1998.

DIRRENBERGER, P. et al. Laminar burning velocity of gasolines with addition of ethanol. **Fuel**, v. 115, p. 162-169, 2014.

EDMUND OPTICS. Edmund Optics, 2014. Disponivel em: <http://www.edmundoptics.com/testing-targets/testing-alignment/schlieren-systems/71-013>. Access in: 14 mar. 2014.

EISAZADEH-FAR, K. **Burning speeds, flame kernel formation and flame structure of bio-jet and JP8 fuels at high temperatures and pressures**. [S.l.]: [s.n.], 2010. ISBN PhD. Thesis, The Department of Mechanical and Industrial Engineering, Northeastern University, Boston, Massachusetts, 2010.

GLASSMAN, I.; YETTER, R. A. **Combustion**. 4ª. ed. Londres: Elsevier, 2008. 773 p.

GU, X. J. et al. Laminar Burning Velocity and Markstein Lengths of Methane–Air Mixtures. **Combustion and Flame**, 2000. 41-58.

GÜLDER, Ö. L. Burning velocities of ethanol-isooctane blends. **Combustion and Flame**, v. 56, p. 261-268, 1984.

GÜLDER, Ö. L. Correlations of Laminar Combustion Data for Alternative S.I. Engine Fuels. **SAE Technical Paper 841000, doi:10.4271/841000**, 1984.

HALTER, F.; TAHTOUH, T.; MOUNAÏM-ROUSSELLE, C. Nonlinear effects of stretch on the flame front propagation. **Combustion and Flame**, v. 157, p. 1825-1832, 2010.

HARTMANN, E. M. **INSTRUMENTAÇÃO E OPERACIONALIZAÇÃO DE UM REATOR DE VOLUME CONSTANTE PARA MEDIÇÃO DE VELOCIDADE DE CHAMA LAMINAR**. Master's Dissertation, UNIVERSIDADE FEDERAL DE SANTA CARATINA, Departamento de Engenharia Mecânica, Florianópolis: 2014.

HUANG, Y.; SUNG, C. J.; ENG, J. A. Measurements of Laminar Burning Velocities for Natural Gas-Hidrogen-Air Mixtures. **Combustion and Flame**, p. 302-311, 2006.

IPCC. http://mitigation2014.org/report/final-draft/. **http:** //mitigation2014.org/, 20 oct. 2014. Disponivel em: <http://mitigation2014.org/>. Access in: 20 oct. 2014.

KELLEY, A. P. et al. Laminar flame speeds, non-premixed stagnation ignition, and reduced mechanisms in the oxidation of iso-octane. **Proceedings of the Combustion Institute**, v. 33, p. 501-508, 2011.

KELLEY, A. P.; JOMAAS, G.; LAW, C. K. Critical radius for sustained propagation of spark-ignited spherical flames. **Combustion and Flame**, v. 156, n. 5, p. 1006-1013, 2009.

KIM, N. I. et al. Flammability limits of stationary flames in tubes at low pressure. **Combustion and Flame**, n. 141, p. 78-88, 2005.

KIM, W. K.; MOGI, T.; DOBASHI, R. Fundamental study on accidental explosion behavior of hydrogen-air mixtures in an open space. **International Journal of Hydrogen Energy**, n. 38, p. 8024-8029, 2013.

KOBAYASHI, H. et al. Burning velocity of turbulent premixed flames in a high-pressure environment. **Twenty-Sixth Symposium (International) on Combustion/The Combustion Institute,** p. 386-396, 1996.

KONNOV, A. A.; MEUWISSEN, R. J.; GOEY, L. P. H. D. The temperature dependence of the laminar burning velocity of ethanol flames. **Proceedings of the Combustion Institute**, v. 33, p. 1011-1019, 2011.

KWON, O. C.; HASSAN, M. I.; FAETH, G. M. Flame/Stretch Interactions of Premixed Fuel-Vapor/O2/N2 Flames. **Journal of Propulsion and Power**, v. 16, p. 513-522, 2000.

LAW, C. K. **Combustion physics**. 1. ed. Cambridge: Cambridge University Press, 2006. 722 p.

LIAO, S. Y. et al. Determination of the laminar burning velocities for mixtures of ethanol and air at elevated temperatures. **Applied Thermal Engineering**, v. 27, p. 374-380, 2007.

MANNAA, O. et al. Laminar burning velocities at elevated pressures for gasoline and gasoline surrogates associated with RON. **Combustion and Flame**, v. 162, n. 6, p. 2311–2321, 2015.

MEHL, M. et al. Kinetic modeling of gasoline surrogate components and mixtures under engine conditions. **Proceedings of the Combustion Institute**, v. 33, n. 1, p. 193-200, 2011.

METGHALCHI, M.; KECK, J. C. **Laminar burning velocity of propane-air mixtures at high temperature and pressure**. [S.l.]: [s.n.], 1980. ISBN Combustion and Flame, Volume 38, 1980, Páginas 143-154.

METGHALCHI, M.; KECK, J. C. Burning Velocities of Mixtures of Air with Methanol, Isooctane, and Indolene at High Pressures and Temperatures. **Combustion and Flame**, 1982. 191-210.

MIAO, H.; LIU, Y. Measuring the laminar burning velocity and Markstein length of premixed methane-nitrogen-air mixtures with the consideration of nonlinear stretch effects. **Fuel**, v. 121, p. 208-205, 2014.

NATIONAL INTITUTE OF STANDARDS AND TECHNOLOGY, 2015. Disponivel em: <http://www.nist.gov/>. Access in: 03 aug. 2015.

NIEMANN, U.; SESHADRI, K.; WILLIAMS, F. A. Methane, ethane, and ethylene laminar counterflow diffusion flames at elevated pressures: Experimental and computational investigations up to 2.0 MPa. **Combustion and Flame**, n. 161, p. 138-146, 2014.

NIKON. http://www.microscopyu.com. **MicroscopyU the source for microscophy education**, 2015. Disponivel em: <http://www.microscopyu.com/articles/optics/images/aberrations/astigfigure2.jpg>. Access in: 03 aug. 2015.

PAGLIUSO, J. D. Biofuels for spark-ignition engines. In: ZHAO, H. **Advanced direct injection combustion engine technologies and development Volume 1:** Gasoline and gas engines. Boca Raton: CRC Press LLC, 2010. p. 298.

PETERS, N. **Turbulent Combustion**. Cambridge: Cambridge University Press, 2000.

PICARD, A. et al. Revised formula for the density of moist. **Metrologia**, n. 45, p. 149–155, 2008.

PITZ, W. J. et al. Development of an Experimental Database and Chemical Kinetic Models for Surrogate Gasoline Fuels. **SAE Paper No. 2007-01-0175**, 2007.

QIN, X.; KOBAYASHI, H.; , T. N. Laminar burning velocity of hydrogen-air premixed flames at elevated pressure. **Experimental Thermal and Fluid Science**, n. 21, p. 58-63, 2000.

RAU, F. et al. Laminar burning velocity measurements using the Heat Flux method and numerical predictions of iso-octane/ethanol blends for different preheat temperatures. **Fuel**, n. 140, p. 10-16, 2015.

REACTION DESIGN. **CHEMKIN-PRO® Software Theory Manual**. San Diego: [s.n.], 2008.

SETTLES, G. S. **Schlieren und shadowgraph techniques:** visualizing phenomena in transparent media. Berlin: Springer, 2001.

SILEGHEM, L. et al. Laminar burning velocity of gasoline and the gasoline surrogate components iso-octane, n-heptane and toluene. **Fuel**, v. 112, p. 355-365, 2013.

SMALLBONE, A. J. et al. Experimental and modeling study of laminar flame speed and non-premixed counterflow ignition of n-heptane. **Proceedings of the Combustion Institute**, n. 32, p. 1245-1252, 2009.

SPALDING, D. B. **Combustion and Mass Transfer**. 1ª. ed. Londres: Pergamon, 1979.

TURNS, S. R. **An Introduction to Combustion:** Concepts and Applications. 2ª. ed. [S.l.]: McGraw-Hill, 1996. 565 p.

US ENERGY DEPARTMENT. Vehicle Technologies Office: Fuel Efficiency and Emissions. **http:** //energy.gov, 23 jun. 2015. Disponivel em: <http://energy.gov/eere/vehicles/vehicle-technologies-office-fuel-efficiency-and-emissions>.

VAN LIPZIG, J. P. J. et al. Laminar burning velocities of n-heptane, iso-octane, ethanol and their binary and tertiary mixtures. **Fuel**, v. 90, p. 2773-2781, 2011.

VAREA, E. et al. Measurement of laminar burning velocity and Markstein length relative to fresh gases using a new postprocessing procedure: Application to laminar spherical flames for methane, ethanol and isooctane/air mixtures. **Combustion and Flame**, n. 159, p. 577-590, 2012.

VELOO, P. S. et al. A comparative experimental and computational study of methanol, ethanol, and n-butanol flames. **Combustion and Flame**, v. 157, p. 1989-2004, 2010.

WANG, Z. H. et al. Effect of H2/CO ratio and N2/CO2 dilution rate on laminar burning velocity of syngas investigated by direct measurement and simulation. **Fuel**, n. 141, p. 285-292, 2015.

WARNATZ, J.; MAAS, U.; DIBBLE, R. W. **Combustion**. 4th. ed. Berlin: Springer, 2006.

WIESER, M. E. et al. Atomic weights of the elements 2011 (IUPAC Technical Report). **Pure and Applied Chemistry**, v. 85, n. 5, 2013.

WON, S. H. et al. **Characterization of Global Combustion Properties with Simple Fuel Property Measurements for Alternative Jet Fuels**. Propulsion and Energy Forum 50th AIAA/ASME/SAE/ASEE Joint Propulsion Conference. Cleveland: [s.n.]. 2014.

ZHAO, H. **Advanced direct injection combustion engine technologies and development**. [S.l.]: Woodhead Publishing Limited, v. 1: Gasoline and gas engines, 2010.

APPENDIX A - Effects of stretch and Lewis number on spherical flame

To understand the effects of stretch over the development of the spherical flame is fundamental to properly interpret the results obtained in the experiments. The discussion presented here is mostly based on LAW (2006).

Let us consider the positively stretched, outwardly propagating flame whose radius r_f is much larger than its thickness. In an interval δt, the flame radius grows by an amount $\delta r_f << r_f, r_T, r_M$, where r_T and r_M are respectively the radii for the thermal and limiting reactant layers. Then the volume for the thermal energy will be increased by an approximate amount:

$$\frac{4}{3}\pi\left(r_T + \delta r_f\right)^3 - \frac{4}{3}\pi {r_T}^3 \approx 4\pi {r_T}^2 \delta r_f \tag{A.1}$$

while that for the reactant concentration by:

$$4\pi {r_M}^2 \delta r_f \tag{A.2}$$

Figure A-1 illustrates the flame radius and the thermal and reactants radii layers.

Figure A-1 – Representation of spherical flame propagation, flame radius and the thermal and reactants radii layers.

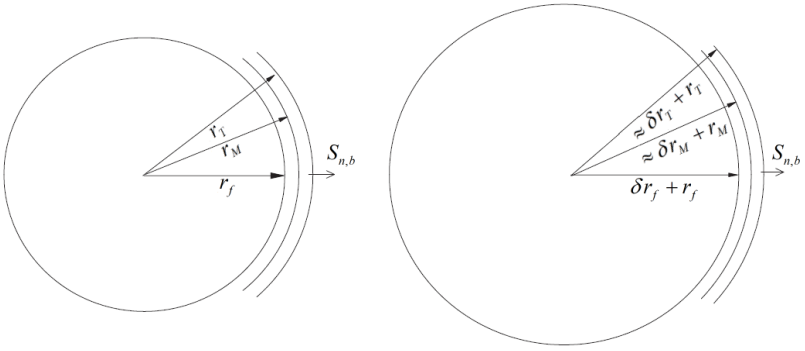

Source: Adapted from LAW (2006).

The increase in the thermal limiting layers structure represents an increased extent of heat transfer away from the reaction region, while an increase in the reactant limiting layer represents an increased amount of reactant supply to the reaction region. Consequently, if $r_T > r_M$, that is, $Le > 1$, then the flame temperature is expected to be reduced from the

adiabatic flame temperature, thus decelerating the flame propagation, while the opposite is true for $Le < 1$.

It is expected that stretch will promote flame propagation, for mixtures with $Le < 1$ and halt flame propagation for $Le > 1$, this relation is expressed by the Markstein length (L_b) calculated in Equation (2.37). L_b is the inclination of the curve that relates the stretched flame speed and the stretch rate. Figure A-2 shows stretched flame speed versus stretch rate for hydrogen flames. For rich hydrogen flames, Lewis number is greater than one, and as the stretch grows, the flame speed reduces, flame with equivalence ratio of 0.9 presents a Lewis number near unity, and the influence of stretch on flame speed is almost null, finally for equivalence ratio of 0.5 when $Le > 1$ stretch accelerates the flame propagation.

Figure A-2 – Stretched flame speed versus stretch rate for hydrogen flame at unburned mixture temperature of 298 K.

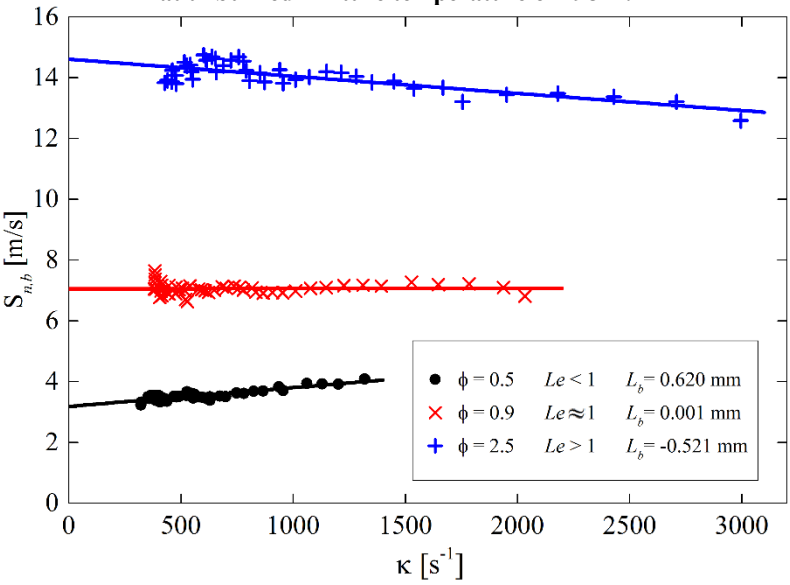

Another important feature discussed by Kelley, Jomaas and Law (2009), is the competition between stretch and energy supplied by the ignition source. This competition can result in the extinction of the propagating flame, for $Le > 1$ if the ignition energy is not sufficient to drive the reaction front to a radius at which stretch effects are reduced, this is the case for lean hydrocarbons flames.

For $Le < 1$ mixtures, the flame does not extinguish as long as a flame kernel can be established. This is reasonable because the initial state of the flame is the strongest, with a flame temperature that is higher than that of the unstretched planar flame. The response of the $Le > 1$ flame, however, is different, for sufficiently large values of the energy input, the flame speed first decreases to a minimum value, and then increases to approach the planar value. For weaker ignition kernels, the continuously decelerating flame cannot recover and eventually extinguishes at a finite size. This results in a 3 regimen flame propagation, represented by Figure A-3, with data of stretched flame speed against flame radius of iso-octane flame at equivalence ratio of 0.75, which corresponds to $Le >> 1$.

Figure A-3 - Stretched flame speed versus flame radius for iso-octane flame (ϕ = 0.75 T_u=398 K).

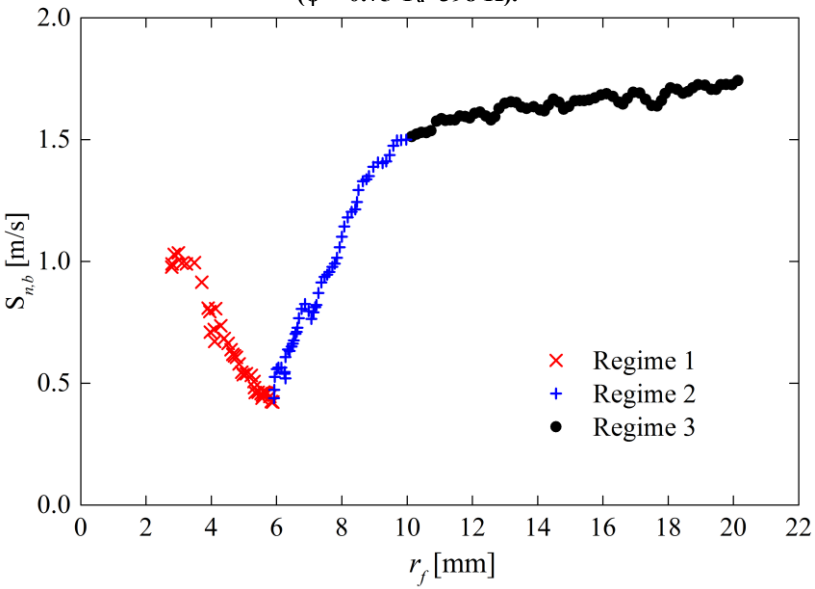

Won, Veloo, *et al.* (2014) explain the three phases. Regime 1 is the ignition energy driven flame propagation regime, where the excessively high flame speed is observed first due to the sudden thermal expansion of the ignition kernel, and later attenuated by the dissipation of thermal energy. Regime 2 is a weak flame regime, where the fuel chemistry starts to populate the radical pool and subsequently establishes the flame structure and sustaining heat release, resulting into the fast transition from a thickened to thin reaction zone. Regime 3 is the normal flame propagation regime, where

the unstretched planar laminar flame speed can be extracted by the linear extrapolation.

To finalize the discussion on flame development it will be addressed the influence of the Lewis number on flame wrinkling, which is the phenomenon shown in Figure 4-3. There are three modes of intrinsic cellular instability, namely diffusional-thermal instability, hydrodynamic instability, and buoyancy-driven instability. Hydrodynamic instabilities are caused by the difference of density of the burned and unburned mixture, and are observed in flames developing in a sufficiently large pressure of unburned mixture. Buoyancy-driven instabilities is induced by a body force, such as gravity. These two instabilities modes, although present, do not explain the difference among the difference of wrinkle in the flames pictured in Figure 4-3. Diffusional-thermal instabilities, which are caused by unbalance of mass and heat diffusion, explain this difference. For the case in the picture (ϕ = 1,4) the Lewis number of ethanol-air mixture is greater than unity, and n-heptane, iso-octane and gasoline smaller.

Law (2006) explain this phenomenon. The initially planar flame must be perturbed, into alternating convex and concave segments toward the unburned mixture, this perturbation is caused by the interaction with the electrodes. Figure A-4 represents the effects of the Lewis number on the instabilities.

Figure A-4 – Nonequidiffusion influence on flame stability.

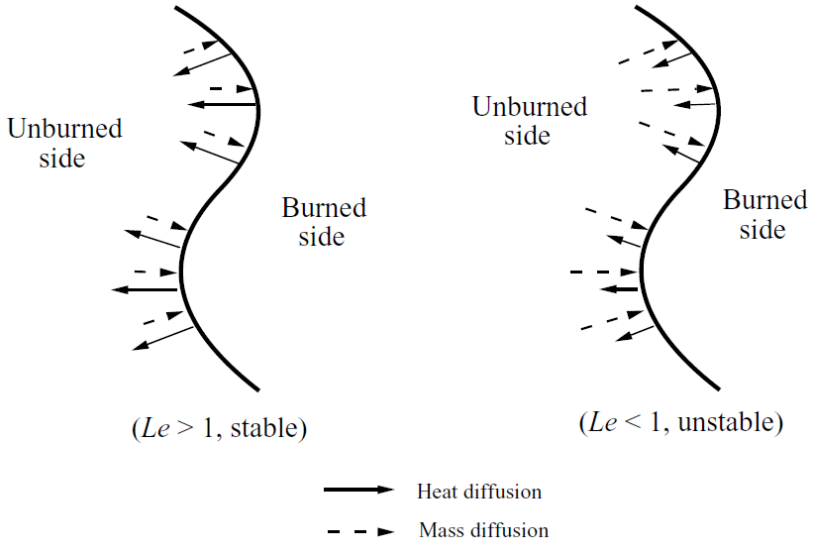

Source: Adapted from LAW (2006).

The concave and convex segments are governed by the same mechanisms of flame stretch addressed in this chapter. For a $Le > 1$ flame, the burning is intensified at the concave segment and weakened at the convex segment, leading to smoothing of the wrinkles. Consequently, such a flame is cellularly stable. Conversely, by the same reasoning a $Le < 1$ flame is cellularly unstable.

APPENDIX B - Uncertainty analysis

Uncertainty propagation calculation is made as already described. In this section, details about the uncertainties of every measurement is explained. The physical variables which uncertainty calculation is pertinent are: pressure of the unburned mixture p_u, mass of injected fuel m_f, unburned mixture temperature T_u, the fuel composition $C_{N_C}H_{N_H}O_{N_O}$, reactor volume V_{CVR}, oxygen molar fraction in air x_{O_2}, universal ideal gas constant R_u, molecular mass of the components MM, unstretched laminar flame speed in relation to the burned mixture $S_{n,b}$, expansion ratio E. This are the variables that are needed to calculate the equivalence ratio and the laminar flame speed using Equation (3.1) and Equation (2.11) respectively.

The standard uncertainty of the measurement equipment together with the data acquisition systems was already asserted in the previous work of Hartmann (2014), the results are summarized in this section.

Each parameter of standard uncertainty presented in this section is used in Equation (3.3), this equation is evaluated individually for every experiment, and the results of the propagated standard uncertainty are plotted as uncertainty bars in the laminar flame speed versus equivalence ratio figures. Correlation of the variables is not considered.

B.1 Static pressure sensor

The initial pressure on the reactor, as already described, is measured by a pressure sensor with a maximum pressure of 200 kPa and an uncertainty of 0.08% of the full scale. The data acquisition system, which is also described in the previous sections, reads the data of the pressure sensor with an uncertainty of 0.015% of the full scale, that is 10 V.

The standard uncertainty of the pressure measurement system (pressure sensor and data acquisition) is $u(p_u) = 0.2\ kPa$.

B.2 Mass balance

The mass balance as already described, measures up to 200 g with an 0.0002 g standard uncertainty. As the mass of fuel injected is the result of the difference of the mass of the syringe prior and after injection, the standard uncertainty of the injected fuel mass is $u(m_f) = 0.0004$ g.

B.3 Thermocouple

The thermocouple that measures the temperature of the unburned mixture is a type K special with a range from -35 to 1260 °C and a standard uncertainty coupled with the acquisition system of $u(T_u) = 1.1\,\mathrm{K}$.

B.4 Fuel composition

All fuels, ethanol, n-heptane, iso-octane, gasoline A and gasoline C where provided by PETROBRAS.

Ethanol presents a purity of 99.5 %, iso-octane and n-heptane: 99.0 %. Gasoline A and C are a complex mixture of several substances, their simplified molecular formulas are represented by $C_{7.55}H_{14.70}$ and $C_{4,85}H_{10.47}$ for gasoline A and C respectively, as data supplied by PETROBRAS.

Surrogates are prepared in 200 mL mixtures each using a burette, the burette presents and standard uncertainty of 0.5 mL. That represents a standard uncertainty of 0.25 % in volume composition for each fuel in the surrogate.

To translate this impurity data into uncertainty the following method is used. Let us use the simplified molecular formula of iso-octane as an example: C_8H_{18}. The 1 % impurity present in the iso-octane samples is assumed to translate directly into uncertainty in the carbon and hydrogen numbers of the molecular formula. Therefore, with uncertainties represented, the simplified molecular formula of iso-octane is: $C_{8.00\pm0.08}H_{18.00\pm0.18}$. For gasoline A and gasoline C a 2% uncertainty is imposed. For surrogate A and C the uncertainty of the burette is added to the uncertainty related to the impurity of the substances.

This method results in an overestimate of the uncertainties, because it is known that other substances present in the fuel samples, classified as impurities, have a similar molecular composition to the most abundant substance, a more precise calculation would result in a minor uncertainty. Table B-1 shows the composition and related standard uncertainty for each fuel.

Table B-1 – Table of uncertainty in fuels molecular composition.

Fuel	N_C	$u(N_C)$	N_H	$u(N_H)$	N_O	$u(N_O)$
iso-Octane	8.00	0.08	18.00	0.18	0	0.000
n-Heptane	7.00	0.07	16.00	0.16	0	0.000
Ethanol	2.00	0.01	6.00	0.03	1.000	0.005

Gasoline A	7.55	0.15	14.7	0.3	0	0.000
Gasoline C	4.85	0.10	10.5	0.2	0.49	0.01
Surrogate A	7.62	0.10	17.2	0.2	0	0.00
Surrogate C	4.76	0.06	11.5	0.1	0.508	0.006

B.5 Reactor volume

The CVR volume is evaluated using a 3D model, in order to assert an uncertainty, due to construction and manufacturing imperfections, it is assumed that the radius of the reactor is ±1 mm than designed, this deviation is assumed as uncertainty. This method results is a calculated volume of 14.8 L and standard uncertainty of $u\left(V_{CVR}\right) = 0.1\ \mathrm{L}$.

B.6 Dry air composition and universal ideal gas constant and molecular masses

Dry air is taken to have the composition of 0.20939 in molar fraction of O_2 as determined by PICARD, DAVIS, *et al.* (2008), other gases are represented by nitrogen. The standard uncertainty is also determined by PICARD, DAVIS, *et al.* (2008) as $u\left(x_{O_2}\right) = 0.00006$.

Universal ideal gas constant and its uncertainty is taken from the 2014 CODATA recommended values available in the NATIONAL INTITUTE OF STANDARDS AND TECHNOLOGY (2015) webpage. It's value is R_u = 8.3144598 $\mathrm{J.mol^{-1}.K^{-1}}$ and standard uncertainty $u\left(R_u\right) = 0.0000048\ \mathrm{J.mol^{-1}.K^{-1}}$.

Atomic weight of carbon, hydrogen and oxygen used to calculate the molar mass of the fuel is taken from the values and standard uncertainties from the 2011 IUPAC technical report WIESER, HOLDEN, *et al.* (2013). Table B-2 shows the values.

Table B-2 – Table of uncertainty in atomic weight of elements.

Element	*Atomic weight (MM)*	*Uncertainty u(MM)*
Carbon	12.010	0.001
Hydrogen	1.0079	0.0001
Oxygen	15.9994	0.0004

Source: WIESER, HOLDEN, *et al.* (2013).

B.7 Unstretched laminar flame speed in relation to the burned mixture

The unstretched laminar flame speed in relation to the burned mixture, is calculated as the intercept od the linear fitting equation that relates stretched laminar flame speed in relation to the burned mixture versus stretch rate, as it is already described. The standard uncertainty related to its value is assumed as the standard deviation of the intercept. I falls for a great majority experiments in the value of $u\left(S_{n,b}\right)=10$ mm/s .

B.8 Expansion ratio

The method for calculate the expansion ratio is already described. In order to assert an uncertainty related to its calculation, the method used is. Calculate the expansion ratio using the ideal composition of the fuel as if it is 100 % pure, and then repeat the calculation with the real purity and assuming the impure fraction is not reactive, the difference from this two values is found to be the standard uncertainty of the expansion ratio. This method yields a value, for a great majority of experiments of $u(E)=0.01$.

B.9 Temperature dependence parameter

The standard uncertainty of temperature dependence parameter is assumed to be the standard deviation of the fitting curve used to perform its calculation.

APPENDIX C - Detailed step-by-step experimental procedure

A. Experiment initialization

1) Turn all dispositive on.
2) Check the 3 USB connections to the PC.
3) Check grip in the window's bolts.
   a) In case heating/cooling occurs, bolts must be opened.
   b) If the temperature is constant the bolts must be tightened in 3 steps of: 5 N.m; 10 N.m; 15 N.m.
4) In the PC open CVR.vi
   a) Monitor the temperature
      i) Click "heating" tab
         (1) Check and control the heating system temperature.
         (2) Control and wait until the heating reaches permanent regime.
   b) Check the camera
      i) Click "Camera" tab.
      ii) Click "Live" button.
         (1) Calibrate optical system positioning, in order to obtain gray tone image.
   c) Test the spark
      i) Click "Pressure" tab.
      ii) Click "spark" button.
      iii) Check reading of the current sensor.
2) Calibrate the mass balance
   a) After the balance is at least 45 min on.
   b) In the balance: Click "tar".
   c) Position the 200 g mass in the center of the balance.
   d) Wait until the balance shows 200.0000 g.
   e) Take the 200 g mass out.

B. Experiment procedure

1) In CVR.vi program enter the following:
   a) Fuel name.
   b) Fuel composition.
   c) Pressure and temperature of the unburned fuel-air mixture.
   d) Equivalence ratio.
2) Clean CVR:
   a) Valve settings:
      i) SV = open.
      ii) NV = closed.
      iii) PV1 = closed.
      iv) PV2 = open.
      v) RVi = open.
      vi) RVo = open.
      vii) VV = closed.
      viii) AV = open.
   b) Control the NV opening and control the pressure measured by the P1 sensor in 130 kPa for 45 s.
3) Create vacuum:
   a) Close SV, NV and AV.
   b) Open VV.
   c) Turn the vacuum pump on.
   d) Wait until the pressure inside the reactor is stabilized to the minimum of the pump capacity.
   e) Close RVi and RVo in this order.
   f) Turn the vacuum pump off.
   g) Open AV.
4) Inject the fuel:

a) Check the “Ideal fuel mass” shown in the “pressure” tab of the “CVR.vi” program.

b) Fill the syringe with fuel

c) Empty the syringe.

d) Place the empty syringe in the balance

e) Click “TAR”.

f) Fill the syringe with the ideal fuel mass.

g) Measure the mass of the full syringe in the balance.

h) Type in the “Full syringe” input the mass measured by the balance.

i) Insert the syringe in the CVR septum.

j) Press the syringe piston to the end.

k) Place the empty syringe in the mass balance.

l) Type in the “Empty syringe” input the mass measured by the balance.

5) Fill the Reactor with air:

a) Close NV.

b) Open SV.

c) Open NV with caution.

d) Open RVi.

e) Control NV and SV until the pressure real and ideal pressure shown in the “pressure” are equal.

f) Close NV, SV and RVi.

g) Wait until temperature inside the reactor is stabilized:

i) In the “heating” tab.

ii) Check the “inner temperature”.

iii) The temperature stabilizes in utmost 7 min.

h) Open RVi.

i) Check total real pressure.

j) Deactivate the static pressure sensor by clicking the green button in the “pressure” tab.

k) Close RVi.

6) Spark:

a) Check in the tab “Camera”:

i) Click “Live”

(1) If the image is not a uniform shade of gray: recalibrate the optical system.

ii) Click “Live”

b) Check if the ignition box is on:

i) Screen lights on.

ii) Initial voltage is the specified.

c) Check if RVi and RVo are closed.

d) Return to the “Pressure” tab:

i) Click the “spark” button.

ii) Follow on screen the pressure evolution.

iii) Click “save video” button.

7) Preparation for next experiment:

a) Close VV.

b) Open RVo and RVi in this order.

c) Return to the step 1 of the experiment proceeding.

C. Finalization of the experimental proceeding.

1) Do the step 1 and 2 of the experiment proceeding.

2) Untighten the bolts of the windows.

3) Set the valves to the positions:

i) SV = closed.

ii) NV = opened.

iii) PV1 = closed.

iv) PV2 = open.

v) RVi = open.

vi) RVo = open.

vii) VV = open.

viii) AV = open.

4) Turn all the devices off.